Dissertation

Distribution and Mixing State of Saharan Dust in the Vertical Column

Airborne observations over the Atlantic Ocean in the Cape Verde region

Zur Erlangung des Grades eines Doktors der Naturwissenschaften (Dr. rer. nat.)
Vorgelegt von Dipl.-Ing. Kirsten Inga Lieke aus Köln
Am Fachbereich Material- und Geowissenschaften
Darmstadt – 2011 – D17

TECHNISCHE
UNIVERSITÄT
DARMSTADT

Gutachter: 1. Prof. Dr. Stephan Weinbruch
2. Prof. Dr. Christoph Schüth

Tag der Einreichung: 20. Januar 2011
Tag der Disputation: 08. April 2011

Widmung

Ich widme diese Arbeit meinem Cousin Jonathan.

Abstract

During the **Sa**haran **M**ineral D**u**st Experi**m**ent (SAMUM) 2008 field campaign, particles with geometric diameters between approximately 0.1 to 25 μm were collected on board of the Falcon sampling aircraft of the Deutsches Zentrum für Luft- und Raumfahrt (DLR, German Aerospace Centre). To investigate the spatial and vertical distribution of aerosol in the Cape Verde region, sampling was performed along the West African coastline and in the Cape Verde region. The chemical composition of these samples was determined by means of electron microscope single particle analysis. The major task of the conducted flights was to observe mixing of Saharan desert dust and biomass burning aerosol from the south Sahel belt. On all days investigated a distinct layer structure of biomass burning aerosol and desert dust layers was observed. The aerosol composition of the small particles (geometric diameter $<$ 0.5 μm) was highly variable and in case of biomass burning strongly dominated by soot with up to 90 % relative number abundance. Internal mixtures of soot particles with mineral dust were not detected. Soot was only observed to mix with secondary sulphate. Biomass burning aerosol particles were enriched in potassium and chlorine originating from the vegetation matrix, and sulphur. After long travel times (aging), particles appeared to be depleted in chlorine and enriched in sulphur. The coarse particles (d $>$ 0.5 μm) were dominated by silicates, which appeared to be mixtures of different minerals. In the Cape Verde region mineral dust is well mixed. For the aerosol arriving from central West Africa a determination of source regions by elemental or mineralogical composition was generally not possible. However, when the air mass followed another transport path, with longer travel time as observed for some high altitude trajectories, the dust origin appeared to be more in the south east of central West Africa, probably in the Bodélé. Refractive indices were calculated for each flight level, revealing a large variance in light absorption, resulting from the high number abundance of soot particles in the biomass burning layers. For a detailed modeling of radiation forcing and resulting effects on climate, the observed layer structure displaying different chemical and physical properties at the respective levels should be taken into account and might lead to some modification of the heretofore known results.

Inhalt der Arbeit

Während der Feldmesskampagne des **Sa**haran **M**ineral D**u**st Experi**m**ent (SAMUM) 2008 wurden Partikel mit einem Durchmesser von d $<$ 0,1 μm bis d $\sim$ 25 μm an Bord des Messflugzeuges Falcon vom Deutschen Zentrum für Luft- und Raumfahrt (DLR) gesammelt. Die räumliche und vertikale Verteilung von in der Kap Verde Region und entlang der West Afrikanischen Küste gesammeltem Aerosol wurde durch elektronenmikroskopische Einzelpartikelanalyse bestimmt. Das Hauptziel der durchgeführten Messflüge war, die Mischung von Wüstenstaub aus der Sahara und Biomasse-Verbrennungs-Aerosol aus der südlichen Sahelzone zu untersuchen. An allen Messtagen trat eine ausgeprägte Schichtung der verschiedenen Aerosoltypen auf. Die Zusammensetzung der kleinen Partikel (geometrischer Durchmesser $<$ 0.5 μm) variierte stark und war im Fall von Biomasse-Verbrennungs-Aerosol deutlich von Rußpartikeln dominiert, wobei der Ruß einen Anteil von bis zu 90 % der Probe ausmachen kann. Es wurden keine internen Mischungen von Ruß mit Mineralstaubpartikeln (Silikaten) gefunden. Ruß trat lediglich in internen Mischungen mit Sulfaten auf, wenn sekundäres Aerosol in hoher Anzahlhäufigkeit vorhanden war. Partikel in Biomasse-Verbrennungs-Aerosol enthielten höhere Anteile an Kalium und Chlor, Elemente die in der Pflanzenmatrix vorkommen, sowie Schwefel. Nach längerer Transportzeit (Alterung) sind diese Partikel reich an Kalium und Schwefel, wobei der Anteil an Chlor stark abnimmt. Die Zusammensetzung der großen Partikel (d $>$ 0.5 μm) wurde deutlich von der Klasse der Silikate dominiert. Diese zeigten sich als Mischungen verschiedener Silikatminerale. Der in der Region Kap Verde ankommende Mineralstaub ist gut gemischt. Eine Zuweisung des gesammelten Aerosols zu möglichen Quellgebieten war generell nicht möglich, wenn die Luftmasse aus dem zentralen West-Afrika kam. Dahingegen zeigte sich ein Unterschied in der Zusammensetzung der Proben in den höheren Schichten, wenn ihre Trajektorien einen anderen, längeren Weg nahmen und möglicherweise einer südöstlicheren Quellregion, nicht nachgewiesen der Bodélé, entstammen. Brechungsindices wurden für jede Flughöhe berechnet. Einhergehend mit der Häufigkeit von Ruß in Biomasse-Verbrennungs-Aerosolschichten zeigte sich eine starke Variabilität der Lichtabsorbtion zwischen den Schichten. Eine derartige Schichtstruktur mit unterschiedlichen chemischen und physikalischen Eigenschaften auf den unterschiedlichen

Höhenniveaus sollten durch entsprechend detaillierte Modelle für Strahlungsbilanz und Klima einbezogen werden, was vermutlich zu entsprechenden Modifikationen bisheriger Ergebnisse führen dürfte.

Table of contents

List of figures

Glossary

- ***Aerosol optical depth (AOD)*** – a quantitative measure of the extinction of solar radiation by aerosol scattering and absorption between the point of observation and the top of the atmosphere (the integrated columnar aerosol load) to express or evaluate direct radiative forcing
- ***BB*** – biomass burning
- ***BBA*** – biomass burning aerosol.
- ***backscatter coefficient*** – in units of m^{-1}. Indicates the attenuation caused by scattering at angles from 90° to 180°. It is one of several coefficients derived from the volume scattering function, each quantifying the total scattering within a particular range of angles.
- ***BSE*** – backscattered electrons.
- ***CCN*** – cloud condensation nuclei.
- ***DLR*** – Deutsches Zentrum für Luft- und Raumfahrt. German Aerospace Centre.
- ***d*** – diameter. Usually referred to as projected area diameter, if other is not declared.
- ***EDX*** – energy dispersive X-ray analysis.
- ***ESEM*** – Environmental Scanning Electron Microscope.
- ***Harmattan*** is a hot, dry wind that blows from the northeast or east in the western Sahara and is strongest in December, January and February. It usually lasts 5 to 6 day and carries large amounts of dust out over the Atlantic Ocean. The Harmattan is a trade wind strengthened by a low-pressure centre over the north coast of the Gulf of Guinea and a high-pressure centre located over north western Africa in winter and over the adjacent Atlantic Ocean during other seasons. In the summer it is undercut by the cooler winds of the southwest monsoon, blowing in from the ocean; this forces the Harmattan to rise to an altitude of about 900 to 1,800 metres.
- ***Ift*** – Leibniz-Institut für Troposphärenforschung Leipzig.
- ***ITCZ*** – inter tropical convergence zone. A band of clouds, usually thunderstorms, that circle the globe near the equator, where winds originating in the northern and southern hemispheres come together.

- ***LIDAR –*** flight detection and ranging is an optical remote sensing technology used to measure different parameters of a remote diffuse object (dust or smoke plume), depending on the scattering of light.
- ***n*** – number of particles.
- ***Radiative forcing –*** the RF represents the stratospherically adjusted radiative flux change evaluated at the tropopause, and is given in units of W m^{-2}. RF refers to global mean RF. Radiative forcings are calculated in various ways depending on the agent: from changes in emissions and/or changes in concentrations, and from observations and other knowledge of climate change drivers. (From IPCC, 2007)
- ***SAMUM*** – Saharan Mineral Dust Experiment research project, funded by Deutsche Forschungsgemeinschaft.
- ***SE*** – secondary electrons.
- ***Stub*** – sample carrier in scanning electron microscopy.
- ***TEM*** – transmission Electron Microscope or Transmission Electron Microscopy.
- ***Trough*** – or Monsoon trough. Elongated areas of low pressure along the intertropical convergence zone as part of the Hadley cell circulation.

Preface

The present study was conducted as part of the **Sa**haran **M**ineral D**u**st Experi**m**ent (SAMUM) during the 2008 Cape Verde field campaign and the following two year period of analysis of samples and interpretation of results.

“Samum” is the name of a small and extremely hot and dry local wind in Arabia and the Sahara. Its temperature often reaches 55 °C, and its relative humidity sometimes falls below 5 %. Intensive ground heating under cloudless sky generates the “SAMUM” or “Simoom”. The word actually means poison wind and refers to the wind’s suffocating effects on the human body (Normand 1920).

The SAMUM-project was a conducted by several groups of departments of for example the “Leibniz-Institut für Troposphärenforschung (Ift)” in Leipzig, the “Deutsches Zentrum für Luft- und Raumfahrt (DLR)” in Oberpfaffenhofen, “Maximilians Universität München”, “Johannes Gutenberg Universität Mainz”, “Technische Universität Darmstadt”, “Universität Bremen” and “Leibniz-Institut für Meereswissenschaften an der Universität Kiel” participated the two big SAMUM field campaigns. Those different groups focused on the different optical, physical and chemical properties of Saharan dust particles respectively, with the aim to improve the understanding of the transport of particles and of the influence that those particles may have in the atmospheric radiation system. In this seven year project, two special issues on the results of two field campaigns, conducted in summer 2006 (SAMUM-1, Heintzenberg 2009) and winter 2008 (SAMUM-2, Ansmann et al. 2011) are published.

The present work was conducted during part two of SAMUM, starting after the SAMUM-2 field campaigns. The major field of the present work was to investigate the vertical distribution and mixing state of particles collected on board of the DLR-Falcon aircraft during the second field campaign.

A large data set was gathered and offered a unique opportunity to study the vertical structure, transport and mixing of aerosol layers off-coast West Africa. As data on the chemical/mineralogical composition and mixing state of Saharan dust in the vertical column are still very limited (e.g., Kandler et al. 2009, Matsuki et al. 2010, Scheuvens et al. 2011), the present work provides important insights in the distribution and mixing of mineral dust and biomass burning aerosol.

List of (own) publications in the scope of and with contribution to or from this work:

- Lieke et al. (2011)
- Kandler et al. (2011)
- Kandler et al. (2011b)
- Ansmann et al. (2011)
- Engelmann et al. (2011)
- Petzold et al. (2011)
- Köhler et al. (2011)
- Schladitz et al. (2011)

A Diploma study (Lieke 2008) was conducted beforehand (May to November 2008). Parts of the results presented therein contributed to the present work and to the above mentioned publications. The present work was conducted from December 2008 to January 2011).

Results were presented on the

- European Aerosol Conference, Aug. 24th to 29th 2008, Thessaloniki, Greece
- 3rd International Workshop on Mineral Dust, Sept. 15th to 17th 2008, Leipzig, Germany
- European Geosciences Union General Assembly, Apr. 19th to 24th 2009, Vienna, Austria
- Japanese Association of Aerosol Science and Technology General Assembly, Aug. 19th to 21st 2009, Okayama, Japan
- European Geosciences Union General Assembly, May 2nd to 7th 2010, Vienna, Austria
- International Aerosol Conference Aug. 29th to Sept. 3rd 2010, Helsinki, Finland

A complete list of (own) publications including conference abstracts is attached to the curriculum vitae of Kirsten Inga Lieke at the end of this work.

1 Introduction and scope

1.1 Aerosol and climate

The Saharan desert is known to be the most important source of mineral dust in the global atmosphere (e.g., Goudie and Middleton 2001). Strong winds and other factors (e.g., Shao et al. 2009) are responsible for the erosion and uplift of dust, which may be then transported over thousands of kilometres (e.g., Huang et al. 2010). Mineral dust particles have a strong influence on the atmospheric radiation budget (see for example Twomey 1991, Tegen and Lacis 1996, Tanré et al. 2003). If absorption of radiation from the sun in the atmosphere exceeds the amount of reflections and emissions back into space, a positive net energy input remains, resulting in an enhanced global mean surface temperature (positive radiative forcing). A negative net energy input of course results in the opposite effect. This corresponds to the definition of positive and negative radiative forcing by the Intergovernmental Panel on Climate Change (IPCC). Due to their physical (shape, size, morphology, aspect ratio) and chemical (mineralogical composition) properties, particles may contribute to either positive or negative radiative forcing, and feedbacks between dust and climate are thus likely to occur (for review of this topic see for example Arimoto 2001 and references therein). Therefore, the characteristics of particles and their distribution in the atmosphere are substantial parameters for calculating local effects and estimating the consequences for the global mean surface temperature.

At Cape Verde islands, a mixing of aerosols is expected due to Saharan dust undergoing a long range transport towards the Americas and biomass burning aerosol being emitted from the huge annual bush fires in the Sahel region, developing a complex layer structure. A corresponding layer structure has been described by Haywood et al. (2008) for ground-based measurement sites across west Africa. While desert dust originates from natural sources, biomass burning is regarded as a strong source for anthropogenic aerosols. It was emphasized by Forster et al. (2007) that for the direct effect of anthropogenic aerosols, there are still substantial uncertainties regarding emission sources and their vertical structure of aerosol, optical properties, mixing and separation from natural background aerosol.

Transport and mixing of aerosols may alter the particles and change the optical properties of the aerosol column. To model a refractive index of the aerosol column, detailed knowledge on the composition and distribution of the particles in the column is of crucial importance. Furthermore, aging effects of mineral dust particles during long–range transport clearly influence their shape, hygroscopic behaviour, radiative effect and properties as ice nuclei (see for example Cziczo et al. 2009).

1.2 State of the art

Aeolian mineral dust has been studied for decades and trace markers for particular source regions were detected (e.g., Schütz and Sebert 1987, Caquineau et al. 2002, Moreno et al. 2006). Dust sources have yet been identified by remote sensing using satellite data (e.g., Prospero et al. 2002, Schepanski et al. 2007). In many studies (e.g., Caquineau et al. 1998, Bates et al. 2001, Blanco et al. 2003, Kandler et al. 2007) element ratios, such as Si/Al, Fe/Ca and mineral phase ratios as Illite/Kaolinite (as derived from elemental or mineralogical analyses of air borne particles and soils), are linked to particular source regions. Different optical techniques (e.g., LIDAR) are used to determine aerosol distribution in a vertical profile.

Several field campaigns, focussing on dust properties and transport, were conducted during the past years: The Puerto Rico Dust Experiment (PRIDE, Reid et al. 2003) in July 2000 and the Saharan Dust Experiment (SHADE, Tanré et al. 2003), took place over the tropical Atlantic between the West African coast and the Cape Verde islands in September 2000. The United Arab Emirates Unified Aerosol Experiment (UAE2, Reid et al. 2008) focused on dust in the southern Arabian Gulf region in late summer 2004. The international African Monsoon Multidisciplinary Analysis (AMMA) program (Redelsperger et al. 2006) included several campaigns over many years which were conducted over western Africa and the adjacent Atlantic to investigate the properties of aerosol particles in that region and their impact on weather and climate. This list is not complete and smaller projects have been conducted ever since, providing important results in is large field of research.
The meteorological phenomena on the large scale are well understood, but dust uplift and transport is also driven by a number of meso and micro scale processes, which

still need to be studied. Underlying physics of wind erosion are described in Shao et al. (2009). Detailed observations revealed the characteristics and season dependencies of dust transport and are summarized for example by Schepanski (2008).

During the AMMA field campaigns, which focused on the mixing of Saharan dust and biomass burning aerosol from agricultural land fires, which are transported towards the West African Monsoon region and across the tropical Atlantic Ocean, Haywood et al. (2008) observed a complex aerosol layering structure. In the source near area on the African continent, Formenti et al. (2008) observed external mixing of biomass burning aerosol and mineral dust particles. Matsuki et al. (2010) present the chemical composition of particles (with $d > 1\ \mu m$) in the aerosol column in the vicinity of Niamey, Niger. As well as Formenti et al. (2008), they observe regional variability of the composition of mineral dust from West Africa. An overview of the recent progresses in understanding physical and chemical properties of mineral dust is given by Formenti et al. (2010). The chemical properties of biomass burning aerosol particles were already described near the source and after short range transport (e.g., Cachier et al. 1995, Gaudichet et al. 1995, Echalar et al. 1995, Li et al. 2003).

1.3 Saharan Mineral Dust Experiment (SAMUM)

Despite the output and success of these above mentioned campaigns, some deficit remained in the understanding of dust-radiation interactions, depending on transportation, mixing and aging of dust with regards to long range transport over the Atlantic, which was part of the motivation in particular of the second SAMUM field campaign. The SAMUM-1 campaign (Heintzenberg 2009) focused on dust mobilization, transport and dust properties in the northern Sahara. The second SAMUM field campaign focused on Saharan dust and biomass burning aerosol from agricultural land fires, which are transported towards the West African Monsoon region and across the tropical Atlantic Ocean. As a part of this second SAMUM campaign, the current work provides an essential contribution to the understanding of mineral dust in the aerosol column and in particular to the understanding of mineral dust mixing with biomass burning in long range transport. Ground based measurements took place on Cape Verde Islands, which lie in the intersection of transported dust and biomass burning aerosol. The results of in-situ particle

measurements are published for example in Kandler et al. (2011, 2011b) and Schladitz et al. (2011). Airborne observations (Lieke et al. 2011, Petzold et al. 2011, Weinzierl et al. 2011) provided a unique opportunity to sample different kind of high resolved data and samples, vertically and horizontally throughout a dust or biomass burning plume.

1.4 Observed parameters

Different analytical techniques are used to characterize chemical and physical properties of mineral dust. In general, bulk measurements and the analysis of individual particles are to be distinguished. Bulk analysis of mineral dust samples can be further subdivided according to the obtained information (mineralogical, elemental, isotopic, or ionic composition) and techniques (for example X-ray diffraction analysis and different applications of mass spectrometry). In the present study, single particle analysis with electron microscopy was used, in order to obtain detailed information on a large number of single particles (size, shape, chemical composition). Particles in the atmosphere are occurring over a wide size range from some nano meters geometric diameter to hundred micro meters. The small particles dominate the number size distribution, whereby the larger particles contribute significantly to the aerosol mass. A size distribution is usually measured with particle counters, which can be also installed on an aircraft, as described for example by Weinzierl et al. (2009, 2011). But referring to the size resolved composition and number abundances of particle classes, the size for every single particle is an important factor derived in electron microscopy. Shape influences the scattering abilities of particles, but in simulations of optical properties and radiative effects of aerosols, spherical model particles or spheroids are assumed (see for example Otto et al. 2009). In electron microscopy an aspect ratio is derived for every single particle, mean values are used in simulations and may vary for different aerosols. The chemical composition of particles is measured with energy dispersive X-ray detection (e.g., Laskin and Cowin 2001). Particles are classified according to their elemental composition (e.g., Ebert et al. 2002), which in most cases can be assorted to mineralogical groups, but a real mineralogical analysis can not be provided by scanning electron microscopy with energy dispersive X-ray analysis (SEM/EDX).

However, the X-ray diffraction analysis (XRD) of bulk samples has identified the most abundant phases of mineral dust (e.g., Prospero et al. 1981, Schütz and Sebert 1987, Ganor 1991, Moreno et al. 2006). Besides quartz, which is ubiquitous in most dust samples, a wide spectrum of other minerals was detected (e.g., feldspars, carbonates, sulphates, and clay minerals). But to approach the mixing state of aerosol and in particular the distribution of these mineral phases in the aerosol particles, it is necessary to apply single particle analysis. Single particle analysis with electron microscopy in the recent years revealed differences in the particles chemistry from different source regions (e.g., Kandler et al. 2007, 2009) and therefore in the reactivity of internally mixed particles (e.g., Krueger et al. 2004). Sokolik and Toon (1999) for example pointed out the dependence of radiative properties on mineralogical composition of single particles. Aerosol particles usually appear as multi component aggregates of minerals with different optical properties. Thus a volume mixing rule is applied to determine a complex refractive index of aerosol particles (e.g., Ebert et al. 2004, Kandler et al. 2007).

1.5 Other aspects of mineral dust

Transported mineral dust (not only from the Sahara) is occurring all over the globe and has a strong influence on populated areas, on people's health and life, on agriculture and soil development, and on marine environments even in remote areas, thousands of kilometres away from the sources. In fact, Saharan dust is transported to the oceans and is contributing as an important nutrient to marine environments (Prospero et al. 1996, Baker et al. 2003, Mills et al. 2004 and others). African dust is a significant contributor to soils of western Atlantic islands (e.g., Muhs et al. 2007). It is the main mineral source that fertilizes the Amazon basin (Swap et al. 1992, Koren et al. 2006), and is responsible for transporting bacteria, fungi and viruses and by that distributing diseases (e.g., Griffin et al. 2001). Among others, Sun et al. (2008) recently reported the impact of Saharan dust on the formation of tropical cyclones in the Atlantic basin. Even in northern Europe transported Saharan dust is frequently observed. Furthermore, dust in general impacts on air quality (e.g., Gatz and Prospero 1996, Prospero 1999b) which today comes increasing in governmental focus.

In agricultural areas, the loss of dust particles leads to gradual land degradation, because fine particles are mostly rich in nutrients and organic matter (e.g., Shao et al. 2009).

1.6 Scope

To asses the direct radiative forcing by particles over the Atlantic Ocean, their distribution (longitude, latitude, altitude) and their variance in space and time should be observed, with focus on the particles chemical/mineralogical composition. Thereby great importance was attached to the mixing of biomass burning aerosol with desert dust and on the state of mixing of these two components in the different regions, e.g., at the Cape Verde Islands and in the south. The aging of aerosol during should be observed and it was expected to see differences in the mineral dust composition due to different source regions. In the present work different aerosol types (Biomass Burning, Desert Dust and Marine) and their distribution in the aerosol column were studied. For that purpose, a large number of particles was collected and analysed and a new version of group classification software was developed and established. From the chemical composition the complex refractive index was calculated for each flight leg. Furthermore, the mixing state was evaluated by using different element indices.
The size-resolved relative number abundance of particles classes was regarded for every single flight level.
The collected samples are part of a four dimensional study (longitude, latitude, altitude and time) and are an essential link in column closure studies, conducted during the Cape-Verde-Field-Experiment 2008 (the results of which will be published in the SAMUM-II Special issue, Tellus 63 B, 2011).

2 Basics

2.1 Aeolian dust

Windblown fine sand, silt, and clay are important components in arid-land ecosystems. Billions of tons (e.g., 5000 $x10^6$ t yr^{-1} estimated by Schütz 1980, 1100-5000 $x10^6$ t yr^{-1} given by Engelstaedter et al. 2006) are emitted into the atmosphere annually. Approximately 20 % thereof is undergoing long range transport, following the major wind systems, and part of it is even transported all around the globe. Due to diurnal patterns of emission, aerosol concentrations vary strongly over time and space (e.g., Kaufman et al. 2002, Huang et al. 2010).

In the following section, the most important factors concerning Aeolian dust are described.

2.1.1 Dust generation

Dust is generated through a number of processes, the most important, wind erosion, is a geological and climatic phenomenon (Shao et al. 2009). Weathering of rocks and soils at the surface produces large amounts of dust, which are emitted into the atmosphere basically by strong surface winds. Dust is mobilized by large-scale frontal systems or numerous small-scale dust devils. Meso-scale mechanisms, such as density currents driven by evaporational cooling of convective precipitations in mountain regions were reported by Knippertz et al. (2007) recently. The dust production is based on physical phenomena such as creeping, saltation and sandblasting of soil aggregates (Gomes et al. 1990, Alfaro et al. 1998). To start lifting from the surface, a threshold force is to be exceeded. This threshold, typically corresponding to a wind speed of at least 7 m s^{-1} at 10 meters above ground level, depends on surface properties like roughness, grain size, and soil moisture. Obstacles like rocks, vegetation and also crusts on soils, increase the threshold velocity required for dust emission (Marticorena and Bergametti 1995). Over large flat surfaces like depressions, where fine loose sediments are accumulated, dust emission is strongest (Prospero et al. 2002).

2.1.2 Dust transport

The mobilized material covers several size classes from sub micrometer range to tens of μm in radius. Particles with d > 50 μm are deposited very rapidly after short distances. Particles with diameters up to about 20 μm possibly go into long range transport. With increasing distance to the source, the size distribution changes and the count median diameter shifts towards smaller dimensions.

An example of measured size distributions for Morocco (Kandler et al. 2009), Cape Verde (Kandler et al. 2011) and previous campaigns (Jaenicke and Schütz 1978, Schütz et al. 2008) is shown in Fig. 1. The measurements in Morocco (MO-2006) showed large variations in the size distribution due to local and regional mineral dust emissions. Mainly local production of dust contributed to the giant particles and significant portions originating from advection contributed to the concentration of the smaller ones. The size distributions at Cape Verde (CV-2008) show only moderately enhanced concentration of larger particles during Saharan dust outbreaks. This is due to long range transport reducing the abundance of particles larger than 25 μm. The size distributions show signatures of anthropogenic influence in the submicron range for particles less than 500 nm in diameter, where little variability of the concentrations can be observed.

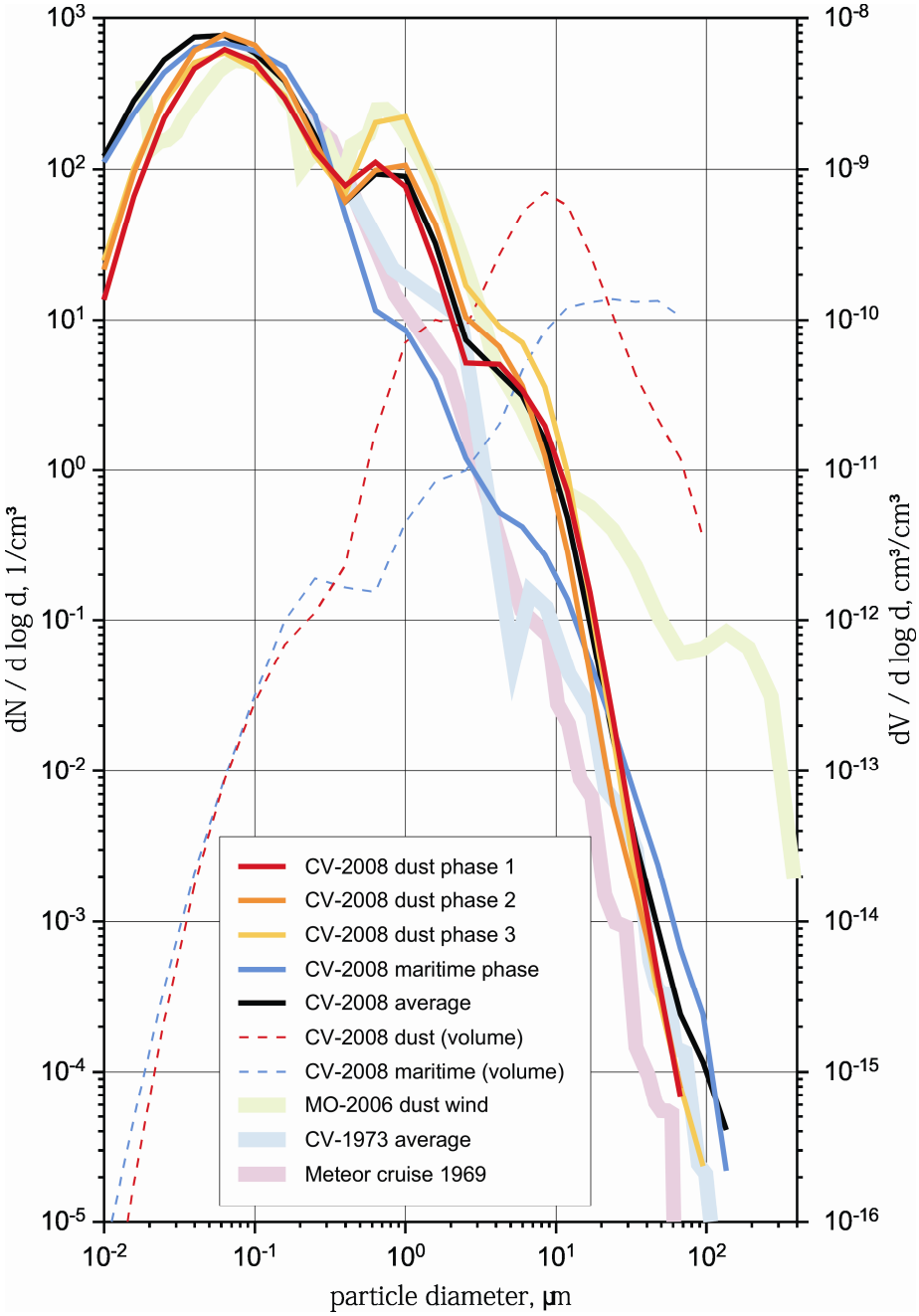

Fig. 1 Boundary layer aerosol size distributions measured at Tinfou, Morocco (MO) 2006, Praia, Cape Verde (CV) 2008 and measurements on board of the research vessel Meteor in 1969 and 1973 in the vicinity of the Cape Verde archipelago and on Sal, Cape Verde. Source: Kandler et al. (2011)

2.1.2.1 Saharan dust transport

Dust is transported within the global atmospheric circulation, and accordingly reflects a large seasonal variability (Moulin et al. 1997). Saharan dust is transported across the Subtropical North Atlantic towards the Caribbean Sea and the Amazon basin. An exemplary illustration of dust transport from Africa over the Atlantic Ocean is given in

Karyampudi et al. (1999). Due to the movement of the inter tropical convergence zone (ITCZ) a winter and a summer pattern can be distinguished.

In summer, dust is transported to the Caribbean Sea, the Gulf of Mexico and even the southern United States, whereby the winter transport of dust follows a more southerly pronounced direction (e.g., Prospero 1999a, Ansmann et al. 2009, Ben-Ami et al. 2009). The winter season is the dry season in south western Africa and therefore the major time for land fires (Govender et al. 2006). These huge annual bush fires in the subtropics region south of the Sahel belt (Crutzen and Andreae 1990) cause huge emissions of biomass burning aerosol (Barbosa et al. 1999), which is then mixed with dust and merging to a complex layer structure (Haywood et al. 2008). Particles are frequently transported southwards with the Harmattan winds causing a persistent smoke load over the Gulf of Guinea and adjacent land (Pelon et al. 2008). To the north of about 10 °N, mid tropospheric southerlies can advect biomass burning aerosol northward gliding up over the relatively cooler and drier desert air (e.g., Knippertz et al. 2011).

2.1.3 Dust sources

Large sources for mineral dust are the major wind erosion regions (Shao et al. 2009). Huge troughs and areas with dry loess sediments combined with strong winds are providing material for uplift. The African, American, Australian, Chinese and Mongolian deserts are large sources for mineral dust in the atmosphere. Dust from East Asia dominates the atmospheric load over China and Mongolia, Korea, Japan, and the North Pacific Ocean (Tanaka and Chiba 2006). But the Saharan Desert is the world's most important source for mineral dust aerosol (Goudie and Middleton 2001).

2.1.3.1 Saharan dust sources

When referring to the *Saharan desert,* dry desert areas spread over the African continent (not necessarily within the geographic boundaries of the Sahara) are meant. There we find sand dunes, salt evaporates and fossil derived sediments, providing a large variety of soil matter. There are prominent source regions for dust production, for example the Bodélé depression in Chad, the Mali-Algerian border, central Libya, Zone of chotts in Tunisia, Foothills of Atlas Mountains, western Sahara and Mauretania and southern Egypt (see Fig. 2 taken from Formenti et al. 2010). The

large Saharan sand seas do not produce mineral dust that can be transported over long distances.

In general, bulk measurements and the analysis of individual particles can be used to characterize and distinguish mineral dust sources (e.g., Kandler et al. 2009, Formenti et al. 2008, Scheuvens et al. 2009).

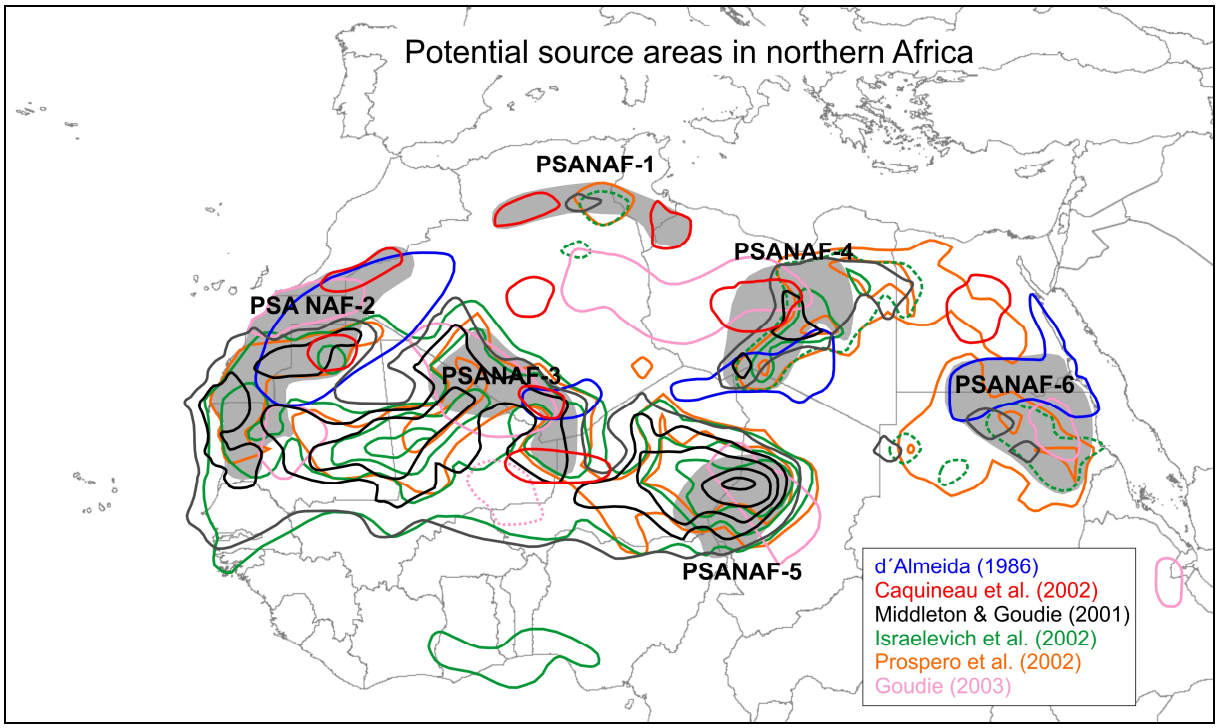

Fig. 2 Map of potential source areas in northern Africa. Source: Formenti et al. (2011)

2.2 Other aerosols

2.2.1 Biomass burning

Biomass burning aerosol is emitted from the huge annual bush fires in the subtropics region south of the Sahel belt (Crutzen and Andreae 1990). It serves to clear land, mainly for agricultural reasons. Biomass burning affects the African continent during the dry season, causing substantial emissions of biomass burning aerosol (e.g., Barbosa et al. 1999) every year. Studies on carbonaceous aerosols have indicated that the intensity of the emissions from tropical biomass burning could compare with that of emissions from fossil fuel burning industrial countries (Cachier et al. 1989). Soot is found to dominate the biomass burning aerosol (e.g., this study). It is generally the major light absorbing aerosol species (Chýlek et al. 1995). Other potassium bearing

particles like condensation salts and vegetation relicts are observed frequently in biomass burning aerosol (e.g., Li et al. 2003, Liu et al. 2000, Gaudichet et al. 1995). As documented below, soot has a very high abundance (up to 95 % relative number abundance in the particles size range below d = 0,5 μm). Moreover, dust and other soil particles are occurring.

2.2.2 Marine aerosol

Marine aerosol arises from sea spray and mainly consists of sodium chloride. Due to the contact of fresh marine aerosol with polluted air masses, the particles might soon experience alteration. Aged sea salt is occurring as sodium sulphate and other sodium-rich particles.

Due to their hygroscopic behaviour, particles might grow fast under humid conditions. The deliquescence relative humidities (DRH) of pure salts are well known (e.g, Tang and Munkelwitz 1993), but due to internal and external mixing might vary on a regional scale. Hygroscopic properties for sub micrometer marine aerosols have been reported for different locations of the world, e.g., the Pacific and Southern Ocean by Berg et al. (1998), eastern Northern Atlantic Ocean by Swietlicki et al. (2000), Southern Atlantic Ocean and Indian Ocean by Massling et al. (2003), for arctic aerosol by Zieger et al. (2010) and for Cape Verde by Schladitz et al. (2011).

When turbulences occur at low altitudes, internal mixtures of mineral dust with sea salt can be observed frequently (Zhang and Iwasaka 2006, Zhang et al. 2006). The influence of humidity on aerosol optical properties, e.g., light scattering, is one of the parameters, which is crucial to estimate direct radiative forcing by aerosol particles.

2.3 State of mixing

Ambient aerosols are often complex mixtures with inorganic and organic components, and their composition can vary substantially with particle size. In addition, for a given size, particles may range from consisting mainly of a single species to aggregates of multiple components. In cases where detailed knowledge is of special interest, a complete and rigorous description of aerosol composition and mixing state may require information on each individual particle.

2.3.1 External mixtures

The aerosol is composed of different species, e.g., sea salt, mineral dust, biomass burning. Aerosol particles may occur externally and internally mixed. If these particles are found separate of each other in a sample (not agglomerated), they are indicated as external mixtures.

2.3.2 Internal mixtures

Agglomerates of particles being associated to different aerosol types (e.g., sea salt, mineral dust, biomass burning) are referred to as internal mixtures. Internal mixing may change the optical properties directly (soot or iron oxide may enhance the light absorption of mineral dust particles) or indirectly through enhancing or reducing the particle solubility (salts may lead to particle growth and thus change the light scattering properties of a particle).

2.4 Climate effects

2.4.1 Direct effects

Direct effects are caused by scattering and absorbing incoming shortwave and long wave radiation. For example plumes of mineral aerosol over dark surfaces are known to have a cooling effect, because in this case the dust increases the planetary albedo. On the other hand, dust may heat the atmosphere over bright surfaces, due to its absorption of radiation at thermal wavelengths. Other types of aerosols may absorb outgoing long wave and/or short wave radiation, due to their mineralogical composition. The net effect (heating or cooling) depends on the surface (land/ocean), and the size and composition of aerosol particles (e.g., Sokolik and Toon 1996, Tegen et al. 1996).

2.4.2 Indirect effects

An indirect aerosol effect tends to cool the global climate by increasing the aerosol concentration and by that leading to smaller cloud droplet size and higher cloud albedo, i.e., brighter clouds (Twomey 1977). The smaller cloud droplet size also inhibits precipitation, leading to an increase in cloud lifetime and coverage (Albrecht

1989). The direct and indirect effects of aerosols are for example summarized in Penner et al. (2001) as part of the third annual report of the IPCC.

2.4.3 Dust radiative forcing

As reported by the Intergovernmental Panel on Climate Change (IPCC) in 2001, positive radiative forcing leads to a global mean surface warming and negative radiative forcing to a global mean surface cooling. Due to their physical (shape, size, morphology, aspect ratio) and chemical (mineralogical composition) properties, particles may contribute to either positive or negative radiative forcing, and feedbacks between dust and climate are possible (for review of this topic see e.g., Arimoto 2001 and references therein). An enhanced absorption of radiation in a layer on a particular level may either stabilize or destabilize the atmospheric layering and thereby provides another independent parameter of air interchange and the formation of a weather pattern. Thus the characteristics of particles and their distribution in the atmosphere are of great interest to estimate the consequences for the global mean surface temperature. The overall dust radiative forcing is complicated through feedback between the energy balance, and the atmospheric dynamics and cloud processes. The energy gain through absorbing radiation in the atmosphere is influencing the stability of the atmosphere and thereby vertical and horizontal wind movement. Wind at the ground is the force of dust emission and uptake, so that by feedback the dust source is influenced. The formation of clouds and precipitation is depending on the aerosol particles, on which the cloud droplets are formed, the cloud condensation nuclei (CCN).

Every material has different abilities (expressed by a refractive index at a certain wavelength) to scatter and absorb solar radiation. Aerosol optical properties depend on size distribution and mineralogical composition. Uncertainties exist in the quantification of the highly variable distribution of the mineral dust components, their optical properties and, therefore, the magnitude and sign of radiative forcing (Solomon 2007). Dust radiative forcing is complicated through mixing of different aerosol types like desert dust and biomass burning. Mixing of aerosol may change the optical properties of aerosol particles (e.g., Haywood et al., 2008).

2.5 Observations of dust

Dust can be observed with in situ measurement techniques or remotely. Detailed observations of the temporal and spatial patterns of the dust load require continuous satellite data. A review of publications regarding continuous observations of aerosols in the climate system from satellites is given by Kaufman et al. (2002). Detailed descriptions of these patterns need continuous model computations considering all relevant processes, including radiation effects of the dust load. The model parameters should be reviewed carefully and be compared with results from in situ measurements regularly.

Remotely sensed dust parameters are for example: Backscatter and extinction coefficient, depolarization, Aerosol optical depth, as well as flux densities. Remote sensing techniques are for example different LIDAR applications (e.g., Tesche et al. 2009, Freudenthaler et al. 2009, Esselborn et al. 2009), and photometer and radiometer measurements, described for instance in Bierwirth et al. (2009) and Toledano et al. (2009).

Dust parameters derived from in situ measurements may be: particle number size distribution, volatile number fraction, hygroscopicity, mass concentration, absorption coefficients, visibility, scattering and backscattering. Detailed description of instrumentation, methods and application data is found in Heintzenberg (2009), Ansmann et al. (2011), and references therein.

Large field campaigns like SAMUM-1 and 2 combine the above mentioned different measurement techniques in so called closure studies.

3 Experimental details

3.1 Sampling equipment

Samples were collected on board of the DLR Falcon aircraft with a set of six two-stage (0.1 – 1 and 1 – 3 μm 50 % cut-off diameter) miniature impactors (e.g., Kandler et al. 2007) and a body impactor mounted in a wing station of the aircraft (Giant Particle Collector, GPaC). The assembly and sampling conditions for the small particles up to d $\sim$ 3 μm, i.e. the miniature impaction system was the same as during the SAMUM-1 campaign (Kandler et al. 2009). For a detailed description of the aerosol inlet and sampling assembly refer to Weinzierl et al. (2009) and references therein.

The aerosol inlet of the DLR Falcon aircraft limits the maximum particle size of collected particles to a diameter of 3 μm (Petzold et al. 2009). In airborne desert dust, much larger particles with diameters up to tens of microns can be expected. No sampling equipment for these large particles is commercially available. The sampling device for large particles described by Levin et al. (2005) cannot be used for the Falcon aircraft. Therefore, it was necessary to develop a new particle sampler to collect large airborne particles. The combination of a two-stage impactor and a giant particle collector allows sampling of particles over a wide size range from below hundred nano meters to some tens of microns.

3.1.1 Giant Particle Collector (GPaC)

The Giant Particle Collector, GPaC was developed by Konrad Kandler for the use under dry condition (no clouds) in the dust laden Saharan air. The first results obtained by the GPaC were gathered by the sampling and analysis as reported in the present work. Therefore a detailed description of this unique instrument is given below and may also be found in Lieke et al. (2011). Preliminary results are first disclosed by Kandler et al. (2010), presented at the International Aerosol Conference Aug. 29th to Sept. 3rd in Helsinki, Finland.

The GPaC is a device for collecting a plurality of samples of airborne particles during a flight. It is provided to be mounted in a wing station of the Dessault Falcon 20-E5 (modified and used as a sampling aircraft by the DLR) and is equipped with a control unit, which controls the retraction and exchange of sample holders. Thereby a

maximum of six samples may be collected one after another during a single flight and at the desired altitudes.

Sample holders, bearing the sample carriers, located at the tip of each bar, can be removed from the bars in order to restore the samples and to change the sampling substrate, as shown in Fig. 3. The substrate diameter is approximately 9 mm.

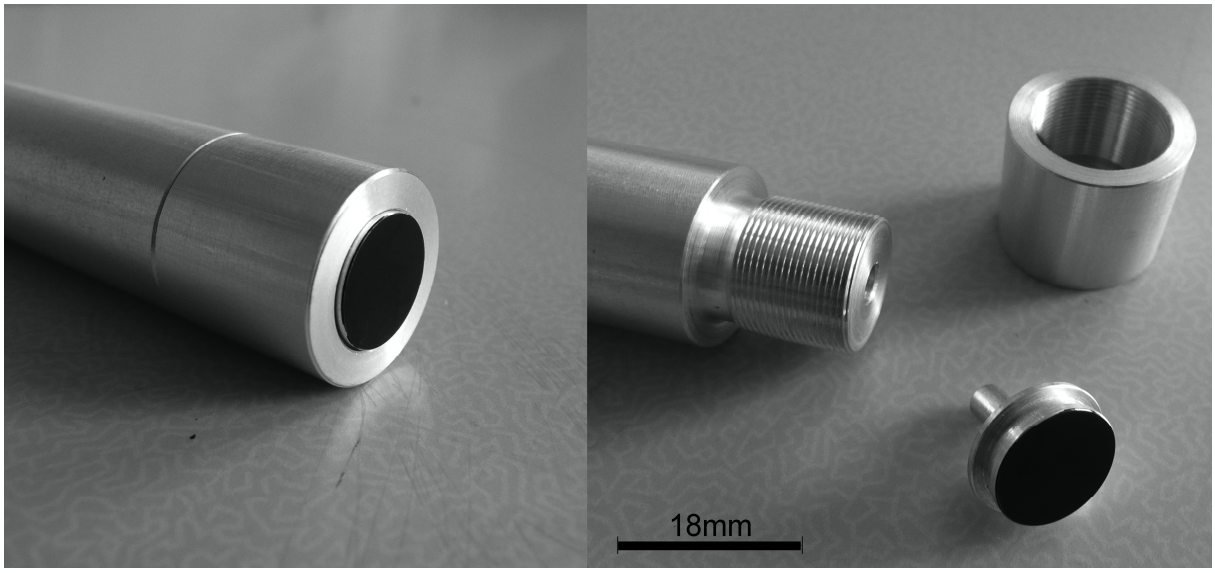

Fig. 3 Giant Particle Collector (GPaC): Sampling bar with tip (left). Demounted tip with sample holder and sample (right), the black area is adhesive carbon substrate

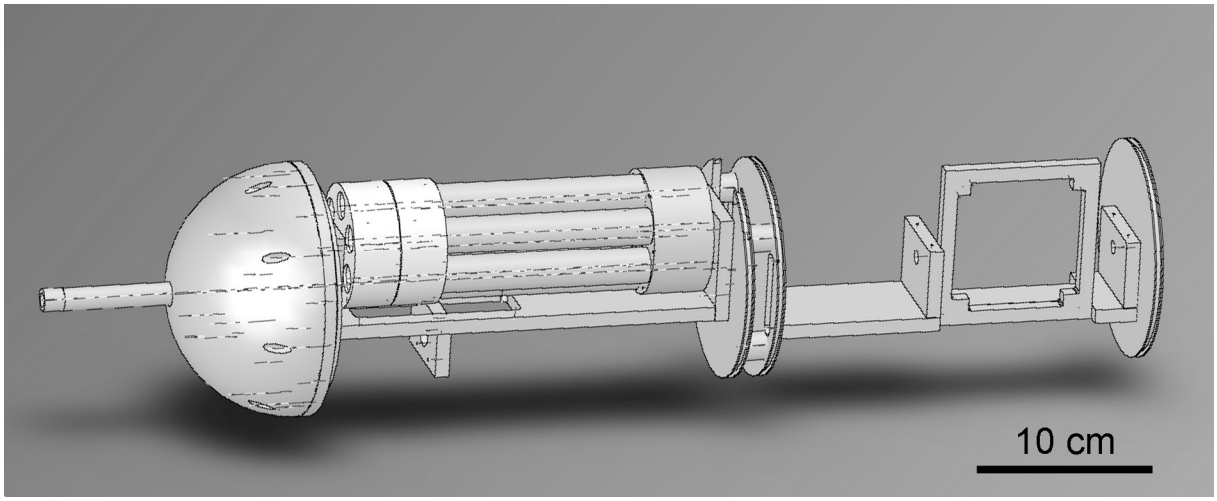

Fig. 4 Giant Particle Collector (GPaC): schematic drawing of the technical component assembly

Due to the interaction of the air flow velocity at the airplane (~ 200 m s^{-1}) and the mass inertia of the airborne particles, particles will collide with (or impact on) the

substrate mounted on top of the bar and will be maintained, as described for body impactors in Willeke (1993). A schematic picture of the GPaC with extended bar is displayed in Fig. 4.

The size of particles is, unlike in jet inertial impactors, not disturbed by a jet or other method of separation, which would lead to a selection of particles due to their aerodynamic diameter.

In principle, all particles are likely to impact on the substrate whereby the airflow due to the speed of the airplane relative to the atmosphere is substituting the acceleration force of a jet. Because of the high flow velocity and due to the lack of separation devices, particles with a low mass inertia are more likely to pass the substrate with the airflow. Any disturbance by the wing or fuselage of the airplane is regarded as insignificant, because the extended bar is projecting ahead of the forward edge of the wing. Therefore, there is no upper limit in size for the deposited particles.

However, the impaction efficiencies for the tip substrate were calculated by extensive computational fluid dynamics (Kandler et al. 2010). The results are shown in Fig. 5.

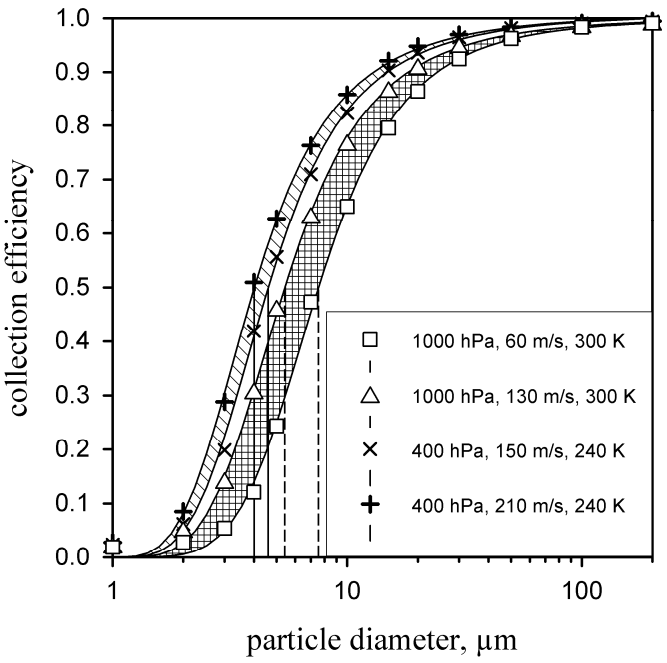

Fig. 5 Impaction efficiency for the tip substrate of the GPaC for different flight conditions. Source: Kandler et al. (2010)

The GPaC was applied for the first time in the vicinity of Cape Verde Islands and the West African coastline. Particles with an average geometric diameter of 0.65 μm to

28.5 μm were found on the substrate and analysed by means of scanning electron microscopy. In Kandler et al. (2010), the number size distribution derived from SEM analysis compared with measurements from optical particle spectrometers as shown in Fig. 6, is discussed.

From the latter figures it can be summarized, that a general form of a typical size distribution is represented, although correction is necessary to derive the values measured by particle counters. However, the GPaC was mainly developed to sample the particles larger than 3 μm geometric diameter. The 50 % cut-off diameter shifts towards smaller particle diameters with increasing speed and decreasing pressure.

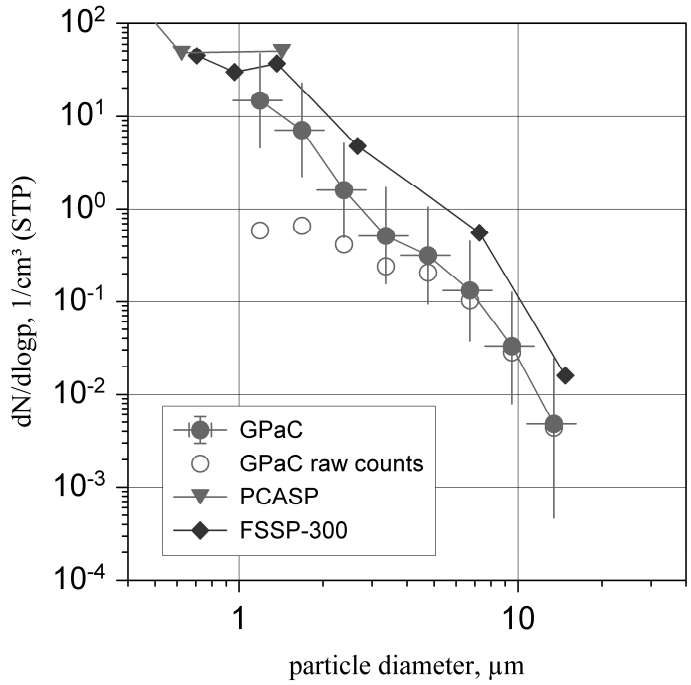

Fig. 6 Number size distributions derived from GPaC by scanning electron microscopy and from optical particle spectrometers (FSSP, PCASP); the open circles show the GPaC data without efficiency correction. Source: Kandler et al. (2010)

3.1.2 Micro inertial impaction system

A set of six micro inertial impactors (MINI) was installed on board of the DLR Falcon aircraft. Each of the six impactors consists of a cascade of two nozzles with aperture diameter of 0.6 mm and 0.25 mm and two substrate holders for different substrates, as explained below (see section sampling substrates). The holders are constructed to let the air pass sideways of the substrate. An inlet guides the air inside the impactor casing, where it is compacted and accelerated at the first nozzle. The air flow passes

the holders, whereby the particles, due to their mass inertia, follow a rather straight flight pass and collide with or impact on the substrate. Lighter particles follow the air flow, which is then accelerated to sonic speed after passing the critical nozzle diameter of 0.25 mm. Those particles impact on the second substrate. For a detailed description and underlying physics please refer to Willeke (1993).

This assembly does not only allow sampling of a wide particle size range, but also provides the advantage, to take six sets of samples during a sampling flight and therefore enables to probe different flight levels. The valves shutting every single impactor were opened and closed by an accompanying DLR scientist. A flight plan was appointed before take off, but could be adjusted to upcoming conditions. The assembly and sampling conditions for the small particles (up to d $\sim$ 3 μm) were the same as during the SAMUM-1 campaign (Kandler et al. 2009). For a detailed description of the aerosol inlet and sampling assembly refer to Weinzierl et al. (2009), and references therein.

3.1.3 Sampling substrates

For the giant, super micron and micron particles (e.g., GPaC and MINI first stage), adhesive carbon foil ("Leittabs", Plano, Wetzlar, Germany) adhered to nickel discs (MINI first stage) and Copper stubs (GPaC) were used. The carbon foil ("Leittabs", Plano, Wetzlar, Germany) was punched out to achieve the suitable size for the used sampling equipment (diameters of $\sim$ 3 mm in case of Mini first stage and $\sim$ 9 mm in case of GPaC).

Due to it's thickness of approx. 0.25 mm, the carbon substrate is suitable only for use in a scanning electron microscope. Filaments of copper are woven into the matrix of carbon, to increase the conductivity. Particles can be imaged and distinguished from the substrate by their chemical contrast, if they contain elements of a higher atomic number than 6 (C). Larger particles can also be detected by their morphology, leading to a stronger (topographic) contrast compared to the substrate. In the automated analysis, only the grey level of backscattered electron images (chemical contrast) was used for particle identification. Therefore, carbonaceous particles and soot in particular are not detected. As those particle groups occur barely in the large particles size ranges, the risk to underestimate the number abundance of those can be neglected.

For the small and submicron particles (MINI second stage), standard carbon coated nickel TEM-grids with formvar foil (polyvinyl formal) S162N9 (Plano, Wetzlar, Germany) were used. The film thickness is 30 to 55 nm (Noli 2010).

Those substrates allow both, scanning and transmission electron microscopy. The very smooth surface grants high topographical contrast even of very small (tens of nms) particles. This advantage was applied for the automated particle analysis in SEM, when only the grey level of secondary electron images was used for particle identification. In TEM, the thickness of the foil allowed the application of electron diffraction and even high resolution (195 000x to 300 000x) imaging, when the particle size and properties allowed the electrons of the incident beam to pass through the sample. For both sampling substrates no preparation prior to analysis was necessary.

All samples were stored and transported under dry conditions (~30 % rH, obtained by silica gel) to avoid modification due to high humidity.

3.2 Analysis

3.2.1 Scanning Electron Microscopy (SEM)

The method of choice was scanning electron microscopy (SEM).

For this study, an environmental scanning electron microscope “ESEM Quanta 200 FEG” of FEI, Eindhoven, the Netherlands with a field emission gun and equipped with an EDAX energy dispersive X-ray microanalysis system was used. The microscope is supported by a software for different single particle analysis applications, which is described further down. This method provides a high spatial resolution. Single particles can be spotted and analyzed with a chemical elemental analysis by the attached EDX system.

For the analysis described in the present work, an Everhart-Thornley-Detector was used for SE images up to a magnification of 20 000x for the small particles on TEM-grids. BSE imaging was used up to a magnification of 4 000x. An annular solid state detector was used which provides a high BSE detection efficiency.

The FEI ESEM Quanta 200 FEG is equipped with an EDAX Phoenix silicium-Lithium detector with an ultra thin beryllium window. According to EDAX Genesis (2006), the spectral resolution is 129 eV at 5.9 keV (Mn K_α line). In principle elements with an

atomic number $Z \geq 5$ (boron) can be detected. For detailed description of method and underlying physics, please see (Reimer 1997, Reed 2005, Goldstein 2007) and others.
In an Environmental Scanning Electron Microscope (ESEM), samples do not have to be analysed under high vacuum conditions, but may be brought under water vapour atmosphere at low pressures (up to app. 40 mbar). This method was developed by Danilatos (1988).
For the present work, samples where pictured before analysis in low vacuum mode (1.1 mbar) and high vacuum mode ($x10^{-6}$ mbar). No obvious change in the appearance and number of particles has been observed and therefore the analysis was conducted in high vacuum mode at 20 kV and spot size 4. Spot size in the used instrument has assigned numbers that range from 1 to 7 with values corresponding to beam current, equivalent diameters are not given by FEI and therefore can not be given here. A working distance of 10 mm (+/- 0.4 mm) was followed in every analysis.
Approximately 70 000 particles where analysed by automated single particle analysis, which is described further down.

3.2.2 Transmission Electron Microscopy (TEM)

Transmission electron microscopy (TEM) was performed with a Philips CM 20 (FEI, Eindhoven, The Netherlands) operated at 200 kV accelerating voltage and a LaB_6 gun. TEM images were recorded with a high resolution CCD camera (KeenView G2, Olympus Soft Imaging Solutions GmbH, Münster, Germany) mounted at the bottom of the transmission electron microscope.
For detailed descriptions of method and underlying physics, please see for example Williams and Carter (1996).

For the present work, TEM was applied only on selected particles, in order to investigate their complex nature and inner structure. However, many air borne particles in the submicron are difficult to investigate with TEM, when samples are not prepared (for example thinned or coated with carbon or gold). Some particles show low beam stability and start to evaporate under electron bombardment. Others are too thick to let the electrons pass. Most mixture particles are multi phase agglomerates. Even though single components or parts of the particle are transparent in one

direction, it is not easy to find another orientation of the same crystal, due to the particles morphology and position on the TEM-grid. TEM high resolution images revealed that most particles are composed of many small mineral crystallites and therefore the electron diffraction pattern might show various reflexions of one particle, originating from either differently orientated grains or different minerals. But at least, TEM helped to confirm the graphitic structure of soot particles, the existence and phase of ammonium sulphate and helped to investigate ammonium sulphate residuals. Also TEM helped to understand the complex nature and composition of silicate-mixture particles and was used to determine the distribution of iron oxide in and on mineral dust particles.

3.2.3 Automated particle analysis in SEM

Automated single particle analysis with EDX is a common tool for the investigation of aerosol chemical composition (e.g., Weinbruch et al. 1997, Ro et al. 2002, Laskin et al. 2003). For this study the SEM-supporting software Genesis Particle Analysis Version 5.10 (EDAX, Mahwah, NJ, USA) was applied.

To prepare the automated analysis, a frame near the centre of the deposition spot on the samples was chosen as the centre of a so called snake matrix (virtual grid) of adjacent fields (starting in the center and circling out), which covers the deposition spot from the centre to the outer edges, in order to prevent over- or underrating of any particles due to separation processes, which might have occurred during sampling. The position coordinates of the stage in the chamber of the microscope are copied to the Genesis software and used as initial point for the stub matrix. An image (as described above) is collected automatically. The software uses the grey level contrasts of secondary electron or backscattered electron images for particle identification, which either due to their morphological or chemical contrast are distinguished well from the underlying substrate. The particle selection may be adjusted by a size threshold with upper and lower limit of some tens of nanometers to some tens of micrometers. The position of the stage relative to the electron beam is actuated by the software, according to the coordinates of detected particles. The chemical composition of the particles (all elements with $Z \geq 6$) was determined by energy-dispersive X-ray microanalysis with a silicium (Li) detector. X-ray count rates were corrected for matrix effects using the so-called ‘standard less’ procedures

provided by the Genesis software. Coordinates, size, shape and a count rate for each element of the spectrum are recorded. The count rate is given in ZAF-corrected atomic weight percent. For each analysed field, one image respectively is saved to an output file, so that for post processing purposes each particle can be visualized together with its individual spectrum and size and morphology information after analysis. The advantages of this method are obvious: the automated analysis, which can be driven without manual control, can run day and night and therefore allows a high number throughput in short time. Secondly, every analysis is based on the same conditions. The influence of a user, and thereby a source for errors is neglected. And finally, all analysis data is maintained for further processing.

3.3 Particle classification method

It was part of the present work to improve the classification method, based on the group particle classification software “groupp”, developed by Konrad Kandler as previously described in Lieke (2008), which was applied and modified for the present study on mineral dust from different source regions. In scope of this work, the version “groupp_2” of the configuration file was developed and applied to classify the particles collected during the SAMUM-2 field campaign, published in Lieke et al. (2011), Kandler et al. (2011b) and Scheuvens et al. (2011). This version worked well for samples of transported Asian dust from Amakusa, Japan and even for samples of the Icelandic Eyjafjalla volcano eruption in April 2010, collected in and over Germany and northern Europe. The applied version was successfully enhanced with the expertise of Dirk Scheuvens in order to distinguish minerals and groups within the silicate class and to classify different mixture particles. However, the complexity of the collected silicates can still not be completely covered by the classification scheme, but may be used as a tool investigate the composition and mixing state of different aerosols. It may be modified and adjusted to different applications by changing the corresponding entries in the configuration file. First, particle groups were defined from the particles found on the samples (as described further down). The classification into groups is based on fitting parameters of elemental ratios. The fitting parameters are listed in the configuration file and assorted, so that an order of priority is derived. For some groups, a particle size limit and a recessed priority argument

were added. Groupp converts ZAF-corrected elemental weight percent (from X-ray count rates) into atom percent and calculates element indices (see below) for the elements of interest. The classification criteria of the current groupp file are listed in appendix A and are recently published in Kandler et al. (2011b). The group list is then extended with a class entry, which summarizes the 42 groups into 12 classes. For displaying and discussion of results, only classes were used.

For smaller particles, the signal to noise ratio is low during automated analysis, so especially the discrimination of soot, sulphate, and quartz is not reliable. Thus, the classification of these particles was performed manually for selected samples, taking into account the X-ray spectrum, morphological features and the characteristic alteration under electron bombardment. The resulting number abundance ratios for soot, sulphate and quartz from the manual classification was then scaled to the number of particles not clearly identified by their chemical composition automatically (i.e., all particles except halogenides, non-quartz silicates, silicate sulphate mixtures, carbonates and iron oxides, refer to appendix A. In order to detect soot particles on carbon coated substrate (Nickel grids coated with polyvinyl formal and carbon, Plano, Wetzlar, Germany), a manual post processing on the small stage samples was necessary. Soot and other very fine mode particles (d $\sim$ 30 to 500 nm) were characterized based on their characteristic morphological appearance.

3.4 Element indices and ratios of elements

The chemical composition of the particles is expressed as element index as described in Kandler et al. (2011b). This index is defined as the atomic ratio of the concentration of the element considered and the sum of the concentrations of the elements Na, Mg, Al, Si, P, S, Cl, K, Ca, Ti, Cr, Mn, and Fe. Element indices and ratios between different element indices are used to describe the complex composition of the particles.

3.5 Particle mixing state

The ratios Al/Si, ((Mg+Fe)/Si) and ((K+Ca+Na)/Si) were used to describe the complex composition of mineral dust. Silicate mixture particles as well as soot and

soot mixtures were investigated by TEM images analysis manually. The applied process for internal soot-sulphate-mixtures is described below and in Kandler et al. (2011b).

For particles smaller than 500 nm diameter, the automatically measured chemical information exhibits a too high uncertainty to apply the chemical ternary mixing. In addition, soot plays an important role in this size range, which is not included in the chemical mixing model. Thus, a manual investigation of mixing state was performed by TEM analysis. Selected particle ensembles were recorded while they were extensively irradiated by the electron beam to remove volatile material. The residues were imaged and investigated with high resolution imaging and EDX. A change in particle volume is obvious, but the projected area diameter did not reduce detectably.

3.6 Determination of refractive index

To determine the complex refractive index of the individual particles, the measured chemical composition has to be simplified because (i) the mineralogical phase could not be determined for each particle in this work and (ii) the spectral optical base properties for the identifiable components are not available in any case. The method for deriving the refractive index from a model composition was applied and described previously in Kandler et al. (2011b) and references here in.

3.7 Sampling location and period

The SAMUM-2a field campaign was conducted from January 14th to February 11th 2008. The station for ground based measurements and meteorological observations, was build up near the airport of Praia, the capital of Cape Verde on Santiago Island laying at 14° 56’ 50.89” N and 23° 29’ 4.31” W, approximately 100 m a.s.l.. The Falcon sampling aircraft and equipment were stationed in a hangar and the facilities of TACV, Cabo Verde Airlines.

The Falcon arrived from the transfer flight on January 22nd. First measurements were performed on this flight with the micro inertial impaction system. The first flight with the GPaC and Minis running in parallel was performed on January 23rd. The last sampling flight was conducted on February 6th.

Apart from that, particles of soil samples collected at Burkina Faso (with courtesy of Marlen Vragel, Karlsruhe Institute of Technology) were analysed and compared to samples of the present work.

3.7.1 Flights

Flights were conducted by the DLR to the south, north and east of the Cape Verde. Each of the sampling flights had a different aim, for example conducting a column closure study over Cape Verde Islands (Ansmann et al. 2011), studying urban influenced dust episodes (Petzold et al. 2011) or investigating biomass burning aerosol (this study).

When planning the flight route, information about the dust load and weather forecast based on satellite data (ECMWF, Meteosat) were taken into account. Data was kindly provided by the DLR-Institute for Atmospheric Physics in Oberpfaffenhofen, Germany and the Barcelona Super Computing Center in Spain.

For a detailed list of flight legs, sampling time and location including the chemical composition and number of analysed particles please refer to appendix B.

3.7.2 Back trajectories

For the calculation of 5-day and 10-day back trajectories, the HYSPLIT (HYbrid Single-Particle Lagrangian Integrated Trajectory) Model was used, access via NOAA ARL READY Website of NOAA Air Resources Laboratory, Silver Spring, MD.

3.8 Meteorological situation

A meteorological overview for Cape Verde region based on ground based observation during the measurement period is given by Knippertz et al. (2011), a short summary of which is given as follows. The meteorological observation period ranges from January 15th to February 15th. During that time, stable atmospheric conditions were prevailing. The wind direction at the sampling station was in the sector of 330° to 40° and the average wind speed was approximately 5.5 m s^{-1}. The observed time period can be subdivided into four dust periods with marine phases before and after. The difference between the dust periods and the marine phases is mainly seen in the mass concentration (only available until Feb. 11th) and LIDAR observations, and in the

significant difference of wind speed. During dust phases, the wind speed was around 4.6±1.5 m s^{-1}, while during the marine periods the wind speed was 7.1±1.4 m s^{-1} in average. The dust phases themselves did not show such differences, compared with each other.

During the dust phases, a stronger diurnal pattern in water vapour mixing ratio and wind direction oscillation is present than during the marine periods (Kandler et al. 2011). This behaviour shows the influence of the dust burden on the local circulation around the island of Santiago. According to Knippertz et al. (2011) this indicates that during daytime in dust situations, where there is a decrease in water vapour mixing ratio, dust laden air is mixed into the marine boundary layer, which does not happen during marine phases.

The dust phases described by Knippertz et al. (2011) are listed below.

- Dust phase 1, 17th to 20th January 2008. A high pressure system moves from the subtropical Atlantic across the Iberian Peninsula into the western Mediterranean Sea. Thereby a tight north-south pressure gradient over the western part of West Africa finally leads to high dust production in Mauretania and neighbouring countries. Air masses arriving Praia in the high pressure altitudes, are clearly linked to this dust emission, while air reaching Praia in the low pressure altitudes (850 – 481 hPa) originates from a widespread area from south western West Africa and the Gulf of Guinea and most trajectories followed an anti cyclonic curve around the archipelago, reaching the Cape Verde from the east. Those air masses may have transported aged biomass burning aerosol. The travel time for the dust from Mauretania was much shorter, and took two to three day from their source to the Cape Verde. At high altitudes, an east flowing clean air mass layer is following the subtropical jet stream.
- Dust phase 2, 24th to 26th January 2008. The high pressure system, that dominated Phase 1 split into two centers causing a strong south-north pressure gradient over the Sahel and southern Sahara. This leads to dust emissions in a wide spread area, covering Mauretania, Mali, Niger, and the Bodélé depression in Chad. This development proceeds on the next day, with a slightly less

southerly pronounced extension. Calculation of travel time and trajectory analysis yield a dust source located further to the southeast than during dust phase 1, mainly in Mali but also in western Niger, with typical transport times of two to five days. The uppermost layer trajectories for Cape Verde show a weak cyclonic curvature in the over all westerly flow. The mid level trajectories show at least a weak contribution of continental air masses, resulting in a shallow smoke dominated layer.

- Dust phase 3, 28th January to 2nd February. A persistent and intense high over France extends far into northern Africa, whereby it south-north pressure gradients cause widespread dust emissions from the Bodélé Depression to the coast of Mauretania. Dust uplift is strongest on 26th and 27th January, but further emissions occur on 28th and 29th January. For Praia this means that the situation is similar as at 25th for the high pressure altitudes from the surface to 801 hPa. On 29th and 30th January, the highest surface mass concentrations are reported over Praia. The mid air level stream is shallower than during other periods and contains less smoke than air masses from the southern parts of the tropical West Africa, leading to a less pronounced smoke layer on January 30th. It is mentioned by (Knippertz et al. 2011) that the westerly flow at upper levels causes rather clean conditions aloft.
- For the rest of the field campaign, the surface mass concentrations at Praia were rather low, caused by the diminishing of the subtropical high. At least, a shallow dust layer prevails until 6th February above 500 m. A subsequent mixing with biomass burning layers above 1 km was observed. At lower heights, trajectories show no contact to dust layers. The “rather clean” layer was observed between 0.5 and 1.5 km.

The fourth period (Feb. 6th to 15th) is not regarded, as sampling was only performed until Feb. 6th.

4 Results

From all samples collected throughout the field campaign, it is obvious at first sight that there is a very distinct layer structure of different aerosol types. Above the Atlantic and in the Cape Verde region, highly stabile conditions for the low pressure altitudes were found. A very similar structure prevailed for most flights: the sequence of layers changed due to the meteorological situation, but remained a clearly detectable layer structure, indicated for example by the presence of different amounts of soot among the small particles.

In total, 40 flight levels from 8 different days (103 samples) were investigated (a detailed description of the flights follows in chapter 4.3). The summarized results for biomass burning, desert dust and marine boundary layer aerosols are described below. There are pronounced differences between the dust and the biomass burning samples, which can be clearly identified by the particle chemical composition. The chemical composition is expressed as relative number abundance of the different particle groups. These particle groups are described in the following section.

4.1 Particle classes

In the following section, particle classes are described including the appending particle groups. Captions are listed and named after particle classes.

The particle classification into chemical classes was performed automatically for particles larger than approximately 0.5 μm. For smaller particles, the signal to noise ratio is low during automated analysis, so the classification of these particles was performed manually, taking into account the X-ray spectrum, morphological features and the characteristic alteration under electron bombardment. The classification criteria for all particle groups (as published in Kandler et al. 2011b) are listed in appendix A.

Silicates. The over all dominating class in the collected samples is of course the silicates class. Feldspars and clay minerals are the most abundant phases. It was therefore tried to separate silicates by their chemical composition, considering trace elements and atomic ratios in order to determine mineralogical finger prints.

The composition of the most abundant silicates in soils was derived from literature (e.g., Anthony et al. 1990, Jasmund 1993).

The particles of the SiAl (Fe) group are characterized by elevated silicium and aluminium contents, whereas iron may occur as an additional component to a small extent. This group is the dominant particle group in many samples and reaches particle number concentrations of 15 to 20 % in the collected samples. As silicium concentrations always exceed aluminium concentrations, the presence of the Al_2SiO_5 (Andalusit, Silimanit, Disthen) can be neglected. The SiAl (Fe) group is interpreted to consist mainly of clay minerals (kaolinite, smectite). As many particles of this group exhibit Si/Al ratios above 2, it seems reasonable to assume significant internal mixing between the above-mentioned clay minerals and a Si-rich phase (quartz) in many particles. A fraction of particles of this group contains iron. One probable explanation for this observation is the admixing of iron oxide nano crystallites, as described further down. Mixing between kaolinite and to a minor extends smectite and Fe-rich chlorites may also occur. These aggregates consist of numerous small grains, causing a higher surface roughness of the particle as described in Scheuvens et al. (2011). Kaolinite particles were determined additionally in TEM images. They often occur as flat small hexagonal flakes with low topographic contrast and therefore their abundance might be slightly underestimated in the automated analysis in the size range between 0.2 μm and 0.5 μm.

The particles of the SiAlK (Fe) group can be subdivided into a subgroup with high potassium contents and a subgroup with relatively low potassium contents. Almost all particles of the high-potassium subgroup exhibit Si:Al:K ratios of 3:1:1 which are indicative for K-feldspar. The particles of the subgroup with low potassium content are interpreted to consist mainly of illite and/or muscovite, but it is to be noted that especially the boundary to the SiAl group is fuzzy. Scheuvens et al. (2011) report that SiAlK particles with elevated iron contents are almost exclusively members of the illite-muscovite subgroup, indicating that iron oxides and iron hydroxides are preferentially associated with illite-muscovite particles and not with K-feldspar.

The mineralogical interpretation of the SiAlNa group is albitic plagioclase. According to Scheuvens et al. (2011), at least in mineral dust during SAMUM-1 most particles reveal Si:Al:Na ratio of 3:1:1. Due to the low number abundance of this group, this result can not be reproduced for the SAMUM-2 samples.

Particles of the SiAlNaCa group, which can be interpreted as Ca-bearing plagioclase (e.g., oligoclase) or as internal mixtures of albite ($NaAlSi_3O_8$) and calcium carbonates are even more seldom.

SiAlNaK is representing the series of alkali feldspars $NaAlSi_3O_8$ to $KAl_2Si_2O_8$ and Nephelin ($(K,Na)AlSiO_4$), a feldspathoid.

The SiAlCaFeMg and SiAlKFeMg groups represent silicate mixed groups characterized by elevated aluminium, iron and magnesium contents, whereas additional calcium or potassium is only present in some particles. The particle number concentrations of these groups are more variable than other groups, probably due to the heterogeneity of particles incorporated within this group. Possible minerals are for example members of the biotite group, the chlorite group, the amphibole group, or the smectite group. Most particles are likely internal mixtures of different minerals. According to Scheuvens et al. (2011) particles with high magnesium contents and relatively high Si:Al ratios (> 3) are probably internal mixtures of palygorskite/sepiolite, clay minerals and iron oxides. The major portion of particles with elevated magnesium and silicium contents can be interpreted as representing minerals of the palygorskite/sepiolite group, which is depicted to often occur among with calcite (e.g., Schütz and Sebert 1987). However, the particle number concentration of this group is generally around 3 to 5 % in the investigated samples, whereas the relative number abundance of calcite is varying. Many SiMg particles contain an additional aluminium component which can best be explained as mixtures of palygorskite/sepiolite with other clay minerals.

The SiCaTi is representing Titanite ($CaTi[O|SiO_4]$), which is barely found on the investigated samples.

The most dominant group with abundances of ~ 50 % within the silicate class are other silicates (Fig. 7). This group is a mixture of silicates (as the above mentioned), and to lesser extent of other components such as calcite and iron oxide. The classification is based the presence of silicium and aluminium and the absence of sulphur. Those particles are occurring in all size regimes. It should be emphasized here, that the mixture are very complex multi phase aggregates, as they miss the criteria for the above mentioned silicate groups, which already include some forms of mixtures. It must thus be concluded, that about two thirds of the silicate class particles are present as mixtures!

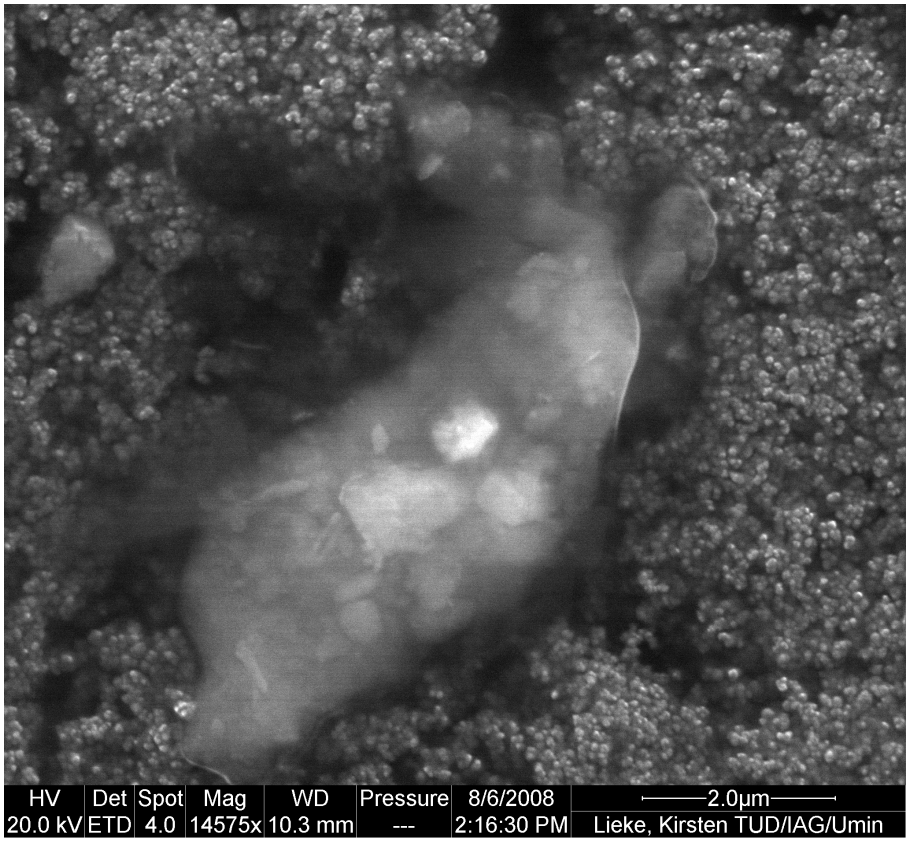

Fig. 7 Secondary electron image of an internally mixed silicate particle (other silicates)

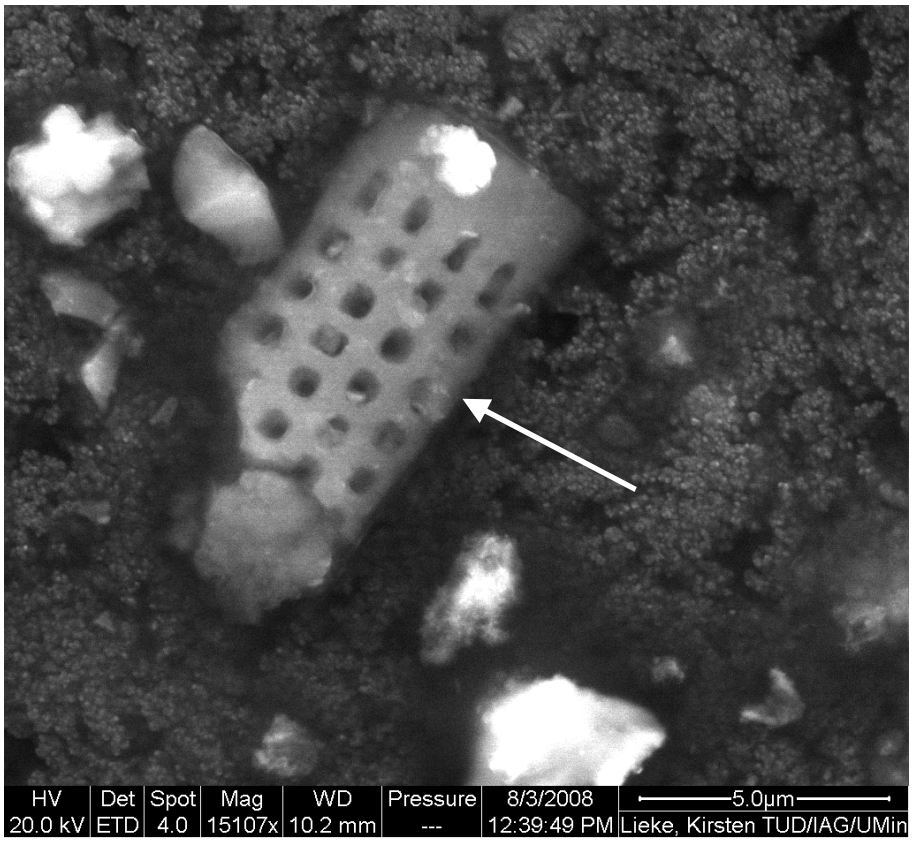

Fig. 8 Secondary electron image of a diatomae fragment (arrow)

Quartz. SiO_2 is one of the main components in Saharan dust. Kandler et al. (2009) described quartz to be the most abundant phase among the super micron range in samples from dust storm events in Morocco: Due to its high mechanical stability, the most quartz grains are ≥ 50 μm. As the aerosol in the Cape Verde region is necessarily long range transported aerosol, the larger particles and thus most likely the quartz grains are present at lower abundances in our samples. Quartz contributes at almost constant amounts of $\sim$ 10 % to the mineral dust. Below 0.5 μm, quartz grains were hardly found. Due to their chemical composition Diatomite fragments are classified into the quartz class, however, only minor amounts could be determined by their characteristic morphology (Fig. 8).

Soot particles are occurring as soot agglomerates and are the most abundant particles in biomass burning samples. Their sources are wide spread bush fires occurring seasonally in the Sahel. Traffic or industry may be a minor source for soot. The soot primary particles show an onion shell structure with disordered graphitic layers (Fig. 9), as previously observed in many studies (e.g., Li et al. 2003, Wentzel et al. 2003). Soot from biomass burning aerosols is often described to be enriched in potassium, chlorine, and sulphur (Artaxo et al. 1998, Gaudichet et al. 1995). In fact, approximately one third of the soot particles contain significant amounts of potassium. X-ray mappings on soot agglomerates did not reveal any inclusions. Instead, potassium seems to be distributed homogenously over the entire particle. It is suspected that potassium is present as nitrate, because a sulphur peak (indicating the alternative presence of potassium sulphates) was not observed. In addition, some particles appeared to be swollen and displayed slight deformation on the surface under electron bombardment, without changing their chemical composition. This observation may indicate the presence of thin coatings of secondary components (nitrates, sulphates, and organics). Internal mixtures with ammonium sulphate were frequently observed and classified as such.

Graphitic soot is a strongly light absorbing component in the atmosphere (e.g., Rosen et al. 1978). Mixing with ammonium sulphate may reduce the absorption and change the hygroscopic behaviour of particles. Condensation of water vapour onto particles below super saturation strongly influences their scattering properties (Hänel 1976) by changing the particle size and refractive index (Covert et al. 1972).

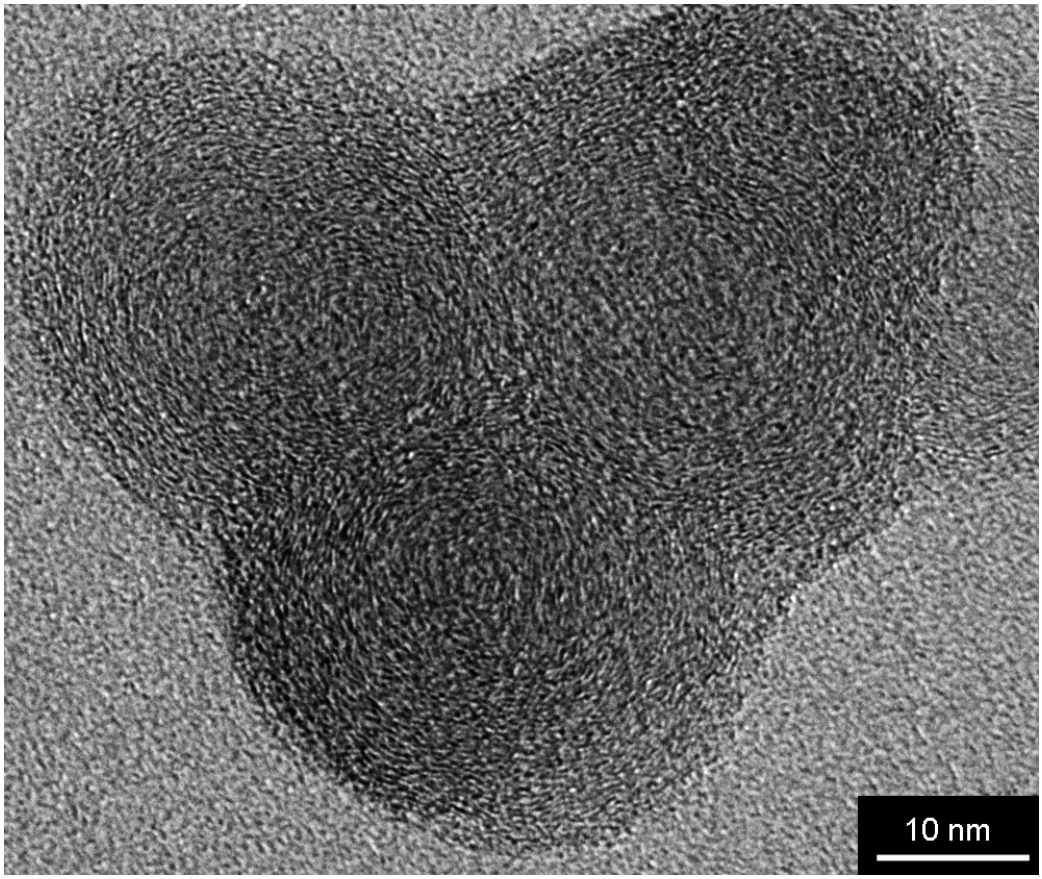

Fig. 9 High resolution TEM image of a soot agglomerate, consisting of three primary particles

Secondary Aerosol. Ammonium sulphate, $(NH_4)_2SO_4$, is present in high abundances in the atmosphere. In the electron microscope, particles appear as sulphur rich droplets with a low stability under the electron beam. Their average diameters on the samples range from tens of nanometers to micrometers, but can be strongly affected by hygroscopic growth or consistent drying due to high vacuum conditions in electron microscope. Ammonium sulphate particles are found to be internally mixed with soot in some cases. Therefore another group was implemented for internal soot-sulphate mixtures. However, the relative number abundances of this group did not exceed 15 %. In the small particles size range, ammonium sulphate is the predominant hygroscopic component, but internal mixture with one or more hydrophobic substances may result in a reduced hygroscopic growth factor (Schladitz et al. 2011). An example of secondary ammonium sulphate particles of different sizes and internal mixtures with sea salt (NaCl) is shown in Fig. 10.

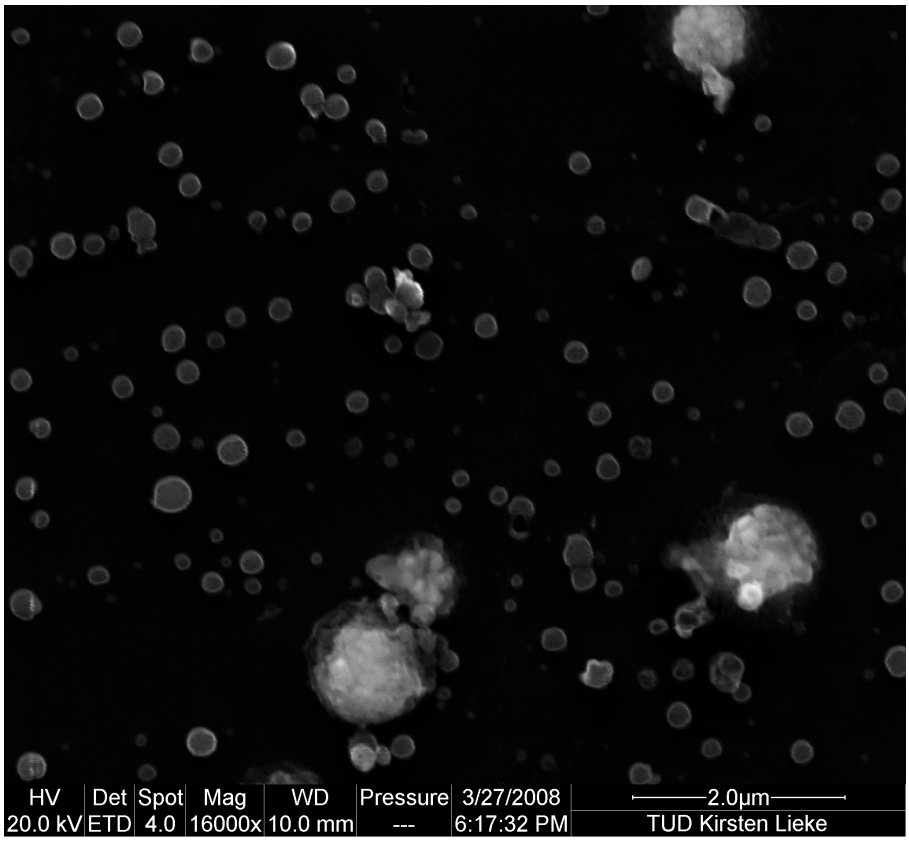

Fig. 10 Secondary electron image of ammonium sulphate particles (small spheres) on carbon foil and internal mixtures of ammonium sulphate with sea salt (large particles)

The group of sodium rich particles is probably composed of sodium nitrate or sodium carbonates, which may occur naturally. However, they are categorized as secondary particles, because they must likely originate from reaction of sodium chloride and/or sodium sulphate with other components in the atmosphere. They may occur with sizes up to some micrometers and are likely to mix with other particles.

Sulphates. Particles, which are classified as sodium sulphate, calcium sulphate or mixtures of calcium and sodium sulphate are found frequently. In addition, other sulphates are detected, which are particles dominated by sulphate but can not be classified as sodium sulphate, calcium sulphate or mixtures of calcium and sodium (for example potassium sulphates or sulphate particles containing calcium and sodium plus potassium and/or other elements). Those particles are summarized in the group of other sulphates.

Sodium sulphates are the most abundant group among the sulphate class. These particles can be associated with marine influence (e.g., aged sea salt) and/or the

presence of anthropogenic SO_2 and H_2SO_4 in the atmosphere. The particle aspect ratio is around 1 for most particles, their shape is mostly rather spherical than sharp edged. Those particles may occur at any size range and are slightly more abundant in samples originating from aged marine and biomass burning aerosols.

Calcium sulphates are particles are likely from a continental source. They may originate from gypsum deposits from dried lakes, which are a typical soil component. It is not known whether the observed particles are gypsum or anhydrite. However, the characteristic composition and ratio of calcium and sulphur allows their classification. The particle size is typically in the micron range, the morphology of particles may be fibrous to bulky, sometimes agglomerates of flat elongated plates (Fig. 11).

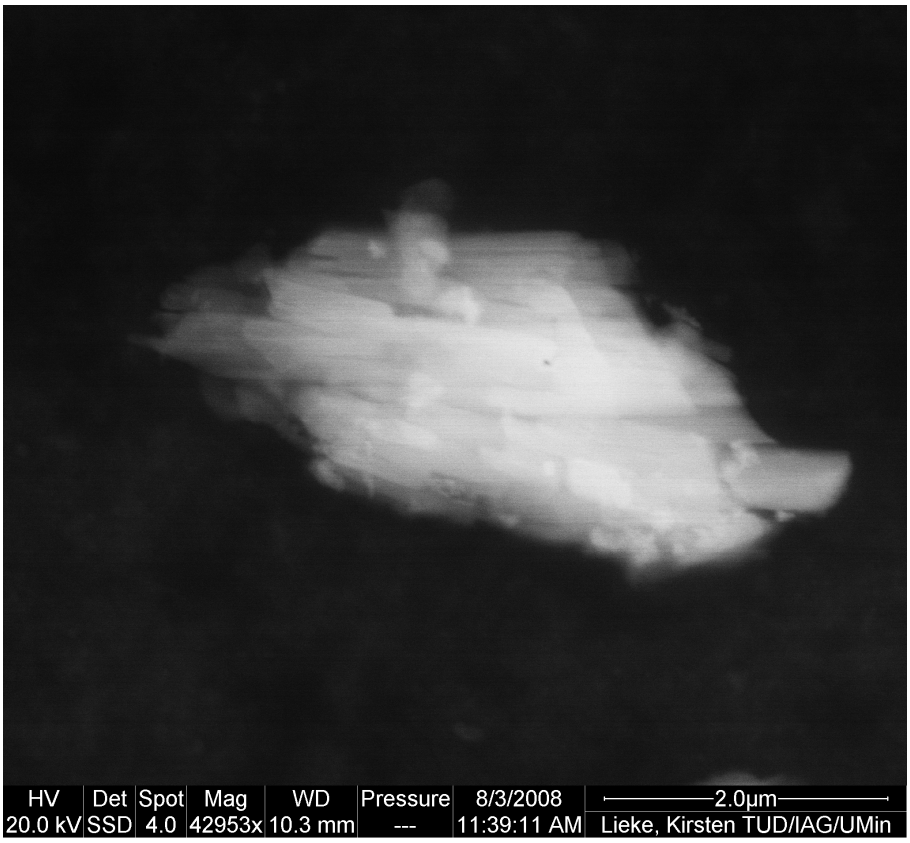

Fig. 11 Backscattered electron image of a calcium sulphate particle

The group of calcium sodium sulphates are not a typical soil component, but are found frequently in the present samples and therefore form an own group. They may be incomplete conversion products of sea salt and calcium sulphate. Their shape is highly varying and they mainly occur in the submicron and micron size range.

Most particles classified as **Carbonates** are calcium carbonate (calcite). The size of the detected particles is in the micron range. High calcium contents are observed in soils from northern and central Algeria, Morocco, Western Sahara, Northern Egypt and Libya (Desboeufs and Cautenet 2005, Schütz and Sebert 1987). Calcium carbonates occurred in the micron size range and are only found on but a few samples. More often Calcite appeared admixed to silicate particles. A pronounced north-south variation of the calcite abundance in the aerosol as found in north West Africa (Kandler et al. 2007, Formenti et al. 2008) could not be observed. Other carbonates are dolomites, which were scarce in our samples, however.

Chlorides. The most abundant particle group within the chloride class is sodium chloride. The most prominent source is the ocean, where fresh sea salt is occurring as NaCl. Even though sodium chloride could also originate from continental sources, it is more likely that the observed sodium chloride particles are sea salt, due the vicinity to the sea and based on trajectory analysis. The particles showed sometime a cubic habitus and usually were of μm size.
In contrast, potassium chloride (KCl) which is also quite often found in the investigated samples, is occurring in the small particle size range (below 0,5 μm) and could be associated to biomass burning. Gaudichet et al. (1995) explain the presence of KCl as a result of salt condensates rapidly forming from elements present in the vegetation matrix during the burning process.

The **Oxides** class covers metal oxides (not SiO_2), the most abundant of which is iron oxide. Iron oxide or hydroxide is detected frequently in our samples. Iron oxide particles mostly consist of several iron containing nanometer-sized crystallites which (in few cases) could be determined as hematite by selected area diffraction in TEM. No evidence for other iron oxide or hydroxide phases (e.g., magnetite, goethite) in particles was found. Iron oxide nano crystallites are frequently found admixed to silicate particles. As Hematite is one of the strongest radiation absorbing components in mineral dust, its distribution within the aerosol is of great interest. Aggregation of hematite with silicates can strongly enhance the radiation absorption by dust at solar wavelength (Sokolik and Toon 1999). Oxides containing titanium and iron are

referred to as iron-titanium oxides. A possible mineral phase (illmenite) could not be determined, as those particles were too few in number. Silicate particles containing iron and titanium (oxides) are observed more often. Titanium oxide, rutil, is occurring a little more often but still scarce so again no mineralogical phase determination could be applied. Primary particles are nanometer- to micrometer-sized. Aluminium oxides and copper oxides are occurring rarely in our samples and might have anthropogenic sources, but in most cases are interpreted as sampling artefacts.

Phosphates. In the present samples, phosphate particles often contain calcium, sodium and magnesium. They appeared in the sub micron and micron size range and their shape was highly variable. According to studies of Graham and Duce (1979), particulate phosphate concentrations are significantly higher over continents than over oceans due to industrial sources and agricultural activities. As the latter is rare in the Sahara, other potential sources for particulate phosphate have to be taken into account like so called “bone bed sediments” (70 % of bone is made of apatite and thus phosphorous is abundant in those sediments) and other phosphate-rich sedimentary rocks. However, due to the low number abundance of particulate phosphate in the investigated samples, the source thereof could not be determined.

The class named **Mixtures** consist of complex multi component aggregates, which are not dominated by the silicate component, but may contain silicates. The Si(Al) + S groups comprise particles that are dominated either by SiAl + S or silicium + S. The particles of the latter group are mainly interpreted to consist of internal mixtures of quartz and sulphate. The sulphate phase of these internal mixtures may be one of the above described sulphates. Within the SiAl + S group all internal mixtures of any alumosilicate (e.g., different clay minerals, feldspars, chlorites) and any sulphate are summarized (Fig. 12). The SiAl + S group is the dominating group among the mixture class. Its abundance is variable, but around 10 % at least are present in every sample. These particles are more abundant in the size range above 0.5 μm, but are present among the small particles as well.

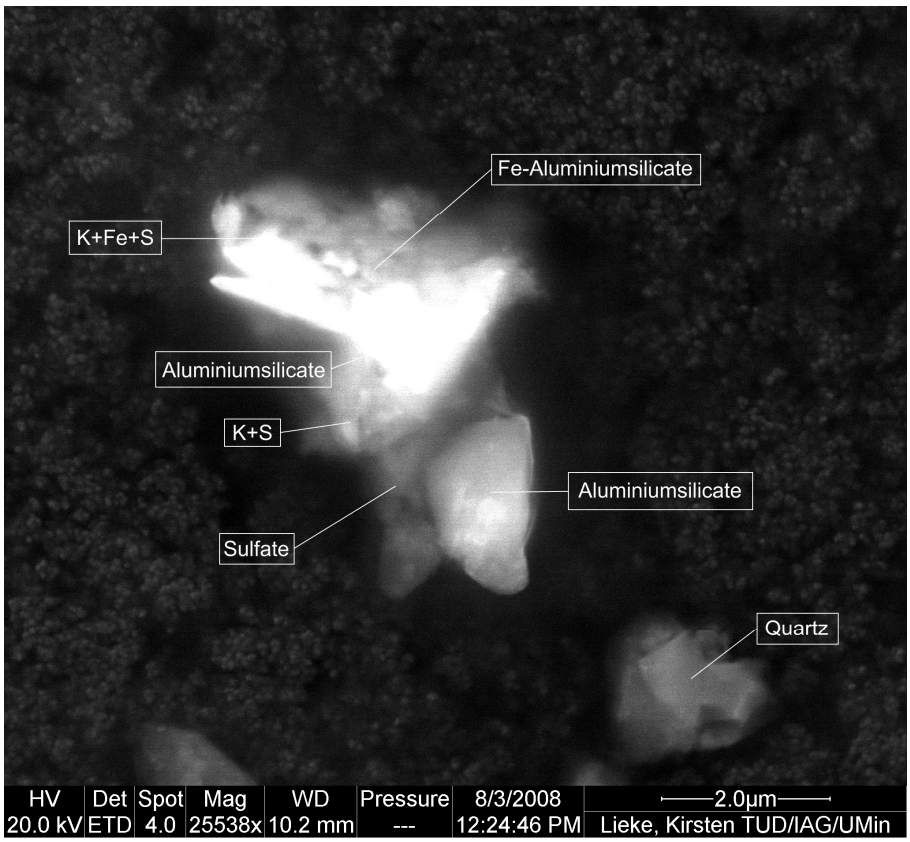

Fig. 12 Secondary electron image of an internally mixed SiAl + sulphur particle

Particles with significant chlorine content mainly belong to two groups. Particles which contain only chlorine as their major component are further characterized by slightly elevated sulphur concentrations and most probably represent altered sodium chloride particles. The second group comprises different internal mixtures of NaCl- or Cl-bearing particles with alumosilicates, and more rarely with quartz or sulphates. The particle number abundance of this latter group is generally low. The Si(Al) + calcium group can be split into SiAl + calcium and silicium + calcium mixtures. The particle number concentration of the latter is small and does not exceed 1 %. This group consists most likely of internal mixtures of a quartz and a calcium carbonate (e.g., calcite). The SiAl + calcium group is slightly more abundant. Mixtures of calcium carbonates and different alumosilicates were usually dominated by the latter and thus included in the above mentioned silicate class. According to Scheuvens et al. (2011), in particles from Morocco Si/Al ratios around 3 are only rarely encountered, and a major contribution of feldspar minerals can thus be excluded. In the present samples, the mixture groups show a similar composition, so that the most reasonable explanation for the composition of many particles of this subgroup is internal mixing

of clay minerals with calcium carbonate (e.g., calcite). Furthermore, in the present samples calcite was determined as component of internally mixed particles in TEM.

Biological particles. Primary biological particles are enriched in organic matter plus phosphorous, potassium, sulphur, calcium, manganese, zinc, chlorine, and others (Artaxo et al. 1998). In this study, the elemental composition including phosphorous, potassium, sulphur, and calcium, as well as the morphology were used to determine and classify particles as biological particles. They might originate as fragments of plants, pollen, spores, and fibres. Tropical forests are a possible source for biological aerosol. However, biological particles are scarce on our samples. In biomass burning samples, plant fragments are likely to occur but rarely found due to the distance from their source. Biological material other than plant fragments was not detected. Diatomea fragments are classified into the quartz class, due to their chemical composition.

Others. The so-called rest group contains all particles, which do not fit into any of the above-described classes. Hence, it represents a vast variety of mixtures of particles dominated by a single element to particles which represent complex internal mixtures. The most abundant group within this class is the potassium dominated particle group. These particles occur solely within the small particles size range and originate from biomass burning. It is suspected that potassium is present as nitrate, as sulphur and/or chlorine peaks were not observed. Their shape is irregular and widely varying. Particles with a characteristic steel-signature (iron, chromium and mangan, in addition to small extents silicium) from time to time occurred on the analysed samples and therefore formed an own group. These particles may originate from (urban or industrial) polluted air masses, but could also be abrasion residues of the used sampling equipment or parts of the airplane. However, a definite source of these particles could not be determined.

4.2 Aerosol types

Different layers of aerosols can be distinguished, and are summarized as the three major types of biomass burning (Fig. 13), desert dust (Fig. 14) and marine boundary layer aerosol. The chemical composition expressed as relative number abundance of the different particle groups shows pronounced differences between the dust, biomass burning and the marine boundary layer samples. Generally, in the size range above 0.5 μm geometric diameter, mineral dust (mostly pure silicates and mixtures of silicates and sulphates) are dominating. Silicate particles show the largest relative number abundance in the super micron size range, contributing about 50 to 85 %. Like in the samples taken on ground level, there is always a small amount of quartz particles present at an almost constant ratio with respect to the amount of silicates. Sulphates (mostly sodium sulphates) are most abundant in the size range between 0.5 and 2.5 μm.

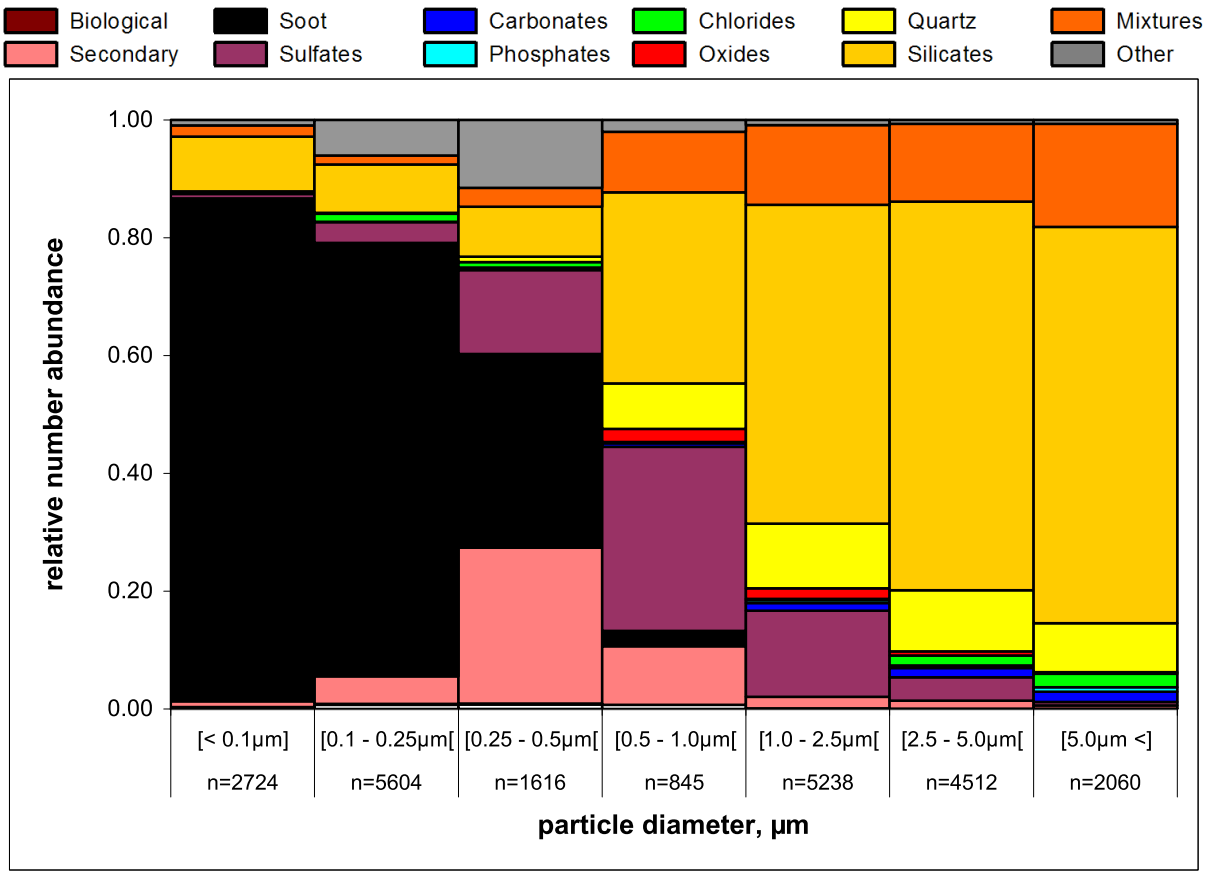

Fig. 13 Biomass burning aerosol, size resolved relative number abundances of particle classes (n = number of analysed particles)

In contrast, the aerosol composition is highly variable below d = 0.5 μm. In the case of biomass burning aerosol layers, soot is strongly dominating (relative number abundance up to 95 %). Mixtures of soot and ammonium sulphate particles are observed frequently, but no mixtures of soot with dust particles. In the dust layers, silicates and silicate-sulphate mixtures are also the most abundant groups (up to 97 %) below 0.5 μm size. Marine boundary layer aerosol was collected at the lowest sampling altitudes (200 and 500 m above sea level), large amounts of sea salt are observed in the particle size range above 0.5 μm. The small particles consist mostly of secondary aerosol (ammonium sulphate) indicating a strong urban influence, when the aerosol was sampled in the vicinity of the coast.

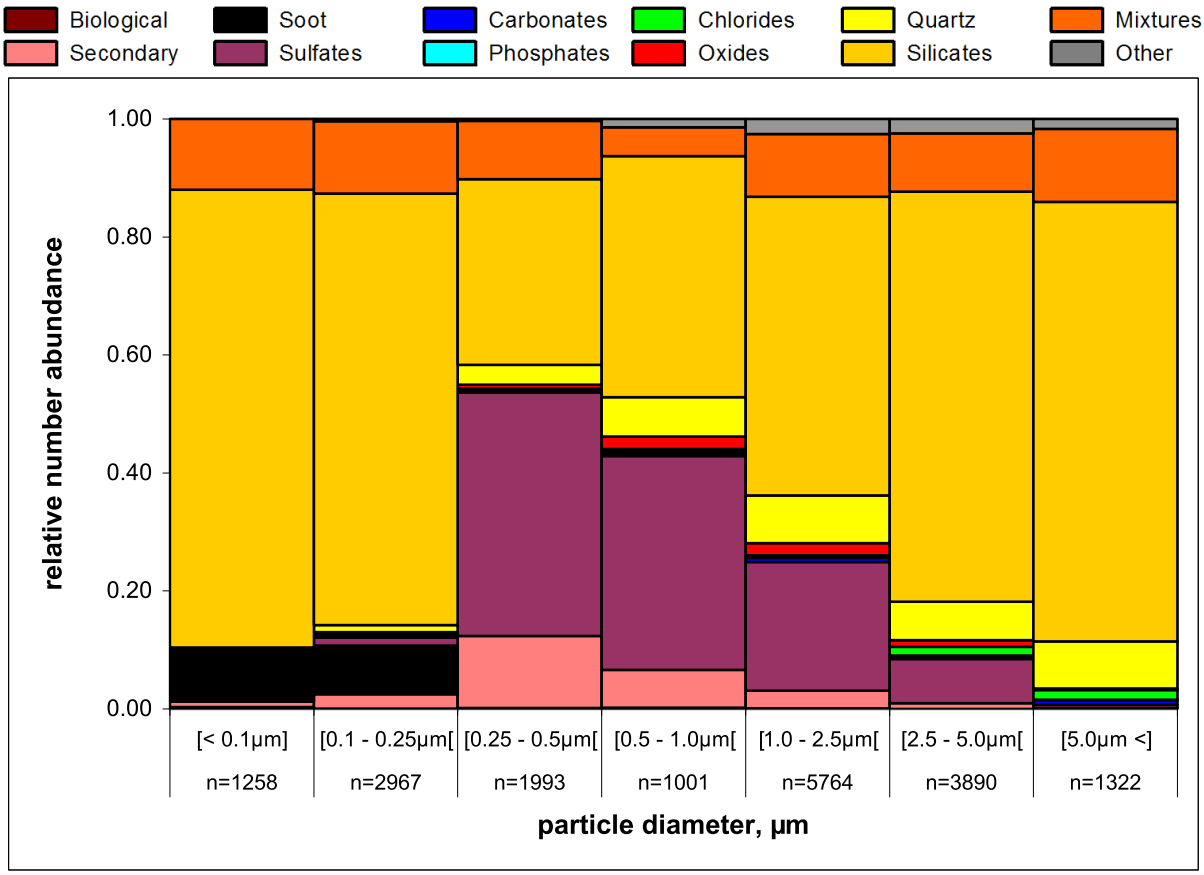

Fig. 14 Mineral dust, size resolved relative number abundances of particle classes (n = number of analysed particles)

Compared to the ground based observations (Kandler et al. 2011b), sodium chloride was observed at much lower concentrations (~ 5 % versus ~ 40 %) in the low (500 m a.s.l.) altitude samples above Cape Verde, indicating that the marine boundary layer is restricted to even lower altitudes. During the whole campaign,

samples from different source regions were collected (Knippertz et al. 2011). As a pronounced north-south gradient was observed for iron oxide and iron-rich silicate abundances in previous investigations (i.e. Kandler et al. 2007), it was expected to see a corresponding variation of abundances of these minerals in our samples. However, despite a general variation, no systematic north-south dependence was observed, indicating that at least the micron range dust particles are well mixed (combining various sources) in the transported aerosol. The contribution of calcite and calcium-dominated particles is negligible, which is contrary to measurements in Tinfou, Morocco (Kandler et al. 2009) during SAMUM-1, where Ca-occurrence could be linked to dust source regions and observations by Formenti et al. (2008). Instead, calcium-dominated particles were found in biomass burning samples from the south.

Figure 15 is a diagram depicting the relative amounts of only the groups of the silicate class and quartz, in order to reveal any variance of the silicate particles between biomass burning and non biomass burning samples in different size regimes. The relative number abundances are listed in Table 1. Within the silicate class, there appears to be no significant difference between the biomass burning and non biomass burning samples. The biomass burning aerosol is almost exclusively represented in the small particles size range, where as mineral dust is present in all particles sizes. However, the abundances within the silicate class are in the same order of magnitude in biomass burning and dust throughout a wide range of sizes.

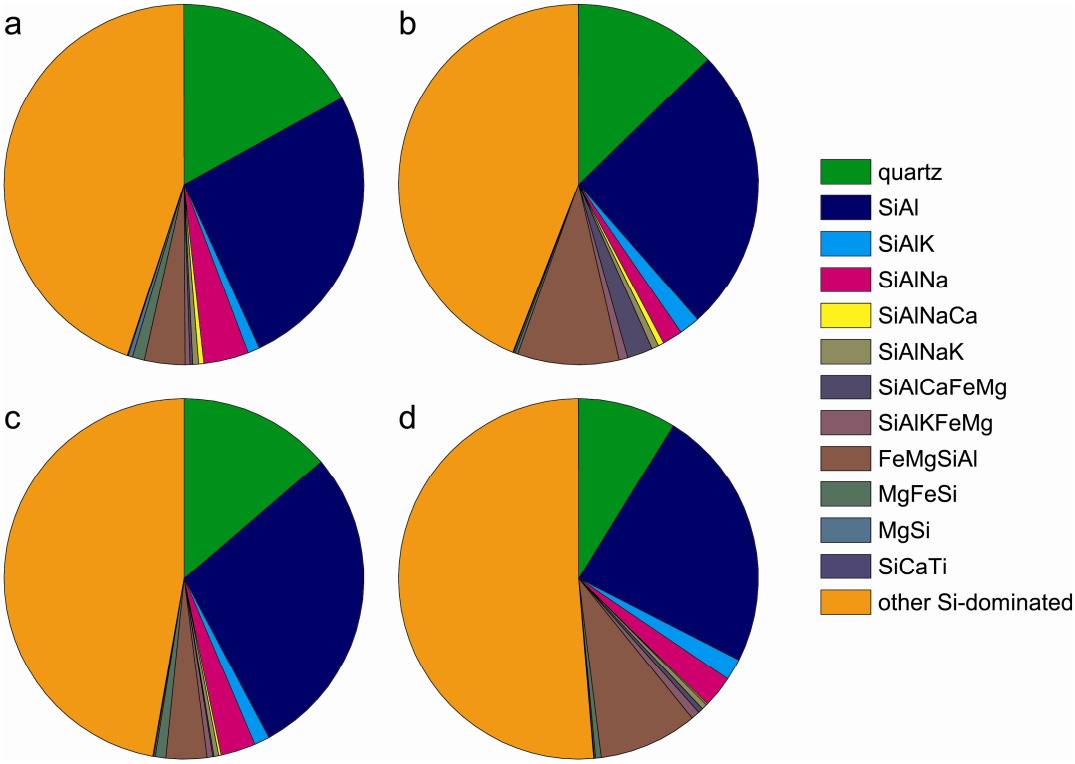

Fig. 15 Relative number abundances of silicate groups and quartz for a) biomass burning aerosol from d = 0.5 – 2.5 µm, b) biomass burning aerosol with d > 2.5 µm, c) mineral dust aerosol from d = 0.5 – 2.5 µm, d) mineral dust aerosol with d > 2.5 µm

Class/sample and [d]	a) BB [0.5-2.5 μm[	c) dust [0.5-2.5 μm[	b) BB [>2.5 μm]	d) dust [>2.5 μm]
quartz	17 %	14 %	13 %	9 %
SiAl	26 %	28 %	26 %	24 %
SiAlK	1 %	1 %	2 %	2 %
SiAlNa	4 %	3 %	2 %	3 %
SiAlNaCa	< 1 %	< 1 %	1 %	< 1 %
SiAlNaK	1 %	< 1 %	1 %	< 1 %
SiAlCaFeMg	< 1 %	< 1 %	2 %	< 1%
SiAlKFeMg	< 1 %	1 %	1 %	1 %
FeMgSiAl	4 %	4 %	9 %	9 %
MgFeSi	1 %	1 %	< 1 %	1 %
MgSi	< 1 %	< 1 %	< 1 %	< 1 %
SiCaTi	< 1 %	< 1 %	< 1 %	< 1 %
other Si-dominated	45 %	47 %	44 %	51 %
Number of particles	n = 6083	n = 6765	n = 6572	n = 6212

Tab. 1 Relative number abundances of silicate groups and quartz for particles with d = 0.5 – 2.5 µm and d > 2.5 µm for biomass burning and mineral dust samples

4.3 Description of flights

Seven sampling flights will be discussed in more detail, as it was possible to sample a variety of aerosol layers during the same flight. A height resolved diagram of relative number abundance in three size regimes is shown for each day and complemented by back trajectories for the different aerosol layers.

4.3.1 Jan. 23rd, 2008, "South"

A sampling flight was performed towards the south Atlantic. This flight was dedicated to sampling of very distinct biomass burning layers (Fig. 16) with high optical depth (AOD) from south west and central Africa that was transported over the Atlantic (Fig. 17). The flight legs were stacked in the range of 9.211° to 10.394° latitude and -20.057° to -19.081° longitude. Samples were collected at altitudes between 3000 and 100 m a.s.l. Sampling locations are marked by a star in the trajectory plots. It should be emphasized here, that the different flight levels were horizontally shifted and occurred one after another, i.e. not an accurate column was sampled. The exact sampling time and coordinates are indicated in the list of samples in the electronic supplement.

This flight revealed three completely different appearing samples of biomass burning aerosol, indicating the differences due to transport and aging within the biomass burning aerosol (Fig. 16). However, in all samples, secondary aerosol and soot are present in the small particles size range. In the large particles size range, mineral dust (e.g., quartz, silicates, and calcite) is prevalent. Mixtures and sulphate indicate the presence of aged marine aerosol. The 100 m a.s.l. flight level sample was collected near the coastline. Its small particles are dominated by ammonium sulphate and soot, which appeared internally and externally mixed. Although the larger particles are dominated by silicates, sulphate is still highly abundant with more than 20 % in the medium size range, indicating the vicinity to the sea. A few fresh sea salt particles were found. The 900 m a.s.l. flight level sample is dominated by soot in the small particles size range, which might be originating from biomass burning in the Sahel. Here the soot appears not mixed. Unexpectedly among the large particles, fresh sea salt is found frequently (relative number abundance ~ 5 %). The aerosol found on the 2000 m a.s.l. flight leg is strongly dominated by secondary and other sulphates,

whereas soot is significantly less abundant. In the 3000 m a.s.l. samples soot and ammonium sulphate are externally mixed with dust in the small particles size range. The particles above 0.5 μm are dominated by mineral dust while other sulphates are less abundant than in the lower flight legs.

The air masses of the upper layers point out to central Nigeria and took their way over Benin, Togo, Ghana, Burkina Faso, Côte d'Ivoire and Guinea, and proceeded towards the Cape Verde. The middle altitude trajectories on 900m started in Mali and Algeria, passed over Niger, Mali and Guinea heading towards Cape Verde. The ground near trajectories started in central Nigeria, meeting and probably mixing with the mid-level trajectories, but than crossing in the northern part, lowered and passed Mauretania and finally Senegal in the low altitudes, making a sharp turn to the south over Cape Verde.

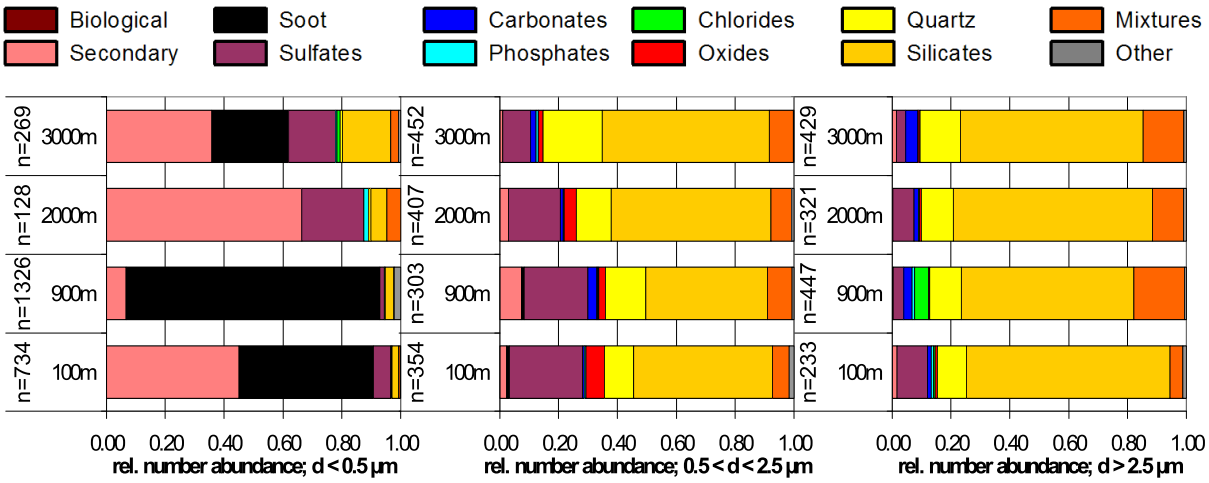

Fig. 16 Relative number abundances of particle classes of Jan. 23rd 2008: Each rows represents 2-3 samples on a given flight level. Left column: geometric diameter < 0.5 µm; middle column: geometric diameter 0.5 – 2.5 µm; right column: geometric diameter > 2.5 µm

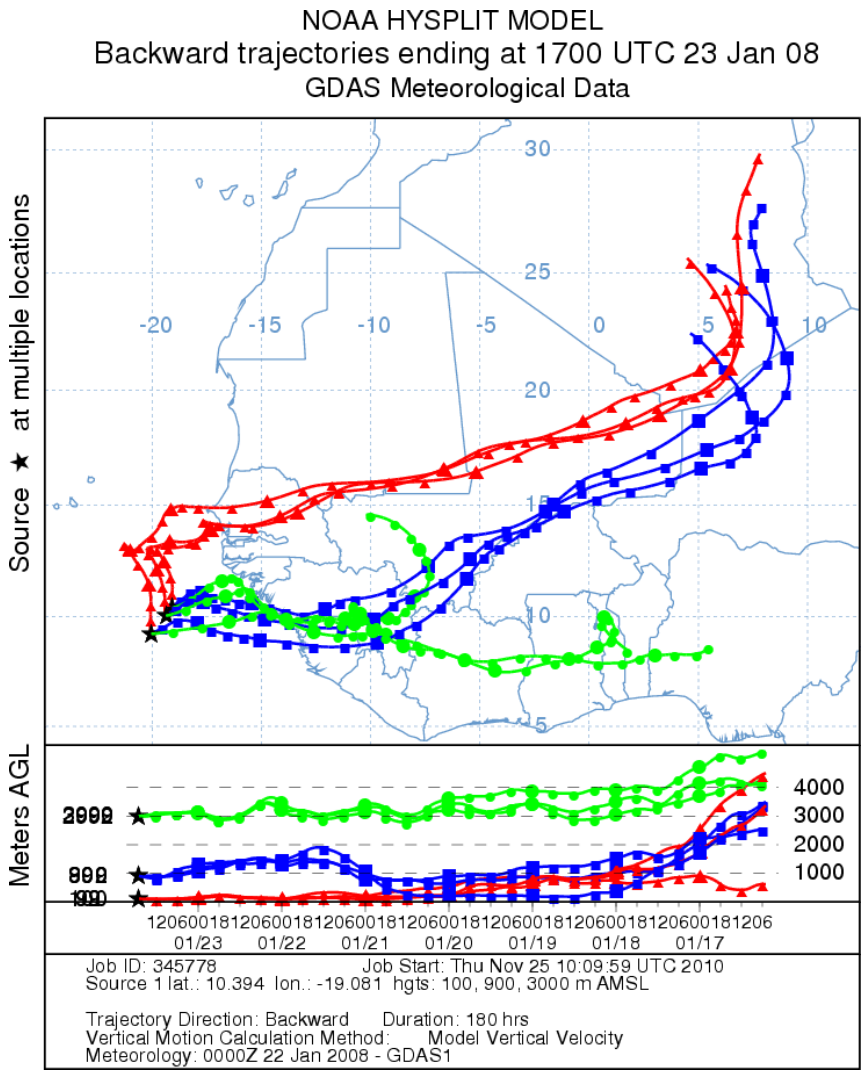

Fig. 17 NOAA HYSPLIT back trajectories for Jan. 23rd 2008

4.3.2 Jan. 25th, 2008, "Praia"

This sampling flight was performed in the vicinity of the Cape Verde Islands. Biomass burning aerosol from the Senegalese region was transported generally west-northwest over the Atlantic ocean, towards the Cape Verde islands (Fig 19). The flight legs where stacked columnar, in the range of 14.886° to 14.986° latitude and -23.472° to -23.553° longitude. Samples were taken on flight levels between 3300 and 200 m a.s.l.

For the flight levels 3300 and 2000 m a.s.l., large amounts of soot and other biomass burning particles are observed in the size range below 0.5 μm (Fig. 18). For larger particles, the relative abundance of the different particle groups encountered at these altitudes is practically identical with pure dust layers. The source of the mineral dust

could be located in the Bodélé depression, where the aerosol was taken up and transported southward, and later (probably after some days) mixed with biomass burning aerosol. At 700 m a.s.l., soot is also dominating the size range below 0.5 μm indicating the presence of biomass burning aerosol. For lower flight levels, mineral dust was observed in the whole size range, i.e. admixture of biomass burning aerosol has not taken place. The dust source for these lower levels is Mauretania, Mali, and Niger (Fig. 19) (Knippertz et al. 2011).

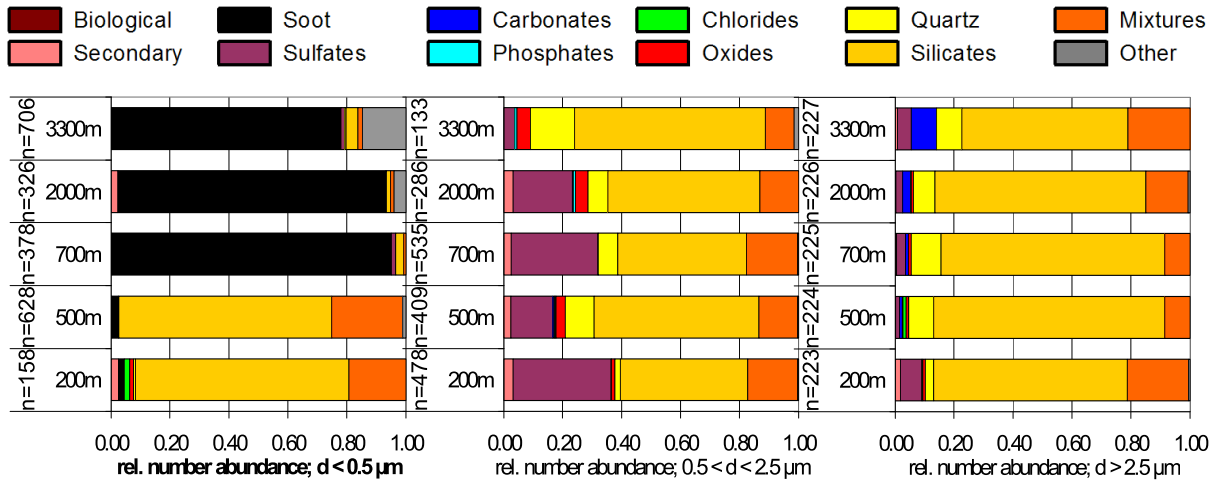

Fig. 18 Relative number abundances of particle classes of Jan. 25th 2008: Each rows represents 2-3 samples on a given flight level. Left column: geometric diameter < 0.5 µm; middle column: geometric diameter 0.5 – 2.5 µm; right column: geometric diameter > 2.5 µm

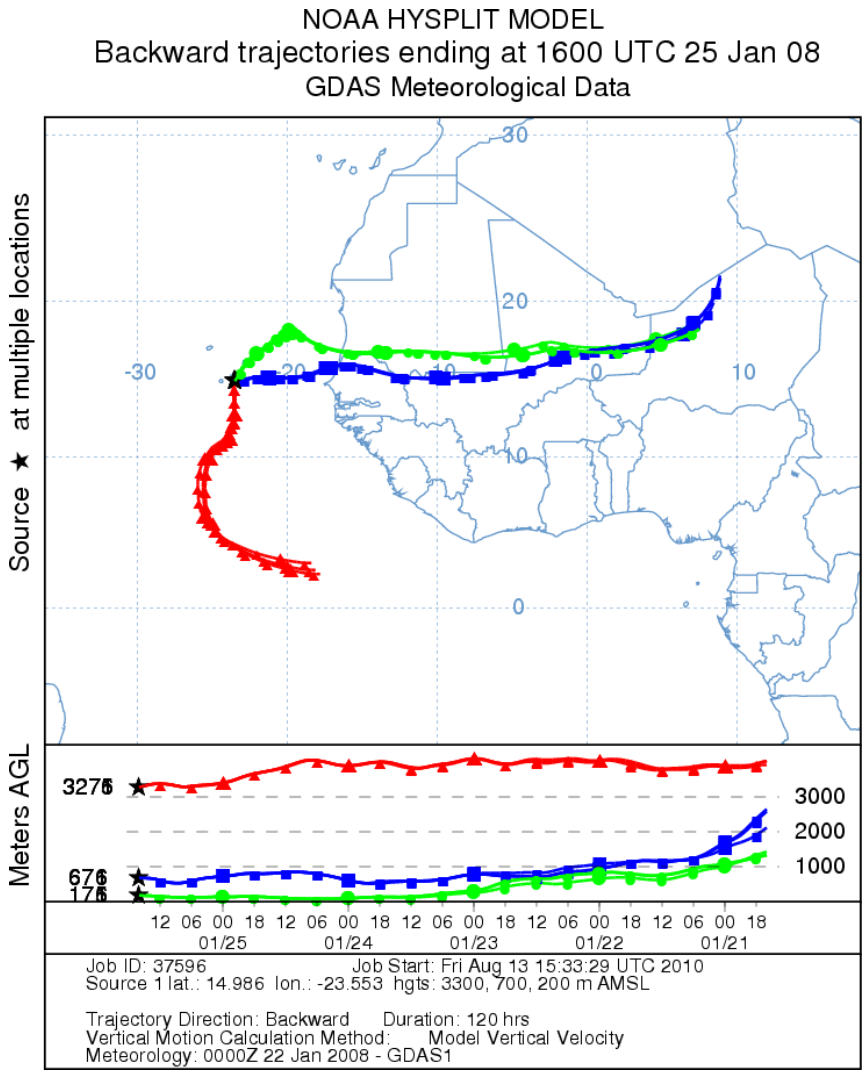

Fig. 19 NOAA HYSPLIT back trajectories for Jan. 25th 2008

4.3.3 Jan. 28th, 2008, "Tenerife"

A flight over the Atlantic towards the Canary Islands was performed, to document the transport of dust from various origins to Tenerife. Samples were taken on two sections. Three sampling legs were set on 500 m a.s.l., within a range of 800 km approximately every 350 km, over the Atlantic south of the Canaries (between 25.159° latitude and -19.223° longitude, and 27.603° latitude and -16.926° longitude). Two flight legs were set 800 m a.s.l. and 1300 m a.s.l. east of Tenerife (28.586°lat/-17.103°lon). Thus the different flight legs are not representing a vertical column, but nevertheless provide insight in the vertical and horizontal distribution of the collected aerosol.

The samples are strongly dominated by mineral dust (Fig. 20), whereas the high abundance of sulphates among the large particles indicates strong but aged marine influence, which is in contrast to the Cape Verde samples, were mostly fresh sea salt was found, if a marine influence was observed. Although some samples are missing, the relative number abundance of particle classes shows no significant variation between the flight legs. This is in accordance with the trajectories paths:

The back trajectory analysis (Fig. 21) shows different paths for the air masses over Europe and northern Africa, but all over Algeria and descended to pass Mali, Mauretania and West Sahara in approximately 500 to 1000 m altitude.

The homogeneity in dust composition in the atmospheric column over the African continent is shown by Scheuvens et al. (2011) for samples from Morocco, Algeria and Tunisia and can be explained by fast mixing with a regional background aerosol after dust entrainment. This intensive vertical mixing most probably caused the observed low inter-layer variation.

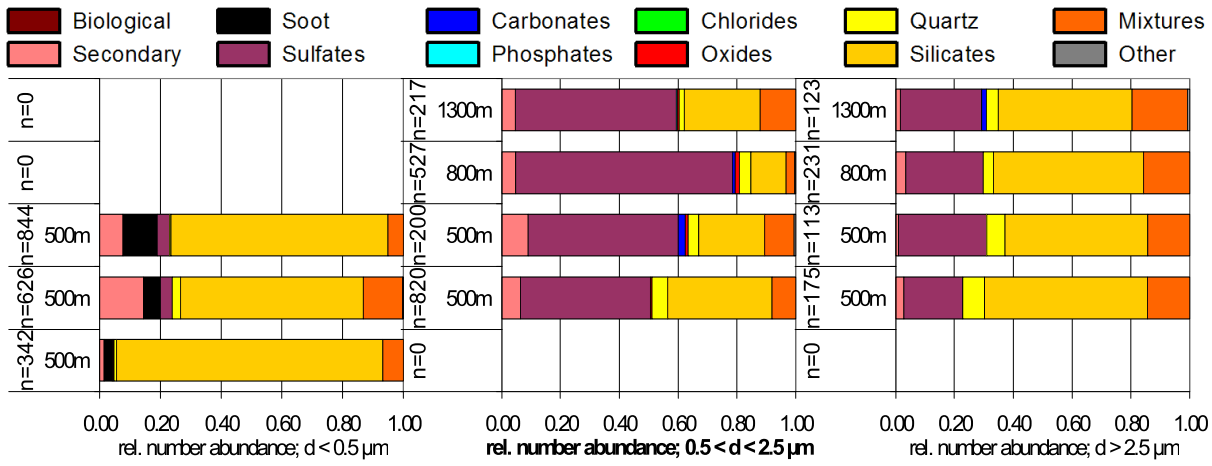

Fig. 20 Relative number abundances of particle classes of Jan. 28th 2008: Each rows represents 2-3 samples on a given flight level. Left column: geometric diameter < 0.5 µm; middle column: geometric diameter 0.5 – 2.5 µm; right column: geometric diameter > 2.5 µm

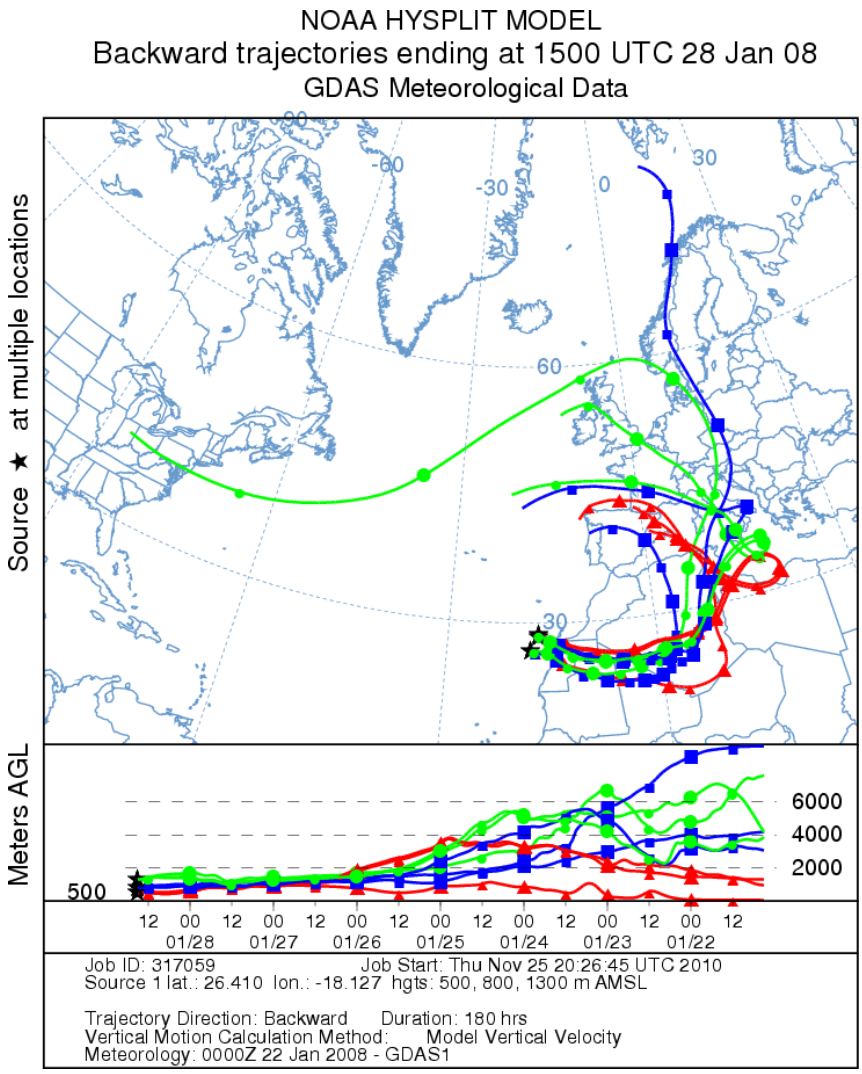

Fig. 21 NOAA HYSPLIT back trajectories for Jan. 28th 2008

4.3.4 Jan. 30th, 2008, "North"

This sampling flight was directed to the north west of the Cape Verde Islands, starting at the latitude of Sao Vicente, passing Santo Antao and following a quasi-Langrangian flight path of approximately 300 km straight over the Atlantic. The flight legs were set in the range from 16.717° to 18.651° latitude and from -25.321° to -26.854° longitude. Samples were collected on 500 and 100 m a.s.l. Due to the accidental loss of samples, the small particles are not included in the analysis. However, the large particles size range is well covered.

All samples are dominated by silicates (Fig. 22). Sea salt and mixtures with sea salt are present, because of the low sampling altitude over the sea. Sulphates indicate an aged sea salt fraction. Interestingly, carbonates, phosphates and iron oxides show

varying abundances between the different samples at the same level with generally higher abundances in the south.

The back trajectory (Fig. 23) ending at the first sampling point descended on Jan 26th from 2000 m down to 500 m on 27th and below the Algerian and Nigerian border, Mali and Mauretania westbound over the Atlantic towards the northern Cape Verde. All trajectories show similar patterns, except for the most southern one. Mali and Mauritania are the most prominent sources, but local influence from the Cape Verde can not be excluded, as the trajectories passed over the islands.

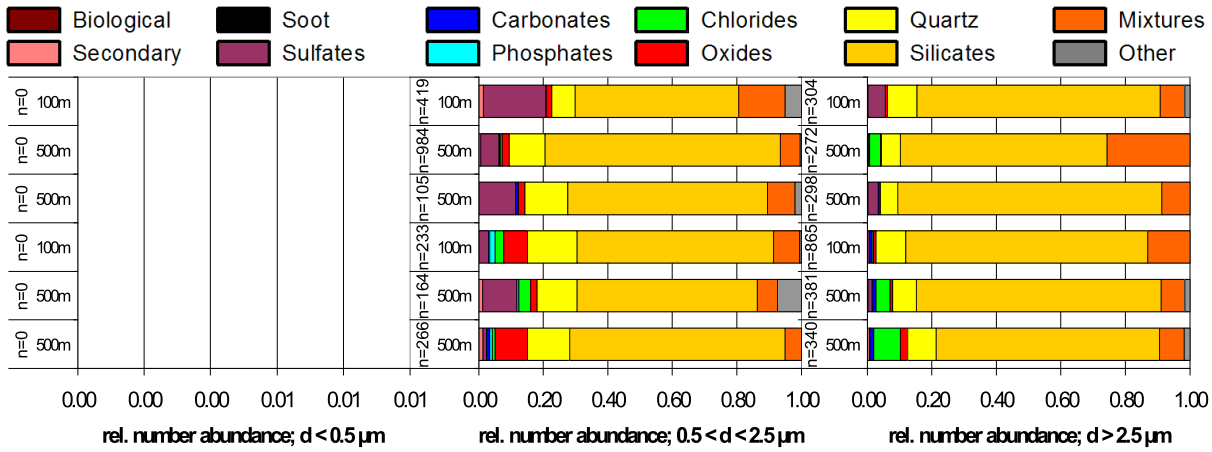

Fig. 22 Relative number abundances of particle classes of Jan. 30th 2008: Each rows represents 2-3 samples on a given flight level. Left column: geometric diameter < 0.5 µm; middle column: geometric diameter 0.5 – 2.5 µm; right column: geometric diameter > 2.5 µm

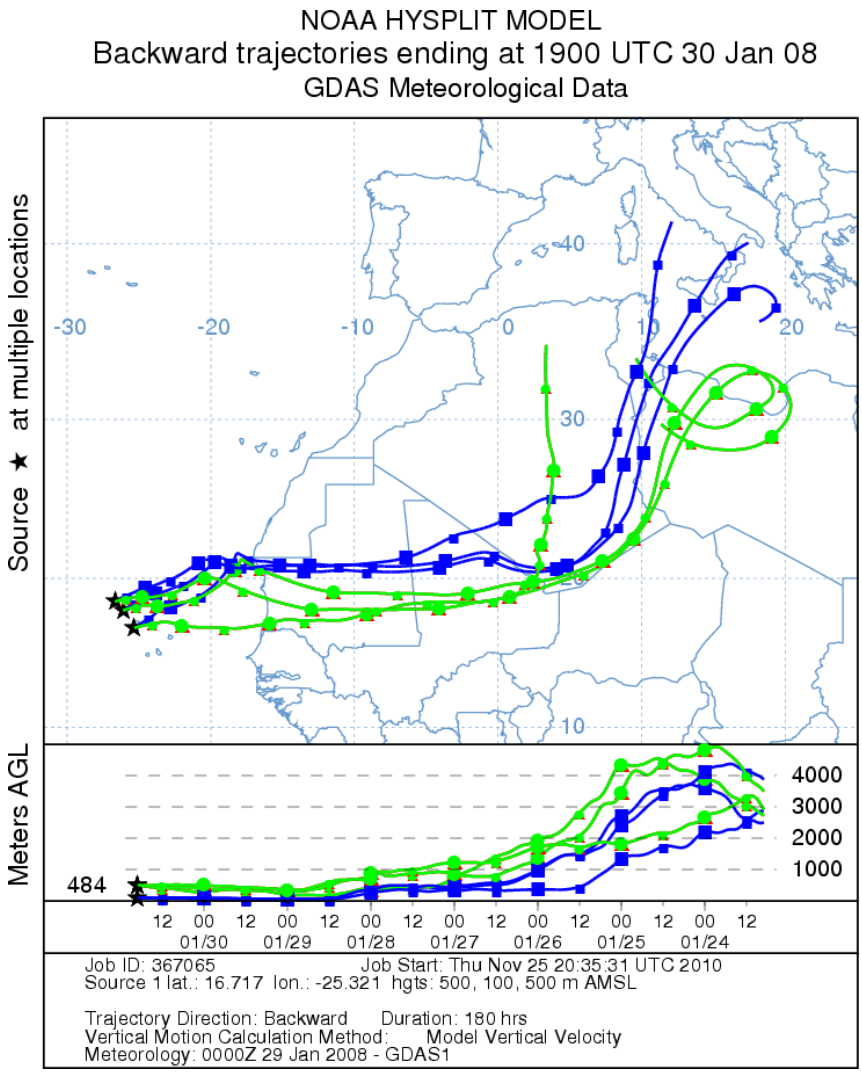

Fig. 23 NOAA HYSPLIT back trajectories for Jan. 30th 2008

4.3.5 Feb. 4th, 2008, "south"

This flight was dedicated to sampling of biomass burning aerosol from south west and central Africa that was transported over the Atlantic (Fig. 25). The flight legs were stacked in the range from 8.909° to 10.291° latitude and from -20.243° to -19.163° longitude. Samples were collected at altitudes between 3300 and 500 m a.s.l. It should be emphasized here, that the different flight levels are shifted horizontally, i.e. not an accurate column was sampled.

Interestingly, the biomass burning aerosol layers are overlaid by an almost pure desert dust layer (Fig 24). This layer shows a high abundance (~ 20 %) of the MgFeSi-group, representing probably olivine or (ortho-) pyroxene, in the size range

0.5 – 2.5 μm. Compared to the other samples, this dust layer is also poor in sulphates, which are usually present in the intermediate particle size range.

All layers below 3300 m a.s.l. show a strong biomass burning component. At 900 m a.s.l. a significant amount (~ 13 %) of potassium chloride was found in the small particle size range, which is interpreted as salt condensate from biomass burning (see below). At the same altitude level, mixtures of soot and ammonium sulphate were present but did not exceed 10 %. At 500 m a.s.l., fresh sea salt from sea spray (~ 18 %) is observed for particles above 2.5 μm size, mixtures of sea salt with silicates and sulphates (~ 10 %) for particles between 0.5 and 2.5 μm diameter. The sulphates of the lower levels contain sodium sulphate and other sulphates in almost equal proportions. Potassium sulphate, which can be allocated to biomass burning, accounts for a quarter of the other sulphates, most of it in the small particle size range.

The 500 m trajectories indicate coastal influence at low altitudes, which is responsible for the sea salt in the sample. The higher trajectories point to Senegal and Gambia as source region for the biomass burning component. This conclusion is supported by the Web Fire Mapper "FIRMS" data (University of Maryland, USA) which detected many fire spots in Senegal, Guinea, southern Mali and the Ivory Coast for the days before Feb. 4th, 2008.

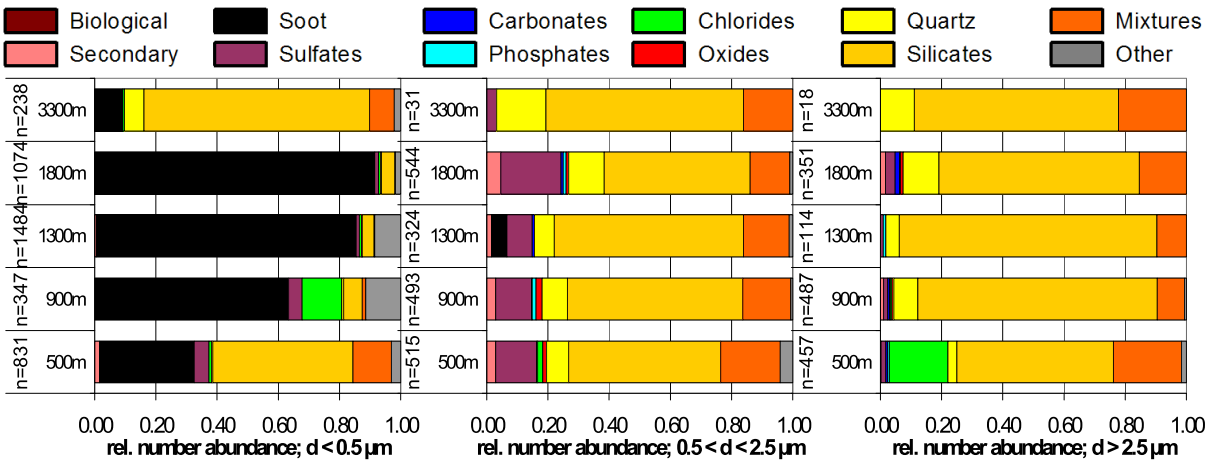

Fig. 24 Relative number abundances of particle classes of Feb. 4th 2008: Each rows represents 2-3 samples on a given flight level. Left column: geometric diameter < 0.5 µm; middle column: geometric diameter 0.5 – 2.5 µm; right column: geometric diameter > 2.5 µm

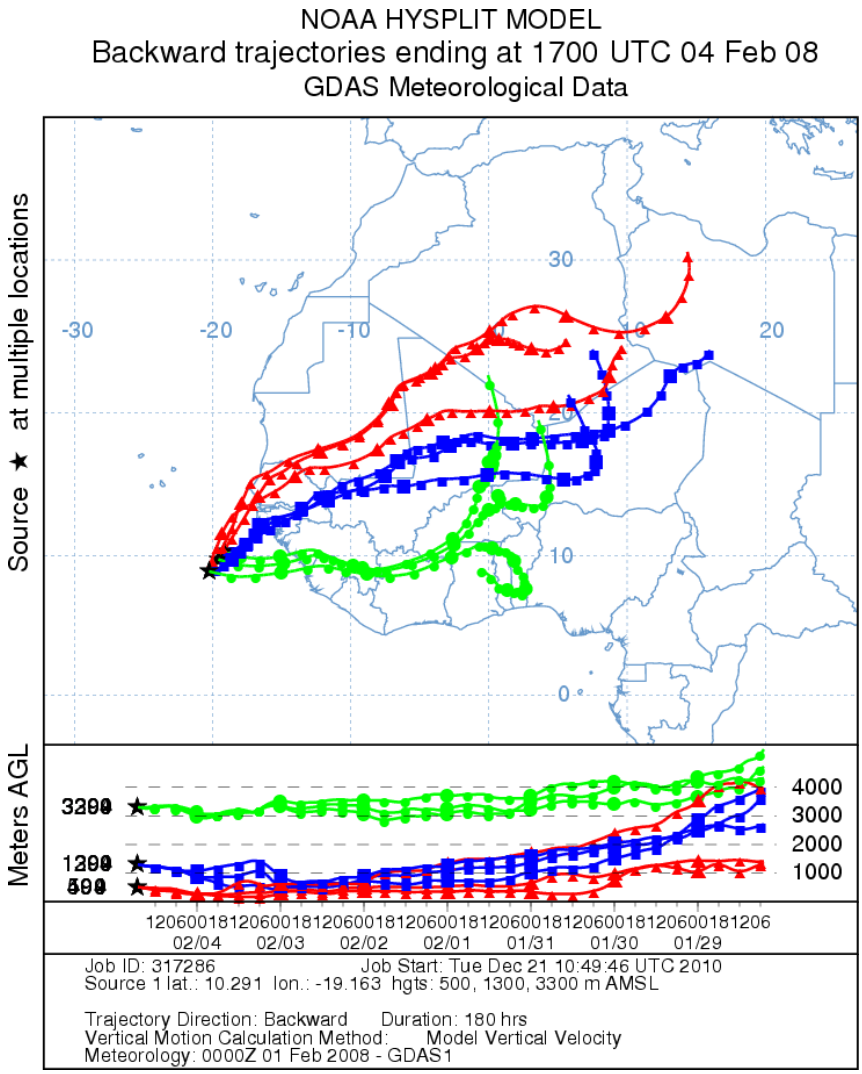

Fig. 25 NOAA HYSPLIT back trajectories for Feb. 4th 2008

4.3.6 Feb. 5th, 2008, "Dakar"

This sampling flight was performed in the vicinity of Dakar and the coast of Senegal, over the Atlantic. Samples were taken on flight levels between 2200 and 500 m a.s.l. within 14.717° and 14.152° and -19.081° and -17.680° longitude. It should be again emphasized here, that the different flight levels are shifted horizontally, i.e. not an accurate column was sampled.

A significant change of composition among the small particles is seen between the three layers (Fig. 26; assuming that both samples taken on 700 m a.s.l. originate from the same layer). The 2200 m a.s.l. samples originate from a biomass burning layer and are dominated by soot and other biomass burning particles in the small particles size range. The 700 m a.s.l. samples are strongly influenced by dust, although soot

and potassium rich particles are present. Both samples originate from the same layer and therefore from the same source, which could possibly be in Mali and adjacent countries. The 500 m a.s.l. flight sample is strongly influenced by coastal air. The large particles are dominated by sea salt. Ammonium sulphate is dominating the particles below 0.5 μm diameter.

Air masses passed Ghana and are lifted to higher altitudes (3000 m – 3500 m) after passing the Ivory Coast. The air mass surrounded the Cape Verde region and turned east, before being transported towards the Atlantic. The 700 and 500 m trajectories showed travel paths for the air masses along the Senegalese coastline, passing Dakar near by in the North West (see Fig. 27).

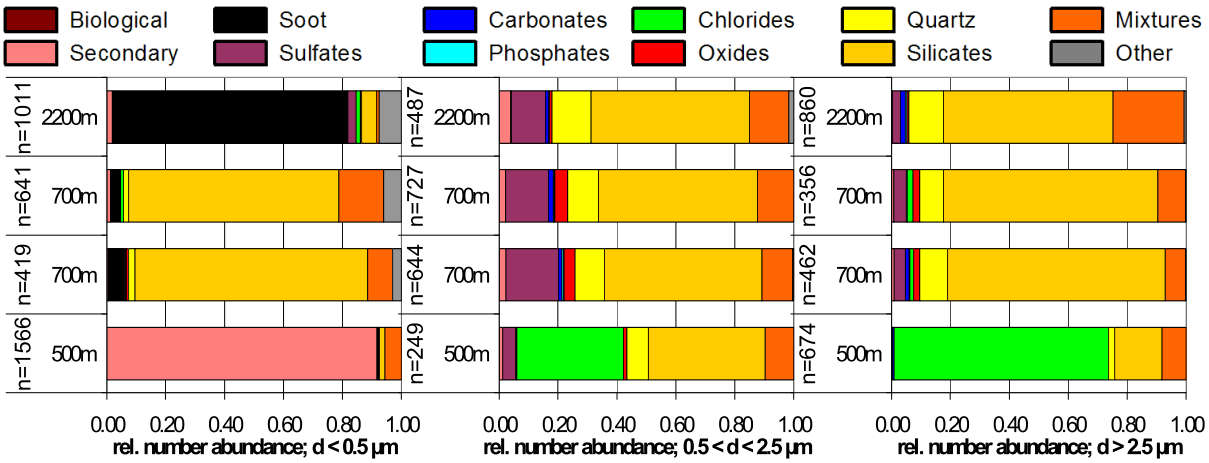

Fig. 26 Relative number abundances of particle classes of Feb. 5th 2008: Each row represents 2-3 samples on a given flight level. Left column: geometric diameter < 0.5 µm; middle column: geometric diameter 0.5 – 2.5 µm; right column: geometric diameter > 2.5 µm

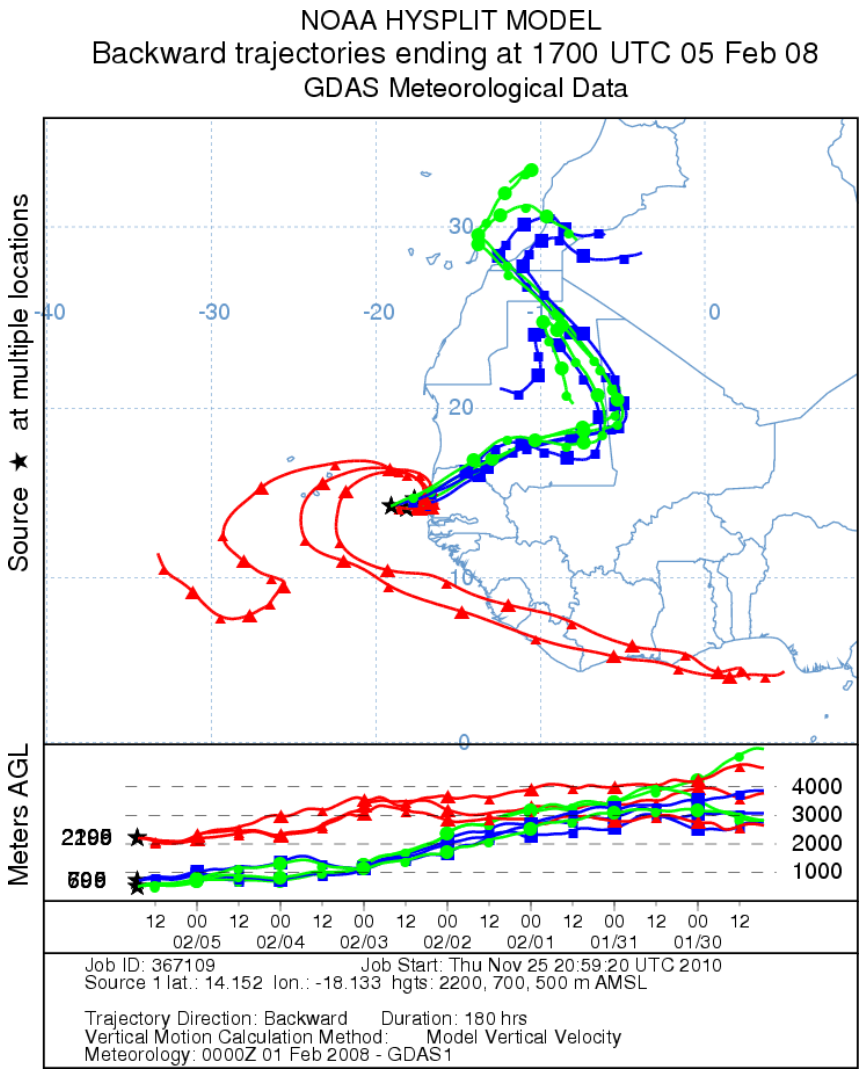

Fig. 27 NOAA HYSPLIT back trajectories for Feb. 5th 2008

4.3.7 Feb. 6th, 2008, "Praia"

On Feb. 6th, a sampling flight took place in the high altitudes (above 2000 m a.s.l.) over the Cape Verde Islands. Biomass burning aerosol samples were collected on 4000, 3700, 3600 and 2000 m a.s.l. All four samples are in the small particle size range dominated by soot and other biomass burning particles (Fig. 28), enriched in potassium. Internal mixtures of soot and ammonium sulphate are observed. The relative number abundance of sulphate particles varies significantly in the micron size range. Calcite and other calcium dominated particles are found in the samples from 3700 m a.s.l. and 4000 m a.s.l. The vast majority of particles in the large size range are silicates.

Trajectory analysis (Fig. 29) shows, that the air masses for the 2000 m flight level passed over the Gulf of Guinea. Other altitude air masses travelled over the continent and south Sahel belt at high altitudes. The biomass burning aerosol of the different layers at 2000 m a.s.l. and the higher levels, respectively, might therefore originate from different source areas.

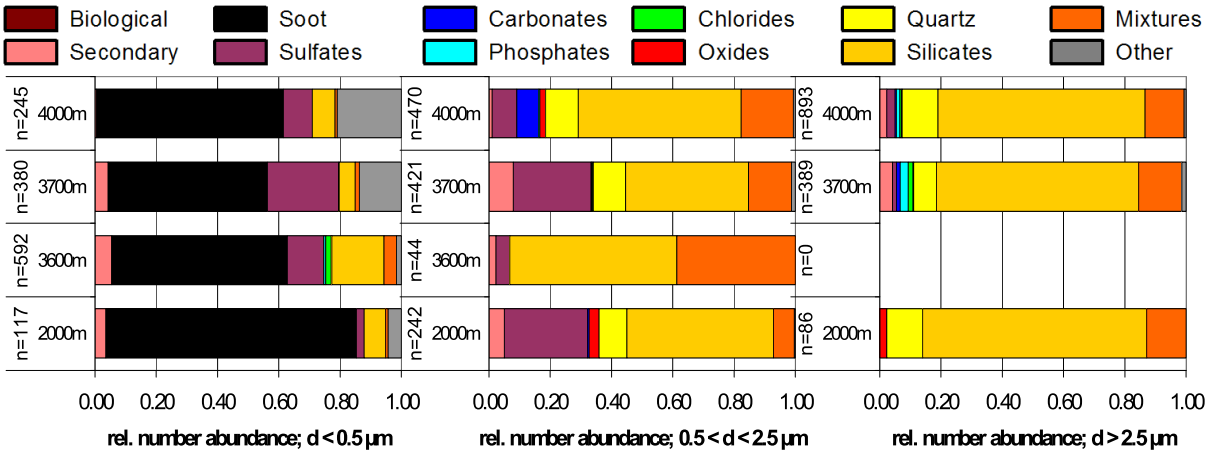

Fig. 28 Relative number abundances of particle classes of Feb. 6th 2008: Each rows represents 2-3 samples on a given flight level. Left column: geometric diameter < 0.5 µm; middle column: geometric diameter 0.5 – 2.5 µm; right column: geometric diameter > 2.5 µm

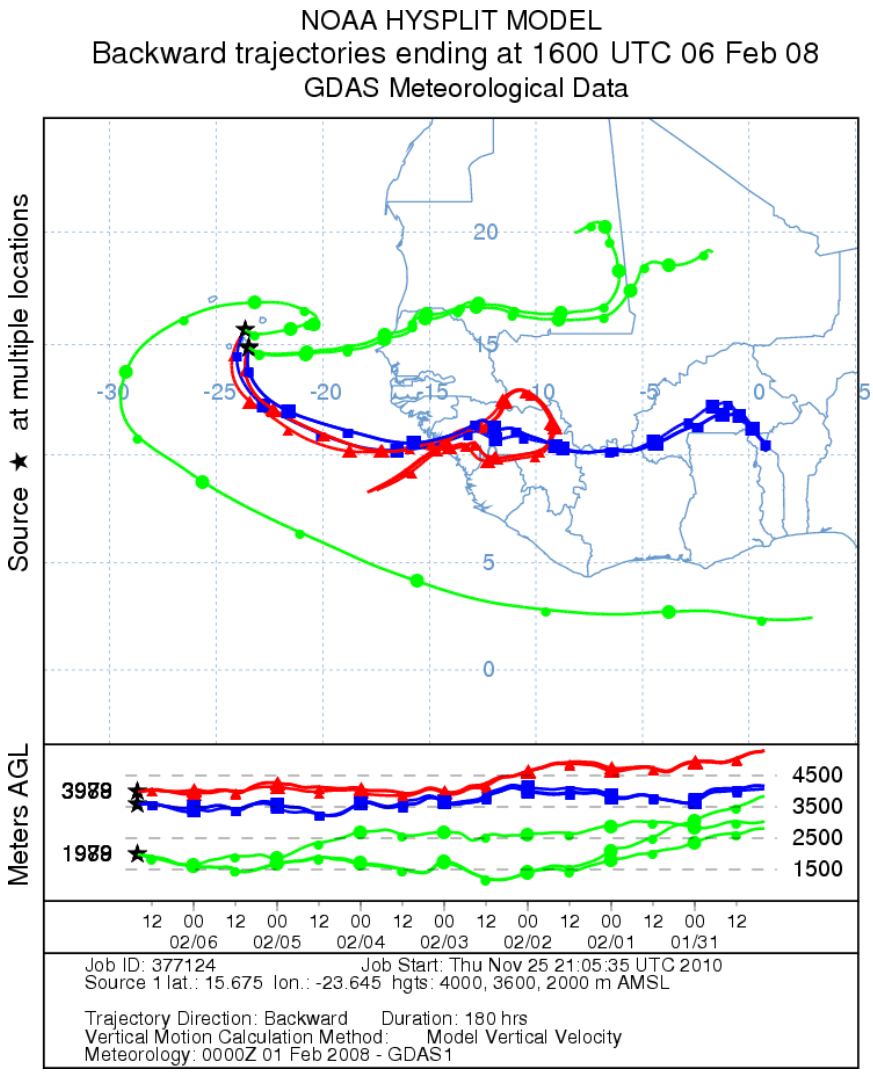

Fig. 29 NOAA HYSPLIT back trajectories for Feb. 6th 2008

4.4 Composition and mixing state of biomass burning aerosol

Biomass burning is occurring annually during the dry winter season in south west and central Africa and was detected for the period of the field campaign as well. The Firms Web Fire Mapper (University of Maryland, USA) reported a large, dense band of fires from western Ethiopia to the Guinean coastline and southern Senegal, as seen in the MODIS Rapid Response image (Giglio et al. 2003, Davies et al. 2004) of this time period (Fig. 30). In the present study, samples of biomass burning aerosol layers are clearly identified by the high number abundance of soot particles and the presence of other tracers for biomass burning, like high potassium contents in small particles.

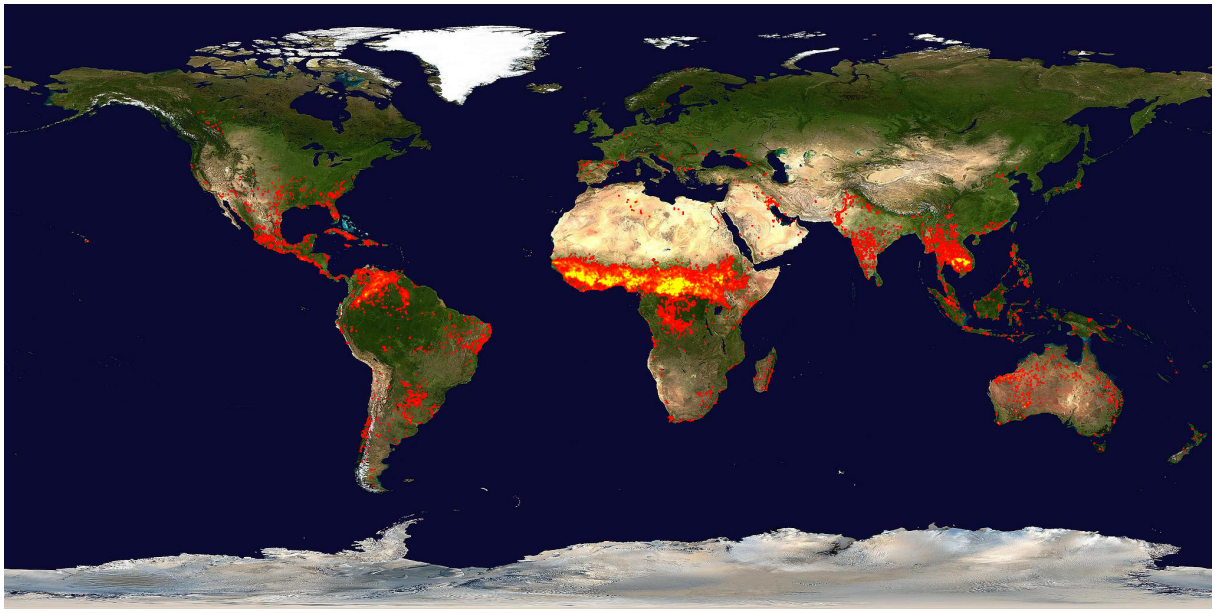

Fig. 30 Fire map from MODIS Rapid Response image for Jan. 21st to Jan. 30th (Davies et al. 2004, Giglio et al. 2003)

4.4.1 Soot

Soot particles were often enriched in potassium, and/or sulphur, which indicate a coating or an uptake of gaseous or liquid residues of biomass burning. In addition, some particles appeared to be swollen and showed a slight deformation on the surface under electron bombardment, without changing their chemical composition. This observation may indicate the presence of thin films of secondary components (nitrates, sulphates, and organics).

As mentioned above, the soot primary particles display an onion shell structure with disordered graphitic layers (Fig. 9), as previously observed in many studies

(e.g., Li et al. 2003, Wentzel et al. 2003). In this study, a typical soot particle occurs mostly as an individual agglomerate (~ 91 %, averaged), only few internal mixtures with secondary aerosol (~ 9 %, averaged, Fig. 31, right) were observed. In single cases, the amount of internally mixed soot with secondary aerosol may even exceed 20 %. In contrast, internal mixtures with secondary aerosol occurred more frequently in the ground based samples (Figs. 11a-b of Kandler et al. 2011b).

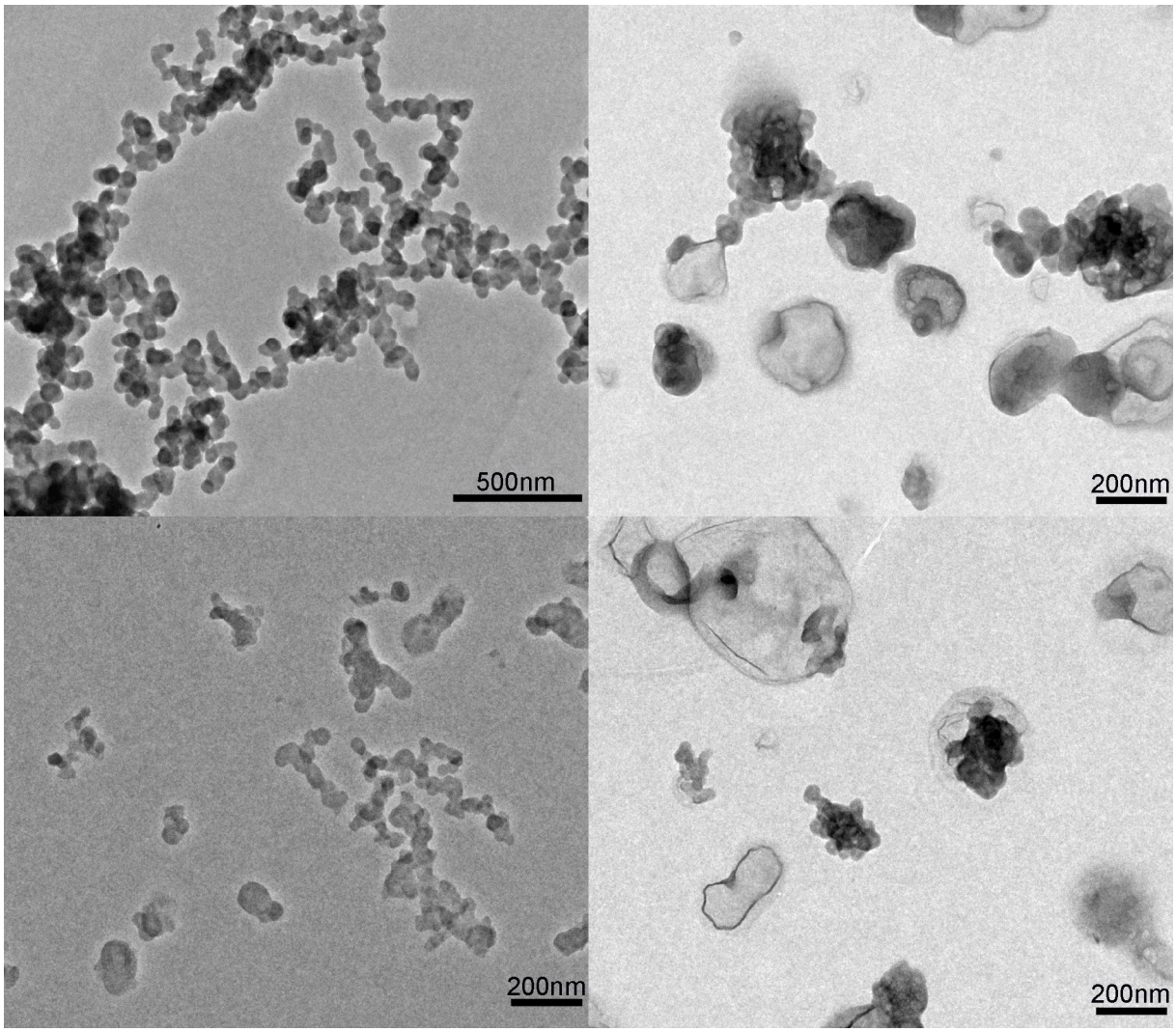

Fig. 31 TEM bright field images of pure and externally mixed soot agglomerates (left) and internal mixtures of soot and sulphates (right)

Approximately one third of the soot particles contain significant amounts of potassium. X-ray mappings on soot agglomerates did not reveal any inclusions. Instead, potassium seems to be distributed homogenously over the entire particle. It is

suspected that potassium is present as nitrate, as a sulphur peak (indicating the presence of sulphates) was not observed.

Silicate particles internally mixed with soot are rare, which is surprising for the aerosol consisting mainly of biomass burning and desert dust. Different forms of agglomerated soot particles were found: primary particles agglomerated to chains, to balls and to other, more complex structures. Soot particles consisting of few (2 - 5) primary particles were most abundant. Chains and other types appeared to be rare. Soot, in any of the occurring types, was never found to mix internally with silicate particles.

4.4.2 Other biomass burning components

The biomass burning layer samples also contain significant amounts of potassium chloride, potassium sulphate and other potassium rich particles (most likely internal mixtures with potassium nitrate). These potassium compounds are prominent tracers for biomass burning from biomass burning (e.g., Andreae et al. 1984, Cachier et al. 1995, Gaudichet et al. 1995, Echalar et al. 1995, Li et al. 2003). Constituents of the potassium and chloride particles are organically bound, present in the fluids of the vegetation and are volatilized during the combustion process (Liu et al. 2000), leading to nucleation and condensation of the potassium salt particles (Gaudichet et al. 1995). According to Li et al. (2003), the extent of aging of biomass burning aerosol may be estimated from the relative abundance of the different potassium salts. A younger plume age is indicated by high potassium chloride contents, where as potassium sulphate and nitrate are more abundant in aged biomass burning plumes. The average $KCl/(K_2SO_4 + KNO_3)$ ratio in our samples is 0.33, which is classified as aged biomass burning aerosol (Li et al. 2003). According to Gaudichet et al. (1995), the S/K and Cl/K ratios can also be used to distinguish fresh and aged biomass burning aerosols. The ratios observed in the present study are typical for aged biomass burning aerosol. The only exception is on Feb. 4^{th} (south), when high amounts of KCl indicate fresh biomass burning. However, for the remainder of the biomass burning aerosols found on the other days, it must be questioned whether plumes of different age can be further distinguished by means of the above ratio. Due to the high spatial frequency of occurring fires, older and younger plumes are likely to mix during the transport time

of two to three days, which results in some average ratio of $KCl/(K_2SO_4 + KNO_3)$ and S/K and Cl/K respectively.

High calcium contents (likely $CaCO_3$) among the large particles in biomass burning samples were only observed on the Jan. 25th and Feb. 6th at high altitudes above 3000 m a.s.l. Calcium carbonate is also described by Gaudichet et al. (1995) and Li et al. (2003) to occur in biomass burning and not being part of soil dust.

In order to check the distribution of biomass burning particles among the different particles size ranges, element indices for potassium, sodium and calcium were calculated.

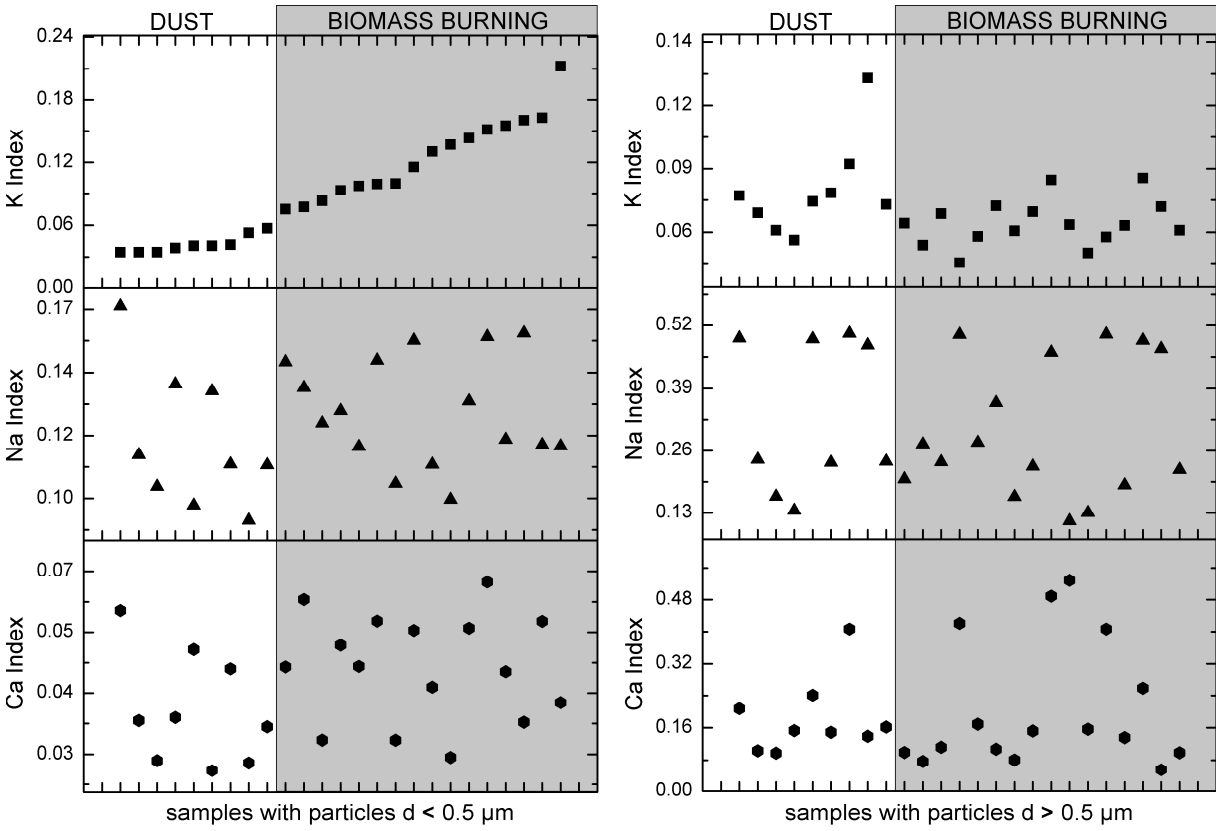

Fig. 32 Element indices of potassium, sodium and calcium plotted for small (left figure, samples with particles d < 0.5 µm) and large (right figure, samples with particles d > 0.5 µm) particles. All samples are sorted according to increasing potassium index of the small particles. Samples from biomass burning layers determined by trajectory analysis and chemical composition are shaded.

In Fig. 32 the samples have been ordered horizontally according to their potassium content, resulting in the effect that all samples associated with dust occurred in the left, low potassium content section of the figure, while all biomass burning samples displayed the higher potassium content and thus only occurred in the right hand

section of the figure. Accordingly, a pronounced difference in potassium index between biomass burning layer and mineral dust layer samples is observed for small particles. In other words the potassium index for small particles may be used as an indicator for distinguishing dust from biomass burning aerosol.

In contrast, no difference in the potassium index is observed for large particles (Fig. 32 right), which are arranged in the same order as the associated small particles samples, indicating that the biomass burning component is only present in the small particle fraction. Element indices for sodium and calcium show no systematic difference between small and large particles and biomass burning layer and mineral dust layer samples, which means that any arrangement of the samples according to the sodium or calcium indices, as well as according to all indices for the large particle samples, would not result in any separation of dust and biomass burning samples.

4.5 Chemical composition and mixing state of mineral dust

Depending on the soil composition in the different source regions, a variation of the aerosol composition should be expected. Mineralogical analysis by X-ray diffraction analysis (Kandler et al. 2011) showed that at least four major silicate groups are present in the aerosol at Praia: plagioclase, K-feldspar, kaolinite and illite, whereby illite was close to the detection limit. In general, the chemical composition expressed as relative number abundance of the different particle classes (Figs. 13 and 14) shows only minor variation within the dust samples. Obviously, it must be concluded that the mineral dust collected during our field campaign is mostly well mixed during long range transport. However, slight differences in composition of silicates can be detected when individual particles are considered.

Most silicate particles are mixtures of different minerals. The highly variable chemical composition of the silicate grains is shown as ternary plots (Fig. 33, 34 and 35). The various positions of a number of particular well known minerals as determined by their ideal chemical composition is shown in the plot of Fig. 33. The fact that the actual measured composition of particles can not be associated with any of these minerals is a clear indication, that most particles are mixtures of different minerals. Like mentioned in Kandler et al. (2011b), the Al/Si ratio exhibits the smallest measurement uncertainty, and varies significantly for different minerals (Fig. 33). The (Mg+Fe)/Si ratio is an indicator for clay mineral aggregates, as feldspars do usually not contain these elements (e.g., Anthony et al. 1990). The (Na+K+Ca)/Si ratio can be used to discriminate between feldspars and clay minerals, the former showing much higher values. The three diagrams in Fig. 34 show the individual chemical composition of silicate particles found in the flight samples of Jan. 25th (Praia), Feb. 4th (south) and Feb. 5th (Dakar).

First of all it is obvious, that the silicates are mostly internal mixtures of different clay minerals (e.g., kaolinite, illite, montmorillonite) and feldspars. Feldspars occur at a much lower abundance as clay minerals (low (Na+K+Ca)/Si and (Mg+Fe)/Si ratios). However, the three sampling days show slight differences in the distribution of particles within the ternary plot. On Jan. 25th (Fig. 34a), and to a lesser extent on Feb. 5th (Fig. 34c) more particles have high Al/Si ratio (> 0.5) and a low (Na+K+Ca)/Si

ratio (< 0.25) indicating a lower presence of feldspar minerals. These differences appear to be related to the back trajectories of the air masses. On Jan. 25th the air masses were transported over the Gulf of Guinea at high altitudes (see trajectories), and the aerosol contains more clay minerals compared to the other samples. In contrast, the aerosol arriving at Cape Verde directly from the continent has higher abundances of feldspars and appears stronger mixed. This becomes even more obvious, when plotting only the samples related to distinct trajectories. The above described plot is shown for three samples respectively with similar trajectories of different days in Fig. 35. The number of particles is comparable (1591 and 1722). Dust moving westwards across the ocean from the African coast is described to derive from different sources and therefore potentially contain different mineral mixtures (Moreno et al. 2006).

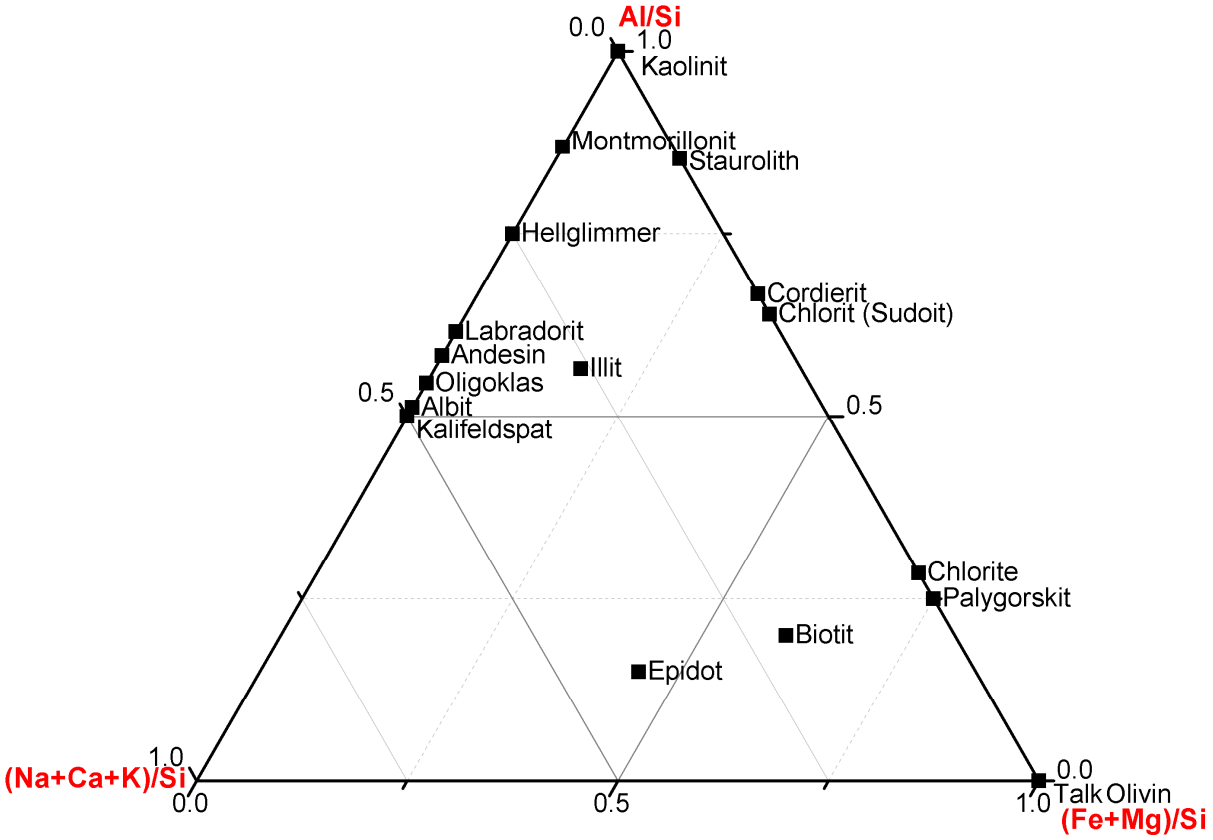

Fig. 33 Ternary plots of silicate minerals (pure phases)

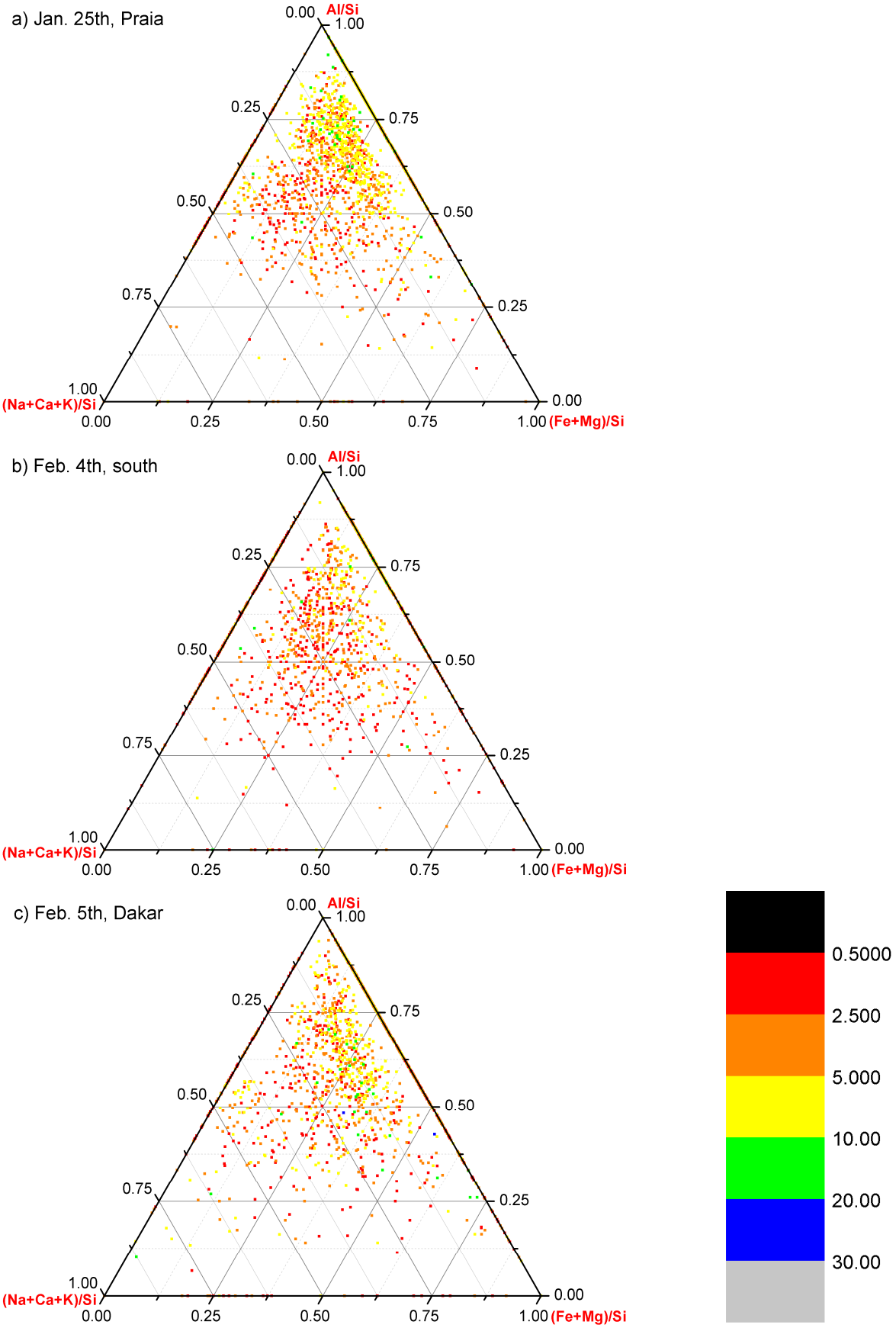

Fig. 34 a - c Ternary plots of silicate particles, particle size is given in colour, values in µm

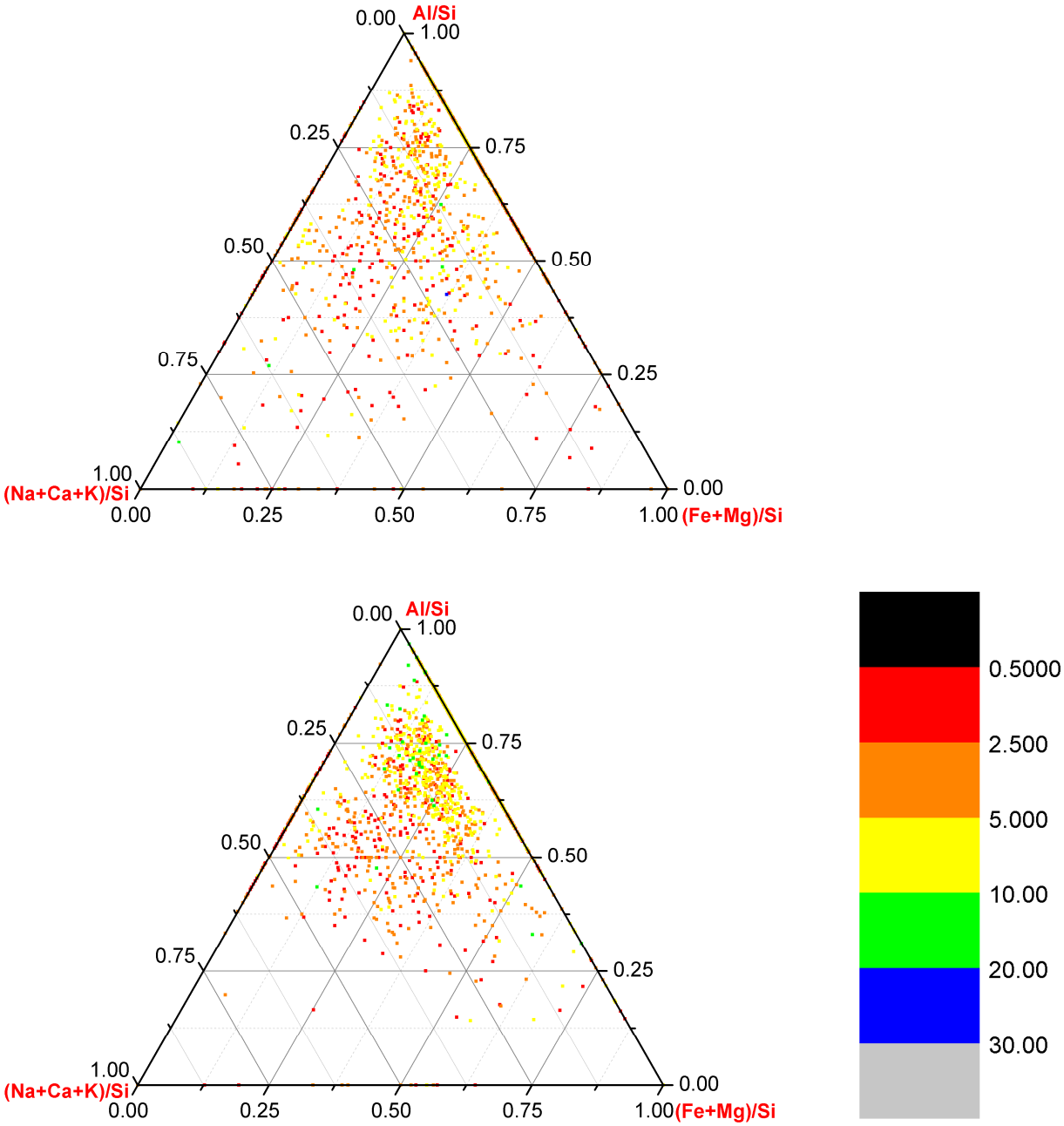

Fig. 35 Ternary plots of silicate particles for distinct trajectories for (upper diagram) mid level, (lower diagram) high level altitudes, particle size is given in colour, values in µm

The complex mixing state of mineral dust can also be seen by TEM, most particles studied consisted of several phases. Many particles classified as silicates (based on the chemical composition by EDX) contain small nano meter sized crystallites of iron oxides either as inclusions or on the surface (Fig. 36). In few cases, the iron oxide grains could be determined by selected area electron diffraction as hematite. Based on

element mapping, small iron oxide crystallites within or on the surface of silicate grains were detected frequently in airborne samples from Morocco (Scheuvens et al. 2011, Figs. 4 and 5 therein). The significance of the iron oxides for radiation transfer is discussed by Kandler et al. (2011b).

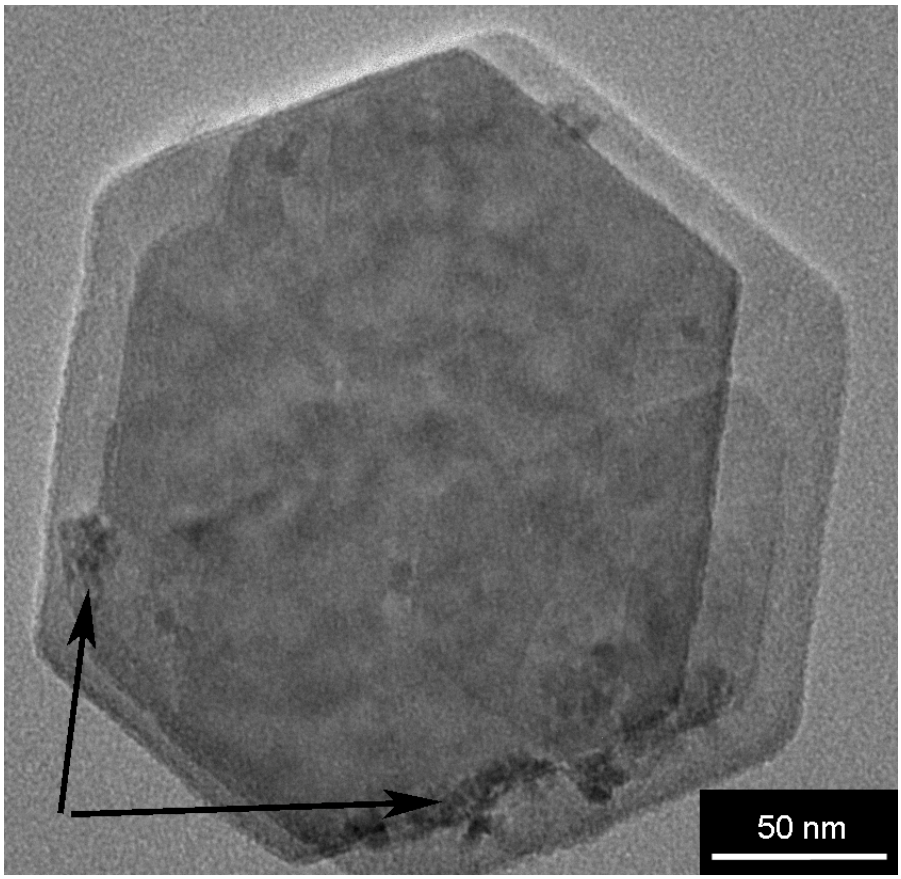

Fig. 36 TEM bright field image of kaolinite particles with iron oxide nano crystallites (arrows)

Beside iron oxides, calcite was also observed internally mixed with silicates (Fig. 37). This figure also shows that the present silicate particle is composed of many small sticks and flakes, which are likely different clay minerals.

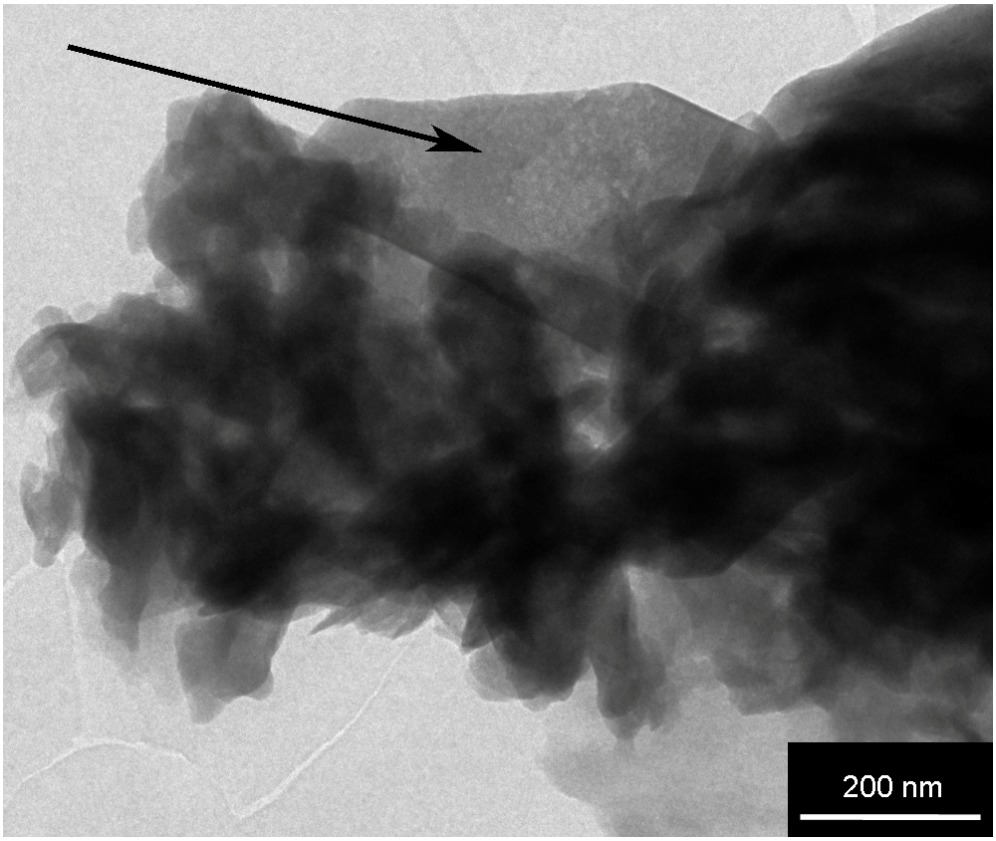

Fig. 37 TEM bright field image of a Ca-rich silicate mixture: Silicate (clay mineral) agglomerate internally mixed with calcite (arrow)

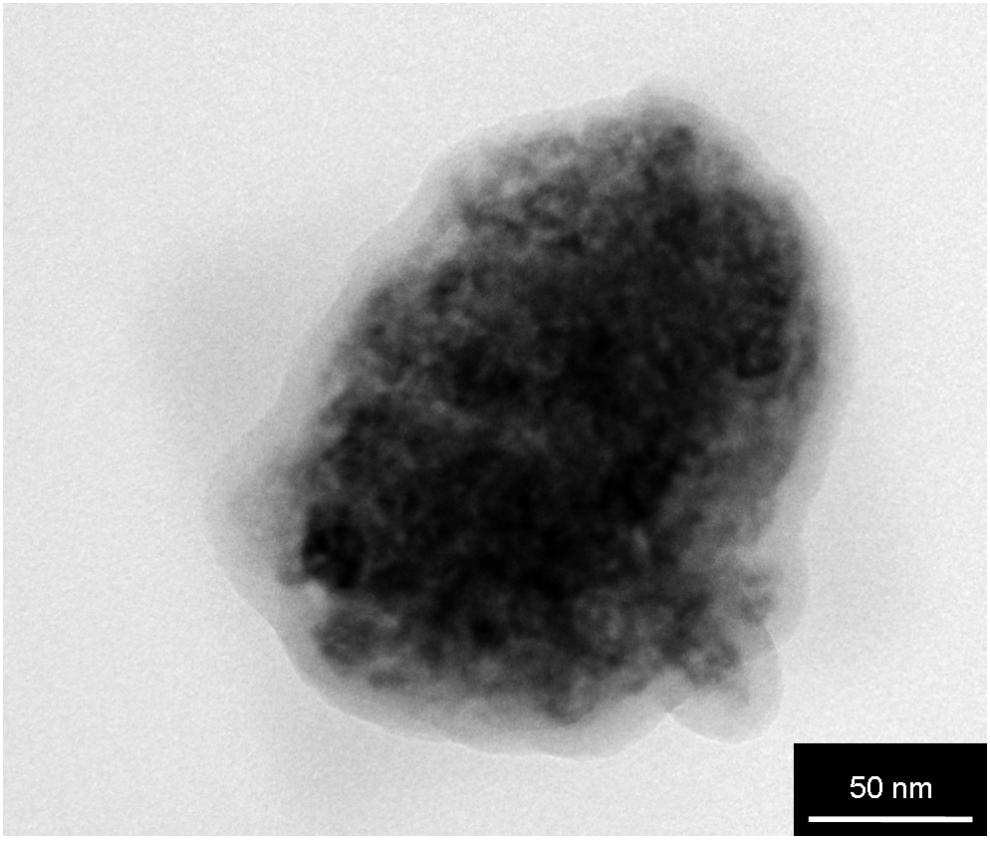

Fig. 38 TEM bright field image of a particle mainly composed of iron oxide nano crystallites

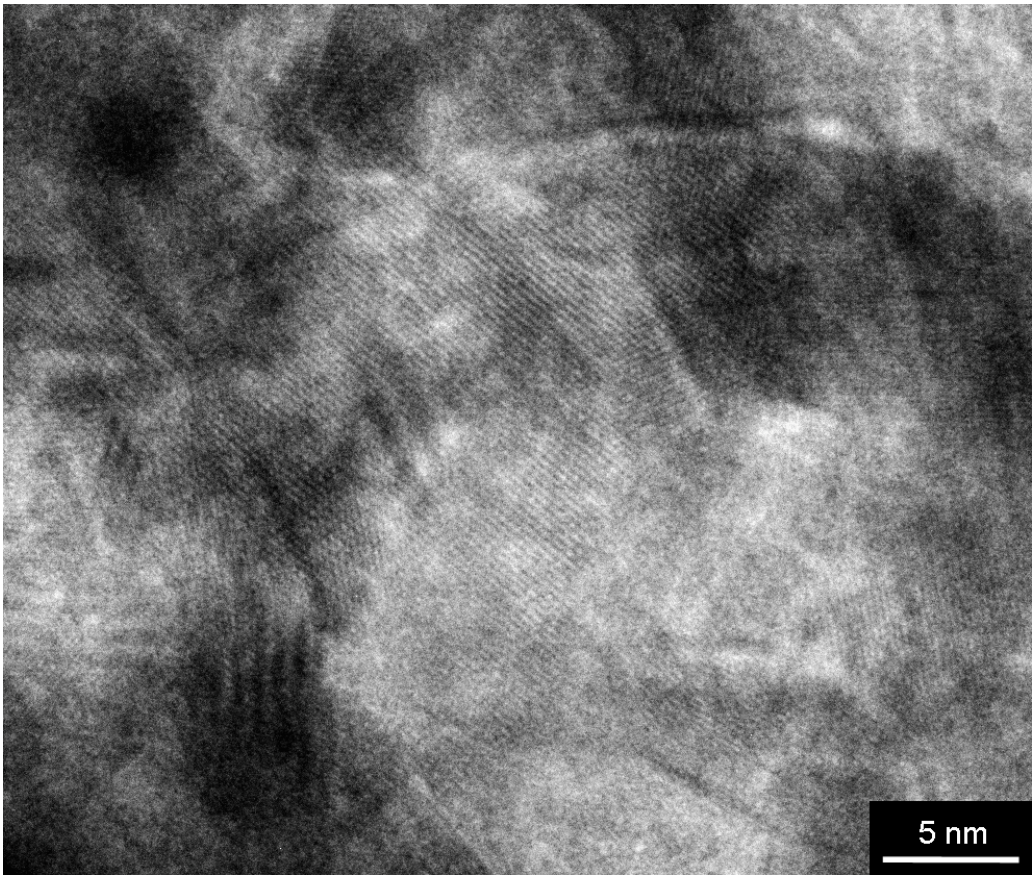

Fig. 39 TEM high resolution image of a bundle of iron oxide nano crystallites

Particles from soil samples of Burkina Faso (unpublished data) showed similar patterns as those described above. Particles were found which consisted of a core build up of iron oxide nano crystallites (Fig. 38). In Fig. 39, those iron oxide nano crystallites are shown in high resolution. The size of the primary crystallite grains ranges from approximately 5 to 10 nm.

In Fig. 40, an amorphous margin was imaged, which was interpreted as coating of 10 to 20 nm thickness over the entire particle. Neither the chemistry nor the origin of the coating could be sufficiently determined, but the fact that this structure was found on nearly all particles investigated by TEM at least leads to the conclusion, that a thin coating is present. However, the present investigations revealed that hematite can be excluded as a coating of the particles in this size range. Instead, iron oxide nano crystallite may be distributed over the complete particle volume and are most likely hematite.

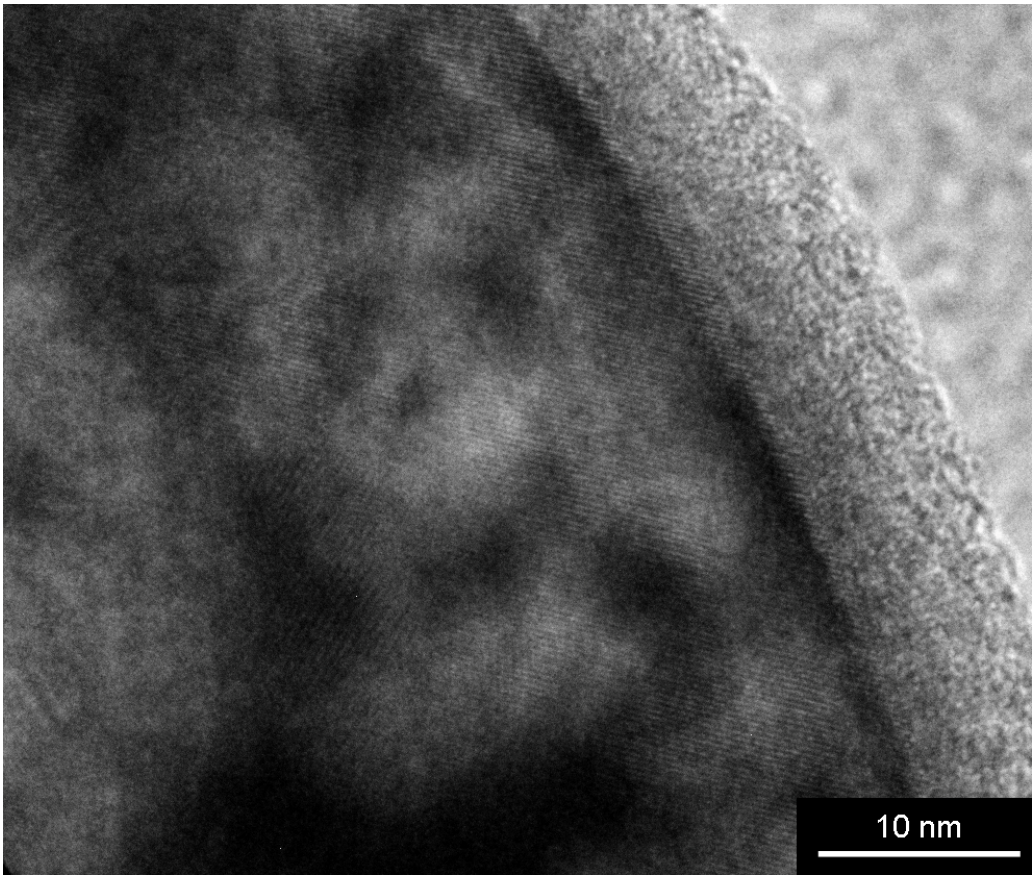

Fig. 40 TEM high resolution image of a silicate particle containing iron oxide nano crystallites and showing an amorphous margin of approx. 10 nm around covering the entire particle

Mixtures of fresh sea salt and dust were hardly found, and no multi phase mixtures of chlorine from sea salt, silicates and sulphates were observed, unlike findings of Zhang et al. (2006) for Asian dust particles. Mixtures between sulphates and silicates were found frequently, whereby silicate was always dominating the particle composition.

The investigations for sulphate coatings on mineral dust particles, as performed in Kandler et al. (2007, 2009), revealed that there is no forthright evidence on a sulphate coating on all investigates particles. The respective method is based on large numbers of particles, so that these calculations may not be conducted for every single flight leg. Large numbers of particles can only be derived by summarizing samples of different flights, as done here for biomass burning and non biomass burning samples. However, for a large number of particles no significant difference between biomass burning and non biomass burning samples was found. When plotting the element concentration per particle volume versus the particle diameter in a double logarithm plot, the linear curve fit of Silicate particles of biomass burning samples has a slope of

2.75, the one of dust samples has a slope of 2.81. It is therefore concluded that sulphate coatings do not significantly contribute to the detectable chemical composition of the particles. The same procedure was applied using the phosphorous index and revealed similar results.

As mentioned in the section above for soot particles, ammonium sulphate residues gave a hint on organic coatings on particles. The coating did not alter or change, after the underlying ammonium sulphate component of the particle obviously disappeared completely. Coatings on dust particles are for example described in Takahama et al. (2010) and support the idea of an organic or at least carbonaceous coating on particles, although the characteristics of the coating in the present study cannot be further determined. Deboudt et al. (2010) recently reported carbonaceous coatings on African dust particles from a site strongly influenced by urban emissions and biomass burning aerosol.

4.6 Refractive index

The layer structure of the aerosol has to be taken into account when modelling the optical properties of the aerosol column. Especially the soot particle abundances show a very high variation between the separate layers. The complex refractive indices were calculated for every flight level. For each size class, an average refractive index was calculated from the refractive indices of the individual particles. In appendix C the averages for wavelengths from the near ultra-violet to near infrared spectral region are given for selected cases. Values for all other days can be taken from file RI_Falcon of the electronic supplement. For the real part, n, values between 1.53 and 1.72 for biomass burning, between 1.55 and 1.70 for marine influenced samples and between 1.55 and 1.63 for dust samples are obtained for a wavelength of 532 nm. The imaginary part shows a strong spectral dependency in contrast to the real part. Four different cases are shown in Fig. 41: (a) biomass burning on Jan. 25th at 3300 m a.s.l.; (b) mineral dust case on Feb. 5th at 700 m a.s.l.; (c) marine boundary layer with possible urban influence on Feb. 5th at 500 m a.s.l.; and (d) mixed marine, dust, and biomass burning aerosol on Feb. 4th at 500 m a.s.l. In general, a tendency of decreasing absorption with increasing particle size is observed, obviously caused by the decreasing amount of soot particles as well as by the decreasing iron content of

the mineral dust with increasing particle size. As a result, this behaviour is pronounced for the biomass burning case and less obvious for the dust and marine cases, where soot is less abundant. The spectral dependency of the absorption shows clear differences between the four separate cases. While for the biomass burning layer (Fig. 41a) there is a high absorption and no dependency on wavelength for the small particles – indicating the dominance of soot in this size range –, the hematite signature becomes clearly visible for particles larger than 500 nm (due to admixed mineral dust). As expected, this behaviour is even more pronounced in the dust case (Fig. 41b), where also the small particles show decreasing absorption with increasing wavelength, though as much as for the particles larger than 500 nm. In the marine boundary layer case (Fig. 41c); the values of the imaginary part of the refractive index are in general much lower, due to the low abundance of absorbing components (soot, hematite). However, as some mineral dust is admixed to the marine aerosol, absorption by hematite plays some role for particles larger than 500 nm. Between 250 nm and 500 nm there is a very low absorption, as only few mineral dust and soot particles were found among the sulphate dominated aerosol. Finally, the mixed aerosol (Fig. 41d) appears as superposition of the three other cases. The small particles have no spectral dependency, reflecting the soot dominance, while the absolute values of absorption are somewhat lower than in the biomass burning case. A similar minimum like in the marine case with low absorption - though less pronounced - is visible between 250 and 500 nm. For particles larger than 500 nm, the hematite spectral signature as main absorbing component of the mineral dust becomes dominant with absolute values of imaginary part between the dust and the marine case.

For the size-resolved complex refractive index, knowledge of the size distribution is not necessary. Calculation of the complex refractive index of the total aerosol requires the particle volume distribution. As the measured size distribution is not available until today, the volume-weighted total composition of the sampled aerosol was not yet calculated.

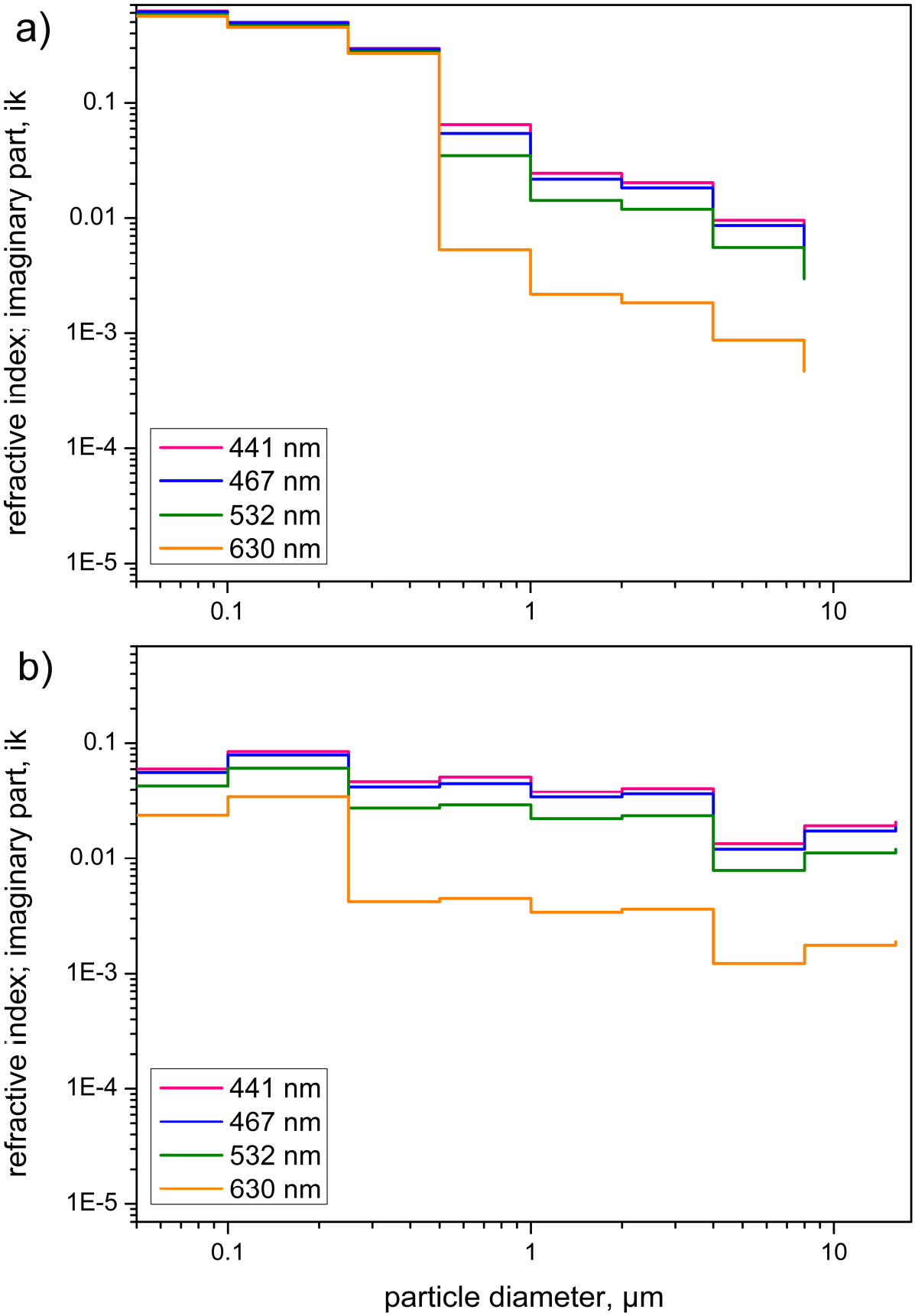

Fig. 41 a (upper) and b (lower) Imaginary part ik of the average refractive index as function of particle diameter at different wavelengths for (a) a biomass burning sample, Jan. 25th, 3300 m a.s.l.; (b) a dust sample, Feb. 5th, 700 m a.s.l.

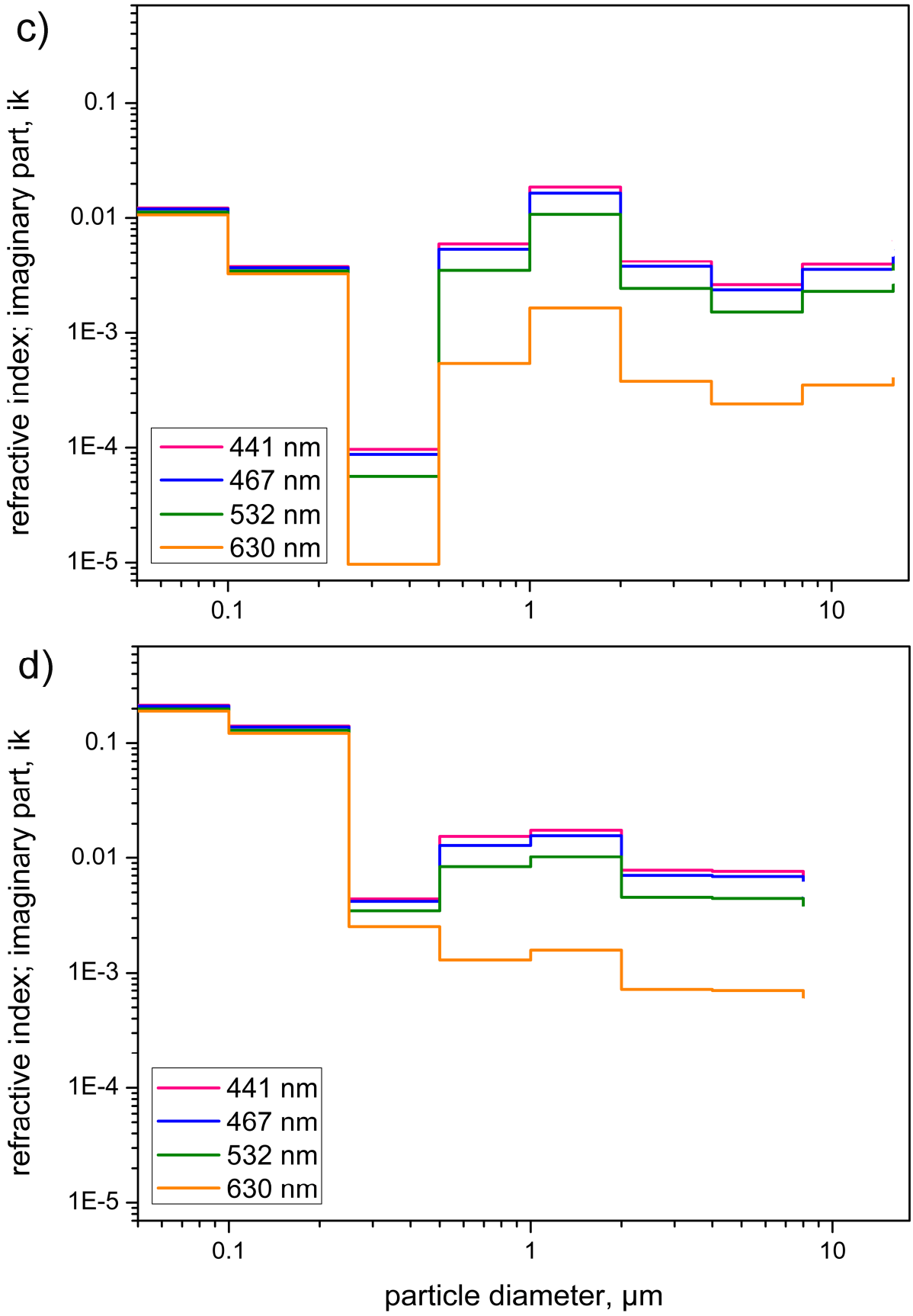

Fig. 41 c (upper) and d (lower) Imaginary part ik of the average refractive index as function of particle diameter at different wavelengths for (c) marine boundary layer aerosol mixed with urban ammonium sulphate, Feb. 5th, 500 m a.s.l.; and (d) marine boundary layer aerosol mixed with biomass burning and dust, Feb. 4th, 500 m a.s.l.

5 Discussion

5.1 Error discussion

5.1.1 Confidence intervals

A confidence interval is known to be a range, calculated from random sample values, that includes the true (unknown) parameter with a certain probability and allows the estimation of how closely the sample matches the true value. The 95 % confidence interval would thus be a range, in which the true population value would be included in 95 of 100 cases, if sampling and analysis would be repeated under the same conditions. The confidence intervals for all particle classes are calculated using the multinomial distribution after Hartung et al. (2005) and are given in the electronic supplement. The absolute width of the confidence intervals decreases with growing number of particles in a size interval. The relative width decreases with growing number abundance of a particle group. Considering for instance the sample (FA_109 of Jan. 23rd, 2008) having a total number of 1320 particles in the small particles size range (d < 0,5 μm), the confidence interval for soot particles with a relative number abundance of 86 % is [81,4 – 89,8] and the confidence interval for silicate particles with a relative number abundance of 3 % is [1,4 – 5,8]. On the other hand, for the sample (FA_129 of Jan. 29th, 2008) with a number of 199 particles in the large particles size range (d < 0,5 μm), the confidence interval for silicate particles with a relative number abundance of 75 % is [60,5 – 86,6], and for the silicate class with a relative number abundance of 9 % is [3,3 – 22,1]. The above mentioned statistical consideration does only refer to the number of analyzed particles. This approach assumes that all analyses are of the same quality.

In the present study, for automated analysis a virtual grid was placed over the impaction spot. Size of the matrix and magnification were chosen to cover most of the particles or a representative cross section from the center of impaction towards the edges. However, as the samples conditions are varying in quality and particle load, it was not always possible to gain about the same number of particles from the same area and sometimes, even the total area available only provided a low number of particles. There is in fact a strong variability in the number of analyzed particles.

5.1.2 Particle collection

By collecting the aerosol particles by means of particle collectors mounted on an airplane, only a small part of a population (e.g., the particles in an aerosol layer) was sampled but was considered to be representative of the actual total population. Of course, any estimates obtained from a sample do only approximate the actual population value.

As above mentioned it was assumed that all analyses are of the same quality and that the sampling and analysis conditions were exactly the same for each sample. In reality this situation can only be approached. Especially the small stage samples experienced strong forces, when the air was accelerated through the nozzle and hit the sampling substrate. In most cases, a part of the foil within the grid was destroyed, but major parts of the sample were still suitable for analysis.

To address in general the significance of a measurement of the mixing state by an off-line single particle analysis method, the coincidence error has to be estimated, i.e. the chance that a newly depositing particle touches another particle, so that the particles can't be discriminated by their shape and internal mixing is detected as an artefact. Kandler et al. (2011b) give the easiest model of coincidence error determination by estimating the chance of touching for a newly impacting, infinitely small particle. This chance corresponds to the area fraction covered by the already deposited particles. The mean area coverage fraction for all ground based samples was 0.025, so the average coincidence error over the sampling time is 0.013. Assuming homogeneous impaction behaviour, the sum of the relative abundances of all mixture groups must be greater than this value to be significant. As the particle load on the flight samples is comparable (0.025 mean area coverage fraction derived by image analysis, ImageJ version 1.43u), this prevails for most of the samples regarded in the present study as well.

5.1.3 Methods of analysis

The vacuum conditions in SEM and TEM may lead to a loss of volatile compounds in or on particles during or prior to analysis. This may also lead to a reduction of the original particle size. Posfai et al. (1998) found a reduction of 50 % of the particles size for complex internally mixed aerosol particles due to high vacuum conditions in TEM. Those particles may be comparable to internally mixed ammonium sulphate

particles of the present study. However, for rather dry mineral dust particles, the reduction of particle size due to loss of volatile compounds (including water) is regarded as negligible. All samples were stored and transported under dry conditions, derived through the presence of silica gel (30 % relative humidity).

The size determination as equivalent projected area diameter may lead to an overestimation of particle size, if the particles are orientated on the substrate. The assumed height of particle might be smaller compared to length and width. The error is assumed to be around 30 to 40 % (Ebert et al. 2002), if the porosity is regarded as being negligible. Contrarily soot agglomerates include a porosity of 26 to 90 % (Ebert et al. 2002) depending on their structure and size. Most soot agglomerates regarded in this study are rather small, but appear in elongated forms. For larger soot agglomerates the porosity might be around 75 %, but the smaller ones composed of only 2 to 5 primary particles (which are most abundant) might have a porosity of 30 – 40 %.

Due to a software error, the size and aspect ratio were not determined accurately for all samples used in the present study. While the size (aquivalent projected area diameter) could be corrected by a factor of √(1,28), the aspect ratio derived by the EDAX Genesis software had to be rejected.

Automated single particle analysis with EDX (also EPMA) is a common tool for the investigation of aerosol chemical composition (e.g., Weinbruch et al. 1997, Ro et al. 2002, Laskin et al. 2003). For characterization of complex aerosol particles, low element concentrations have to be taken into account. X-ray analysis intensities do not yield reliable quantitative results. A rough quantitative information is derived through normalization of the considered elements (as mentioned in chapter 3.3), corrected for matrix- and geometric effects. It is to be emphasized, that the intensities do not necessarily represent the real element concentration within the particle; however, the approach is suitable to sort particles into the above mentioned groups and classes. ZAF correction was applied to asses the differing magnitude of X-ray emission, due to atomic number (Z), absorption (A) and fluorescence excitation (F) in the sample, but not for particle shape effects. The concentration of carbon, nitrogen, oxygen, cupper and nickel in the particles cannot be determined accurately due to a contribution of the sampling substrates or weak signals. As a result, nitrogen compounds and organic matter could not be investigated quantitatively. Effects based on the complex particle

geometry compared to ideal polished samples may occur (Goldstein 2007) and interactions with the underlying substrate can not be neglected. If the geometric effects are not corrected, large errors for the mean values up to 15 % (relative) are incurred (Weinbruch et al. 1997). Particles size and shape effects (Armstrong 1991, Ro et al. 2002, Laskin et al. 2006) could not be regarded in this work.

5.1.4 Particle classification method

Uncertainties remain in the selection of the classification criteria ranges, separating one group from another. In particular the assignment of different mixture classes is debatable. However, the classification criteria were only determined after considering a large number of individual particles. Classification criteria were carefully compared to those published by other Authors (e.g., Ebert et al. 2002, Vester et al. 2007, Kandler et al. 2007, 2009) using the same or at least comparable methods. The uncertainty is diminished when summarizing the particle groups in to classes. However, the classification criteria for groups are listed in appendix A.

Sampling artefacts were occurring mainly on the impactor samples and were more frequently found on the small stage. The characteristic chemical composition and morphology was determined by TEM analysis on the small stage samples and they were excluded from the classification by their chemical composition. Those particles were mainly composed of the elements iron, chlorine, silicium, chromium, manganese (sorted by decreasing abundances) and others to minor extent. Particles were conical sticks in the range of some tens of nanometers or agglomerates of those sticks. TEM high resolution images and electron diffraction revealed a crystalline structure of different orientations. The source of these particles could not be sufficiently determined, but they most likely can be assorted to metallic ingredients in the rubber gasket of the impactors and the aircrafts aerosol inlet, which have a similar chemical composition. Another possible source for Fe-Cl-bearing particles are high temperature combustion processes as occurring in waste incineration (see for example Wang et al. 2001). However, the particles mentioned above are present in almost every sample. Particles of a point source (like a local waste incineration) would not frequently occur on all sampling days and at all sampling coordinates.

Al-bearing sampling artefacts appeared only on the GPaC samples and could be associated to the mechanical parts and housing of the GPaC. They occurred as chips

and could be excluded from the analysis by their characteristic morphology and count rates.

The element index used in the present study is not an exact quantification of elemental contents but may be regarded as a systematic tool for mixing state discrimination.

5.2 Distribution and mixing state in the aerosol column

The Aerosol of the Cape Verde region, off the West African coastline and over Senegal and Dakar, is composed of transported Saharan mineral dust, sea salt and aged sea salt, soot from biomass burning of huge bushfires throughout the Sahel, and secondary particles (ammonium sulphate). A variation of these components in number abundance was observed locally and within the aerosol column.

5.2.1 Aerosol layer structure

The evaluation of the samples taken on each of the sampling days revealed a distinct aerosol layer structure. Layer structures over the Cape Verde and adjacent Atlantic region with such a large lateral extension were not documented before. The layer structure depends on meteorological conditions. Typically, biomass burning layers, desert dust layers, and mixed layers can be clearly identified above the marine boundary layer by aerosol chemical composition. The small particle composition is highly variable and in case of biomass burning samples dominated by soot. Mixtures of soot with silicates were not observed.

The layer structure (Figures 16 to 28) displays high stability over long range distances. The chemical compositions of particles on different flight levels are clearly different. The biomass burning layer is distinct from the mineral dust layer as characterized by the high relative number abundance of soot particles and other biomass burning aerosol. For the same layers, an increased number of non-volatile fine mode particles in biomass burning aerosol size distributions was observed (Weinzierl et al. 2011). Desert dust layers comprise a relative higher number abundance of silicate particles over all size ranges. Those silicates are composed of internal mixtures of different minerals. The silicate particles from the Saharan desert

are well mixed, however, differences in composition may be observed for different transport paths.

Biomass burning aerosol layers were observed over a large lateral extension, while there are no hints to a vertical mixing above the West African Atlantic and in the Cape Verde region. During SAMUM-2 strong southward extensions of the Azores High across the western Mediterranean and northern Africa controlled the strength of the Harmattan winds transporting mineral dust from Western Sahara to Cape Verde. To the south, synoptic-scale midlevel easterlies led to an efficient transport of biomass burning aerosol from land-fires over southern West Africa (Knippertz et al. 2011).

The enhanced absorption of radiation by soot has obviously a stabilizing effect on the layer structure. A theory regarding the general layer structure is described in Fig. 12 of Haywood et al. (2008) and depends on warmer, ascending air (biomass burning aerosol) which is forced to rise over colder, dust laden air. A resulting temperature inversion leads to a stabilizing effect, which obviously lasts over long range transport (as for example shown in the present study).

5.2.2 Mixing state

Due to the high stability of aerosol layers, internal mixtures of different aerosol types (e.g., sea salt internally mixed with dust and biomass burning) are seldom, in contrast to samples of Asian dust (Zhang et al. 2003a, 2006). The observed internal mixing of mineral dust obviously occurs prior to (long range) transport and thus prior to the mixing of biomass burning air masses with dust laden aerosol. Accordingly, no internal mixtures of these two components are observed. Mixtures of mineral dust and sea salt may occur through turbulent mixing close to the sea level (marked through fresh sea salt particles incorporated in the complex aggregates (Zhang et al. 2003a)) or prior to long range transport by mixing of old marine air masses with freshly emitted dust (marked through aged sea salt). Air masses, which are described as “clean” (Heinold et al. 2011, Knippertz et al. 2011), are usually indicated by a lower abundance of the silicate class, resulting in a dominance of sulphate particles in the large particle size range in the samples. Those samples might reflect a background aerosol, whereas the sulphate might represent aged sea salt as described above. Another explanation might be the industrial and urban pollution from large urban settlements along the Gulf of Guinean coast, which may contribute to the high

amount of absorbing aerosol in this region. If dust laden air is mixed into the background, the relative number abundance of sulphates is reduced. From the chemical composition it can not be answered whether the layers which obviously belong neither to biomass burning nor desert dust, are composed of marine or background aerosol. As they contain a large number of other sulphates (sodium sulphates most abundantly) they might represent a marine influenced background aerosol, probably with very aged sea salt.

Internal mixtures of mineral dust (i.e., silicate particles) with soot were not observed in the present study, while external mixing occurred between small soot particles and large mineral dust particles. Deboudt et al. (2010) report externally mixed soot and mineral dust at a sampling location near the Atlantic coast, where Saharan dust plumes mix with biomass burning aerosol. The occurrence of solely external mixtures was described previously by Haywood et al. (2008) and Formenti et al. (2008). On the other hand, Hand et al. (2010) reported the evidence of internal mixtures of soot with mineral dust particles by airborne observations in the vicinity of Niamey, Niger. It should be mentioned that the examples shown therein are rather large particles (d $\sim$ 10 μm, agglomerates of soot chain-like particles with large silicate particles) which are likely occurring near the source, but probably not going into long range transport. The present study does not provide a definite answer to the question, why the external mixing (obviously) only affects large particles. It is therefore recommended to focus on this question in subsequent studies.

Internal mixtures of dust with fresh sea salt were rare. Although some of the samples were taken at low level altitudes above the sea, marine boundary layer aerosol was not very dominant and often restricted to the very low altitudes (200 m a.s.l.). This indicates a high stability of layers with almost no vertical mixing, probably due to the lack of turbulences.

The mixing state of silicate particles is slightly variable. Clay minerals, in particular kaolinite, and feldspars can be regarded as a major constituents in mineral dust particles. Iron oxides (most likely hematite nano crystallites) and to a minor extent calcite, contribute significantly to the chemical composition of silicate mixtures.

5.2.3 Coatings

Deboudt et al. (2010) observe an organic coating on marine and carbonaceous (i.e., soot) particles. This may be due to strong pollution influence of African cities.

The frequent occurrence of coatings consisting of organic compounds or nitrate can not be neglected and TEM investigations posed strong hints on their existence on all kinds of particles (as described above for soot, silicates and ammonium sulphate particles). Coatings have been observed in all kinds of particles by Takahama et al. (2010), for Asian dust by Li and Shao (2009) and Zhang et al. (2003b), and for African dust by Deboudt et al. (2010). Knowing the composition of particle coatings would be interesting regarding the effects they can have (for example on the cloud condensation ability of particles).

As mentioned in Kandler et al. (2011b), nitrate and organic components could not be regarded for refractive index determination, but it is rather assumed that their impact on the overall refractive index is low i) due to their most probably small volume contribution and ii) due to comparatively low light absorption (Hoffer et al. 2006, Schkolnik et al. 2007). However, absorption amplification effects (Schnaiter et al. 2005), (Worringen et al. 2008)) can't be accounted for by the model (applied in this study for deriving a complex refractive index).

Amplification effects occur for example, when black carbon (soot) and a non absorbing component (e.g., sulphate or water) mix internally or when soot particles are coated with non absorbing secondary organic matter (Schnaiter et al. 2005).

There are many hints on organic, carbonaceous or other (nitrate) coatings on all kinds of particles (silicates, ammonium sulphates, soot), although the chemical composition thereof could not be determined in the present study. In order clarify, whether they alter or change with distance to the source region and whether they could be linked to transport paths of the aerosol, it would be required to analyze the chemical composition of the coatings

5.2.4 Biomass burning

The biomass burning aerosol is almost exclusively represented in the small particles size range, whereas mineral dust is present in all particles sizes. In many cases, not even a single silicate particle is found among the small particle size range of biomass burning samples, as it is in dust samples. The question remains, where the larger

mineral dust particles in the biomass burning layers originate from. The contribution of local soil particles due to thermal uptake can be neglected (as suggested by other studies e.g., Haywood et al. 2008), because the silicate particles show the same chemical composition in biomass burning samples as in dust samples, rather than a fingerprint of local soils. Large mineral dust particles might have been present in the background air stream, which provided the air for the burning process. The fact that biomass burning is frequently injected into an already turbid, dusty environment was described by Haywood et al. (2008) and Formenti et al. (2008) as observed during the AMMA field campaign.

Tar balls, which Deboudt et al. (2010) associated with a biomass burning influence in their samples, were not detected. They may probably not be visible on the present samples, due to their chemical composition.

In this study, Potassium served as a tracer for biomass burning. The aging of biomass burning aerosol was observed using element indices ratios of potassium and sulfur and chlorine, respectively. It is shown that the observed aerosol in most cases is aged. If such state of aging implies, that all particles are coated (probably with non absorbing components) this may have a strong influence on the absorption properties of biomass burning aerosol.

Biomass burning aerosol seems to be restricted to the small particles size range. Those layers include large amounts of mineral dust in the large particles size range, but never internally mixed with soot.

5.2.5 Mineral dust

Regarding the differences in silicate composition for the highest trajectories (as described above), a period of strong dust production in the Bodélé during the period of measurements is described (Heinold et al. 2011, Knippertz et al. 2011). The observed differences within the silicate class could possibly be linked to long range transport from the Bodélé with easterly waves. The mineral dust composition at the source with a low feldspar contribution is represented in the samples. Clay minerals, in particular kaolinite, can be regarded as a major constituent in mineral dust particles. The observed variety of elemental ratios in silicate particles, differing from an ideal elemental ratio in silicate minerals, is driven by the agglomeration of smaller

particles on larger ones or with each other. Those agglomerates clearly dominate the aerosol transported over the Atlantic. Aging effects were not observed.

Iron is one of the most important compounds of mineral dust with respect to atmospheric processes (radiation transfer, ice nucleation, input of nutrients into ecosystems). It can be present in particles as different species (e. g., Lázaro et al. 2008). Iron can be incorporated into the crystal structure of clay minerals where it does not influence optical properties significantly (Karickhoff and Bailey 1973). In contrast, Jaffe (1988) showed an increase of refractivity in isostructural series, with increasing density, which is obviously correlating with the iron content. However, the large variety of iron content in silicates as observed in the present study is possibly caused by iron oxide nano crystallites, which in most cases could be identified as hematite. Nine out of ten investigated particles contained hematite, as determined by electron diffraction (reflections matching lattice distances of hematite) whereas no other iron oxide phases could be detected. A quantitative estimation of the total iron oxide content can not be made within the present study, but obviously those iron oxide nano crystallites are abundant in mineral dust, as also shown in other studies (e.g., Kandler et al. 2009, Scheuvens et al. 2011) and therefore should play an important role, regarding the radiative forcing. Average total iron contents for African mineral dust of 6 to 8 % are given by Lafon et al. (2004), whereby half of the iron content is supposed to be iron oxide.

In the present samples, neither the iron content nor the calcite containing mixtures could be linked to possible source regions, which proofs a strong mixing of mineral dust prior to long range transport and probably close to the source.

5.2.6 Refractive index

The complex refractive indices determined in the present work are significantly different for various aerosol types encountered. Soot and hematite (the latter incorporated into the mineral dust) are the dominating light-absorbing compounds. Their spectral signature is clearly visible in the corresponding size ranges. In the biomass burning cases, the small particles size range is dominated by soot absorption, while the large particles size range is still mineral dust-dominated. In the mineral dust case, also the small particles show a hematite spectral signature, though less pronounced as for the large particles. A decrease in absorption for all wavelengths

with increasing particle size is visible, which decrease is the strongest for the biomass burning case. In the marine case, the particle absorption is generally lower, as the aerosol mass is dominated by sea-salt and sulphates. Still, the spectral features of soot and hematite are visible. The same is true for the mixed case, appearing as the average over the other cases.

Conclusions

This study clearly demonstrated that the aerosol in the vertical profile over the Cape Verde region can not be regarded as one homogeneous mixture of different particles. In principle, an enhanced absorption of radiation in a layer on a particular level may either stabilize or destabilize the atmospheric layering and thereby provide another independent parameter of air interchange and the formation of a weather pattern. However, the mere existence of the distinct layer structure seems to indicate that the stabilizing effects are dominating.

To model the radiative effect of the aerosol column, it is necessary to regard the present layer structure. Quijano et al. (2000) demonstrated by model radiances (as observed by a satellite) that, in the presence of absorbing aerosols, the observed optical depth can be over- or underestimated by a factor of two or more, depending on the relative position of different aerosol layers. The sensitivity of shortwave radiation fluxes on changes in the vertical distribution of layers was quantified by Gomez-Amo et al. (2010). They found that notable changes occur in the surface and top of the atmosphere diffuse fluxes, strongly depending on the boundary layer properties, probably caused by urban (e.g., strongly absorbing) and marine (highly scattering) aerosol particles. In the present study it was shown, that the imaginary part of the refractive index within the column is highly variable due to the abundance of soot particles. Biomass burning aerosol has a significant effect on the atmospheric radiation budget due to its strong absorbing properties and is known to have a warming effect. The negative effect from ammonium sulphate can be diminished by internal mixing with soot (Lesins et al. 2002). Chapter 4.6 demonstrated the variability in the relative contributions of biomass burning and mineral dust aerosols to the scattering and the absorption. In addition, the vertical extension of the layers in the aerosol column is to be estimated from LIDAR measurements. A current model (Heinold et al. 2011) combines recent developments in mineral dust modelling and accounts for aerosol radiative effects on dust and smoke transport and captures the observed complex layering of the mixed aerosol plume. However, the physics underlying radiative forcing are rather complicated since for instance reflection of wavelengths high in the atmosphere which otherwise would be absorbed from lower layers may prevent a positive radiative forcing by for instance soot in a lower layer.

Therefore, to assess the effect of layered aerosols upon the surface radiation budget, an enhanced radiative transfer model study would have to be applied including this layer structure and comprising the newly available data as received during the SAMUM-2 field campaign and in parts presented in this study.

It was unexpected to find mineral dust and biomass burning aerosol (still) externally mixed after long range transport and with obviously large lateral extent. It can be assumed that due to the stability of layers, this separation of different aerosol types lasts even further over the mid Atlantic towards the American continent.

A general observation was that, within the Cape Verde region and thus a remote area in terms of long range particle transport, it was not possible to distinguish source regions for mineral dust particles. Despite that, as observed in only few samples, a difference in southward transported high altitude air masses was observed, which proofs that the influence of the source region composition can not be neglected.

In the present samples, neither the iron content nor the calcite containing mixtures could be linked to possible source regions, which proofs a strong mixing of mineral dust prior to long range transport and probably closed to the source.

Internal mixtures of silicate particles (representing mineral dust) and sulphates (most probably aged sea salt) are occurring frequently to varying abundances, whereby no pronounced height dependence could be observed. This leads to the assumption that air masses already carrying aged marine aerosol mix with fresh mineral dust, which than proceeds into long range transport over the Atlantic Ocean.

There are many hints on organic, carbonaceous or other (nitrate) coatings on all kinds of particles (silicates, ammonium sulphates, soot), although the chemical composition thereof could not be determined. It would thus be an interesting task to analyze the extent and chemical composition of the coatings, in order to consider the resulting modification of the refractive index.

The results in the present work also leads to the question, why there occurs no internal mixing of biomass burning and desert dust aerosol.

Now, for different regions over the Atlantic Ocean, very detailed particle data in the aerosol column can be provided, in addition to existing data in the aerosol column over the continent (as above cited). The existence of a layer structure and the detailed knowledge of the composition of the layer structure pose the question whether the

combination thereof affects the surface radiation budget by radiative forcing of particles.

While many properties of particles could be gathered by means of scanning electron microscopy, which provided important data for determining the conditions of mixtures, this method has rather limited capabilities when considering organic coatings and the inner structure of more complex multiphase particles.
Therefore, further investigations were preformed by means of transmission electron microscopy which yielded supplementary findings.
Transport mechanisms which finally lead to the formation (or non-formation) of particle mixtures, may only be described by means of large scale transport models. The radiation absorption efficiency of different aerosols stacked in several layers above one another will have to be calculated by means of radiation transfer modelling.
In that respect, the refractive indices derived by the present study, will provide at least a first approach and clearly indicate that aerosol layers arising from biomass burning are most important for the radiation absorption efficiency.
The data from the single particle analysis by electron microscopy directly affect the radiation models (Köhler et al. 2011) as well as the models for correction and calibration of other measuring devices on board of the Falcon aircraft (Petzold et al. 2011). Aerosol properties derived by LIDAR measurements (Gasteiger et al. 2011, Gross et al. 2011, Engelmann et al. 2011) could be evaluated under consideration of the additionally obtained information on size and morphology as well as the chemical composition of the gathered aerosols. The present particle data provide important reference values for future model studies.
Source areas of mineral dust apparently only play a minor role on long range distances. Nevertheless, by an even more in depth exploration it would be desirable to investigate the aging of biomass burning aerosols, in particular with regard to coatings on soot particles, which appear to have an amplification effect on the absorption properties of the aerosol.

Acknowledgements

I acknowledge the NOAA Air Resources Laboratory (ARL) for the provision of the HYSPLIT transport and dispersion model and/or READY website (http://www.arl.noaa.gov/ready.php) used herein.

This work was conducted within in the SAMUM project. Financial support by the DFG (Deutsche Forschungsgemeinschaft) is gratefully acknowledged. I like to thank TACV Cabo Verde Airlines for great logistic and financial support. The field campaign strongly benefitted from logistic support by Antonio Fortes. The DLR (German Aerospace Center) provided the sampling aircraft and supported this thesis with data. PD Dr. Andreas Petzold, Dr. Bernadett Weinzierl, Susanne Mund and Andreas Veira are gratefully thanked for logistic support and useful discussion.

Christian von Glahn and Klaus-Dieter Wilhelm (Johannes-Gutenberg-Universität Mainz) were deeply involved in the development and construction of the Giant Particle Collector. Carmen Emmel (former Johannes-Gutenberg-Universität Mainz) helped with the collection of samples. I like to thank Dr. Lothar Schütz (Johannes-Gutenberg-Universität Mainz) for logistic support, for providing literature and for useful discussions, which accompanied my work throughout the field campaign and the years after.

Prof. Hans-Joachim Kleebe and his group at the Technische Universität Darmstadt are thanked for access to the transmission electron microscopes and for technical support. Special thanks are to Dr. Nathalie Benker and Jens Kling for guiding support with TEM operation.

I thank Prof. Daizhou Zhang for his bountiful hospitality and the opportunity he provided me to study at the Prefectural University of Kumamoto in Kumamoto, Japan and also for giving me the opportunity to travel to China. Financial support by the Haiwa Nakajima Foundation for my stay in Japan is gratefully acknowledged.

I like to thank my Professor Stephan Weinbruch for his trust in me, his guiding support and useful discussion for many years. Last but not least, I am deeply grateful to Dr. Konrad Kandler (Technische Universität Darmstadt) for supervising and instructing me, which more than anything else enabled me to conduct the present work. He basically developed and generously provided the Giant Particle Collector. Dr. Dirk Scheuvens and PD Dr. Martin Ebert (Technische Universität Darmstadt) are

thanked for useful discussion. Furthermore I thank Thomas Dirsch and Astrid Zilz for logistic support, and beyond that for their cordial friendship and good advices. The working group (so far they have not been mentioned above) I want to thank for useful discussions and of course for cheering me up with coffee, candy and comics (probably wouldn't have made it without all that).
I thank my parents and my partner Jens for their encouragement, in particular my father Dr. Winfried Lieke for reading.

I thank all commissioners for reading the present study.

References

ALBRECHT, B. A. (1989): Aerosols, cloud microphysics, and fractional cloudiness, Science 245, 1227–1230.

ALFARO, S. C., GAUDICHET, A., GOMES, L. AND MAILLE, M. (1998): Mineral aerosol production by wind erosion: aerosol particle sizes and binding energies, Geophysical Research Letters 25, 991–994.

ANDREAE, M. O., ANDREAE, T. W., FEREK, R. J. AND RAEMDONCK, H. (1984): Long-range transport of soot carbon in the marine atmosphere, Science of The Total Environment 36, 73–80.

ANSMANN, A., BAARS, H., TESCHE, M., MÜLLER, D., ALTHAUSEN, D., ENGELMANN, R., PAULIQUEVIS, T. AND ARTAXO, P. (2009): Dust and smoke transport from Africa to South America: LIDAR profiling over Cape Verde and the Amazon rainforest, Geophysical Research Letters 36, doi:10.1029/2009GL037923.

ANSMANN, A., PETZOLD, A., KANDLER, K., TEGEN, I., WENDISCH, M., WEINZIERL, B., MÜLLER, T. AND HEINTZENBERG, J. (2011): Saharan Mineral Dust Experiments SAMUM-1 and SAMUM-2: What have we learned?, Tellus B 63, submitted Oct. 2010.

ANTHONY, J. W., BIDEAUX, R. A., BLADH, K. W. AND NICHOLS, M. C.: Handbook of mineralogy, Mineral Data Publishing, Tucson, Arizona 1990.

ARIMOTO, R. (2001): Eolian dust and climate: relationships to sources, tropospheric chemistry, transport and deposition, Earth-Science Reviews 54, 29–42.

ARMSTRONG, J. T. (1991): Quantitative Elemental Analysis of Individual Microparticles with Electron Beam Instruments, Plenum Press Electron Probe Quantitation, 261–315.

ARTAXO, P., FERNANDES, E. T., MARTINS, J. V., YAMASOE, M. A., HOBBS, P. V., MAENHAUT, W., LONGO, K. M. AND CASTANHO, A. (1998): Large-scale aerosol source apportionment in Amazonia, Journal of Geophysical Research - Atmosphere 103, 31837–31847.

BAKER, A. R., KELLY, S. D., BISWAS, K. F., WITT, M. AND JICKELLS, T. D. (2003): Atmospheric deposition of nutrients to the Atlantic Ocean, Geophysical Research Letters 30, doi:10.1029/2003GL018518.

BARBOSA, P. M., STROPPIANA, D., GRÉGOIRE, J., CARDOSO P. AND JOSÉ M. (1999): An assessment of vegetation fire in Africa (1981-1991): Burned areas, burned biomass, and atmospheric emissions, Global Biogeochemical Cycles 13, 933–950.

BATES, T. S., QUINN, P. K., COFFMAN, D. J., JOHNSON, J. E., MILLER, T. L., COVERT, D. S., WIEDENSOHLER, A., LEINERT, S., NOWAK, A. AND NEUSÜSS, C. (2001): Regional physical and chemical properties of the marine boundary layer aerosol across the Atlantic during Aerosols99: An overview, Journal of Geophysical Research 106, 20767–20782.

BEN-AMI, Y., KOREN, I. AND ALTARATZ, O. (2009): Patterns of North African dust transport over the Atlantic: winter vs. summer, based on CALIPSO first year data, Atmospheric Chemistry and Physics 9, 7867–7875.

BERG, O. H., SWIETLICKI, E. AND KREJCI, R. (1998): Hygroscopic growth of aerosol particles in the marine boundary layer over the Pacific and Southern Oceans during the First Aerosol Characterization Experiment (ACE 1), Journal of Geophysical Research - Atmosphere 103, 16535–16545.

BIERWIRTH, E., WENDISCH, M., EHRLICH, A., HEESE, B., TESCHE, M., ALTHAUSEN, D., SCHLADITZ, A., MÜLLER, D., OTTO, S., TRAUTMANN, T., DINTER, T., HOYNINGEN-HUENE,

W. VON AND KAHN, R. (2009): Spectral surface albedo over Morocco and its impact on radiative forcing of Saharan dust, Tellus B 61, 252–269.

BLANCO, A., TOMASI, F. DE, FILIPPO, E., MANNO, D., PERRONE, M. R., SERRA, R., TAFURO, A. M. AND TEPORE, A. (2003): Characterization of African dust over southern Italy, Atmospheric Chemistry and Physics Discussions 3, 4633–4670.

CACHIER, H., LIOUSSE, C., BUAT-MENARD, P. AND GAUDICHET, A. (1995): Particulate content of savanna fire emissions, Journal of Atmospheric Chemistry 22, 123–148.

CACHIER, H., BREMOND, M.-P. AND BUAT-MENARD, P. (1989): Carbonaceous aerosols from different tropical biomass burning sources, Nature 340, 371–373.

CAQUINEAU, S., GAUDICHET, A., GOMES, L. AND LEGRAND, M. (2002): Mineralogy of Saharan dust transported over northwestern tropical Atlantic Ocean in relation to source regions, Journal of Geophysical Research 107, 4251–4263.

CAQUINEAU, S., GAUDICHET, A., GOMES, L., MAGONTHIER, M., CLAUDE, A. AND CHATENET, B. (1998): Saharan dust: Clay ratio as a relevant tracer to assess the origin of soil&8208;derived aerosols, Geophysical Research Letters 25, 983–986.

CHÝLEK, P., VIDEEN, G., NGO, D., PINNICK, R. G. AND KLETT, J. D. (1995): Effect of black carbon on the optical properties and climate forcing of sulfate aerosols, Journal of Geophysical Research 100, 16325–16332.

COVERT, D. S., CHARLSON, R. J. AND AHLQUIST, N. C. (1972): A Study of the Relationship of Chemical Composition and Humidity to Light Scattering by Aerosols, Journal of Applied Meteorology 11, 968–976.

CRUTZEN, P. J. AND ANDREAE, M. O. (1990): Biomass Burning in the Tropics: Impact on Atmospheric Chemistry and Biogeochemical Cycles, Science 250, 1669–1678.

CZICZO, D. J., FROYD, K. D., GALLAVARDIN, S. J., MOEHLER, O., BENZ, S., SAATHOFF, H. AND MURPHY, D. M. (2009): Deactivation of ice nuclei due to atmospherically relevant surface coatings, Environmental Research Letters 4, 1748–9326.

DANILATOS, G. D.: Foundations of environmental scanning electron microscopy, in: Advances in electronics and electron physics. Vol.71, Hawkes, P. W. (Ed.) 109–250 1988.

DAVIES, D., KUMAR, S. AND DESCLOITRES, J. (2004): Global fire monitoring using MODIS near-real-time satellite data, GIM International 18, 41–43.

DEBOUDT, K., FLAMENT, P., CHOEL, M., GLOTER, A. AND SOBANSKA, S. C. C. (2010): Mixing state of aerosols and direct observation of carbonaceous and marine coatings on African dust by individual particle analysis, Atmospheric Chemistry and Physics submitted, 38 pp.

DESBOEUFS, K. V. AND CAUTENET, G. (2005): Transport and mixing zone of dust and sulphate over Tropical Africa and the Atlantic Ocean, Atmospheric Chemistry and Physics Discussions 5, 5615–5644.

EBERT, M., WEINBRUCH, S., HOFFMANN, P. AND ORTNER, H. M. (2004): The chemical composition and complex refractive index of rural and urban influenced aerosols determined by individual particle analysis, Atmospheric Environment 38, 6531–6545.

EBERT, M., WEINBRUCH, S., RAUSCH, A., GORZAWSKI, G., HELAS, G., HOFFMANN, P. AND WEX, H. (2002): Complex refractive index of aerosols during LACE 98 as derived from the analysis of individual particles, Journal of Geophysical Research 107, doi:10.1029/2000JD000195.

ECHALAR, F., GAUDICHET, A., CACHIER, H. AND ARTAXO, P. (1995): Aerosol emissions by tropical forest and savanna biomass burning: Characteristic trace elements and fluxes, Geophysical Research Letters 22, 3039–3042.

EDAX (2006): Genesis V. 5.2 Handbook, Mahwah, NJ, USA.

ENGELMANN, R., ANSMANN, A., HORN, S., ESSELBORN, M., FRUNTKE, J., SEIFERT, P., ALTHAUSEN, D., TESCHE, M. AND LIEKE, K. (2011): Doppler LIDAR studies of heat island effects on vertical mixing of aerosols during SAMUM-2, Tellus B 63, submitted Nov. 2010.

ENGELSTAEDTER, S., TEGEN, I. AND WASHINGTON, R. (2006): North African dust emissions and transport, Earth-Science Reviews 79, 73–100.

ESSELBORN, M., WIRTH, M., FIX, A., WEINZIERL, B., RASP, K., TESCHE, M. AND PETZOLD, A. (2009): Spatial distribution and optical properties of Saharan dust observed by airborne high spectral resolution LIDAR during SAMUM 2006, Tellus B 61, 131–143.

FORMENTI, P., RAJOT, J. L., DESBOEUFS, K., CAQUINEAU, S., CHEVAILLIER, S., NAVA, S., GAUDICHET, A., JOURNET, E., TRIQUET, S., ALFARO, S., CHIARI, M., HAYWOOD, J., COE, H. AND HIGHWOOD, E. (2008): Regional variability of the composition of mineral dust from western Africa: results from the AMMA SOP0/DABEX and DODO field campaigns, Journal of Geophysical Research - Atmosphere 113, doi:10.1029/2008JD009903.

FORMENTI, P., SCHÜTZ, L., BALKANSKI, Y., DESBOEUFS, K., EBERT, M., KANDLER, K., PETZOLD, A., SCHEUVENS, D., WEINBRUCH, S. AND ZHANG, D. Z. (2010): Recent progress in understanding physical and chemical properties of mineral dust, Atmospheric Chemistry and Physics Discussions 10, doi:10.5194/acpd-10-31187-2010.

FORSTER, P., RAMASWAMY, V., ARTAXO, P., BERNTSEN, T., BETTS, R., FAHEY, D. W., HAYWOOD, J., LEAN, J., LOWE, D. C., MYHRE, G., NGANGA, J., PRINN, R., RAGA, G., SCHULZ, M., VAN DORLAND, R., BODEKER, G., BOUCHER, O., COLLINS, W. D., CONWAY, T. J., DLUGOKENCKY, E., ELKINS, J. W., ETHERIDGE, D., FOUKAL, P., FRASER, P., GELLER, M., JOOS, F., KEELING, C. D., KINNE, S., LASSEY, K., LOHMANN, U., MANNING, A. C., MONTZKA, S., ORAM, D., O'SHAUGHNESSY, K., PIPER, S., PLATTNER, G. K., PONATER, M., RAMANKUTTY, N., REID, G., RIND, D., ROSENLOF, K., SAUSEN, R., SCHWARZKOPF, D., SOLANKI, S. K., STENCHIKOV, G., STUBER, N., TAKEMURA, T., TEXTOR, C., WANG, R., WEISS, R. AND WHORF, T.: Changes in Atmospheric Constituents and in Radiative Forcing, Intergovernmental Panel on Climate Change. Cambridge University Press, Cambridge, United Kingdom and New York, USA 2007.

FREUDENTHALER, V., ESSELBORN, M., WIEGNER, M., HEESE, B., TESCHE, M., ANSMANN, A., MUELLER, D., ALTHAUSEN, D., WIRTH, M., FIX, A., EHRET, G., KNIPPERTZ, P., TOLEDANO, C., GASTEIGER, J., GARHAMMER, M. AND SEEFELDNER, M. (2009): Depolarization ratio profiling at several wavelengths in pure Saharan dust during SAMUM 2006, Tellus B 61, 165–179.

GANOR, E. (1991): The composition of clay minerals transported to Israel as indicators of Saharan dust emission, Atmospheric Environment 25, 2657–2664.

GASTEIGER, J., WIEGNER, M., GROSS, S., FREUDENTHALER, V., TOLEDANO, C., TESCHE, M. AND KANDLER, K. (2011): Modeling LIDAR-relevant optical properties of complex mineral dust aerosols, Tellus B 63, submitted Oct. 2010.

GATZ, D. F. AND PROSPERO, J. M. (1996): A large silicon-aluminum aerosol plume in Central Illinois: North African desert dust?, Atmospheric Environment 30, 3789–3799.

GAUDICHET, A., ECHALAR, F., CHATENET, B., QUISEFIT, J. P., MALINGRE, G., CACHIER, H., BUAT-MENARD, P., ARTAXO, P. AND MAENHAUT, W. (1995): Trace elements in tropical African savanna biomass burning aerosols, Journal of Atmospheric Chemistry 22, 19–39.

GIGLIO, L., DESCLOITRES, J., JUSTICE, C. O. AND KAUFMAN, Y. J. (2003): An Enhanced Contextual Fire Detection Algorithm for MODIS, Remote Sensing of Environment 87, 273–282.

GOLDSTEIN, J. I.: Scanning electron microscopy and X-ray microanalysis, 3. ed., corr. print., Springer, New York, NY, 690 pp. 2007.

GOMES, L., BERGAMETTI, G., COUDEGAUSSEN, G. AND ROGNON, P. (1990): Submicron Desert Dust – a sandblasting process, Journal of Geophysical Research - Atmosphere 95, 13927–13935.

GOMEZ-AMO, J. L., DI SARRA, A., MELONI, D., CACCIANI, M. AND UTRILLAS, M. P. (2010): Sensitivity of shortwave radiative fluxes to the vertical distribution of aerosol single scattering albedo in the presence of a desert dust layer, Atmospheric Environment 44, 2787–2791.

GOUDIE, A. S. AND MIDDLETON, N. J. (2001): Saharan dust storms: nature and consequences, Earth-Science Reviews 56, 179–204.

GOVENDER, N., TROLLOPE, S. W. AND VAN WILGEN, B. W. (2006): The effect of fire season, fire frequency, rainfall and management on fire intensity in savanna vegetation in South Africa, Journal of Applied Ecology 43, 748–758.

GRAHAM, W. F. AND DUCE, R. A. (1979): Atmospheric pathways of the phosphorus cycle, Geochimica et Cosmochimica Acta 43, 1195–1208.

GRIFFIN, D., KELLOGG, C. AND SHINN, E. (2001): Dust in the Wind: Long Range Transport of Dust in the Atmosphere and Its Implications for Global Public and Ecosystem Health, Global Change & Human Health 2, 20–33.

GROSS, S., GASTEIGER, J., FREUDENTHALER, V., WIEGNER, M., GEIß, A., SCHLADITZ, A., TOLEDANO, C., KANDLER, K., TESCHE, M., ANSMANN, A. AND WIEDENSOHLER, A. (2011): Characterization of the planetary boundary layer during SAMUM-2 by means of LIDAR measurements, Tellus B 63, submitted Nov. 2010.

HAND, V. L., CAPES, G., VAUGHAN, D. J., FORMENTI, P., HAYWOOD, J. M. AND COE, H. (2010): Evidence of internal mixing of African dust and biomass burning particles by individual particle analysis using electron beam techniques, Journal of Geophysical Research - Atmosphere 115, doi:10.1029/2009JD012938.

HÄNEL, G. (Ed.): The properties of atmospheric aerosol particles as functions of the relative humidity at thermodynamic equilibrium with the surrounding moist air. In Advances in Geophysics, Advances in Geophysics19, Academic Pr., New York, 312 pp. 1976.

HARTUNG, J., ELPELT, B. AND KLÖSENER, K. H. (Eds.): Statistik. Lehr- und Handbuch der angewandten Statistik ; mit zahlreichen, vollständig durchgerechneten Beispielen, 14. Aufl., Oldenbourg, München, 975 pp. 2005.

HAYWOOD, J. M., PELON, J., FORMENTI, P., BHARMAL, N., BROOKS, M., CAPES, G., CHAZETTE, P., CHOU, C., CHRISTOPHER, S., COE, H., CUESTA, J., DERIMIAN, Y., DESBOEUFS, K., GREED, G., HARRISON, M., HEESE, B., HIGHWOOD, E. J., JOHNSON, B., MALLET, M., MARTICORENA, B., MARSHAM, J., MILTON, S., MYHRE, G., OSBORNE, S. R., PARKER, D. J., RAJOT, J. L., SCHULZ, M., SLINGO, A., TANRÉ, D. AND TULET, P. (2008): Overview of the Dust and Biomass-burning Experiment and African Monsoon Multidisciplinary Analysis Special Observing Period-0, Journal of Geophysical Research 113, doi:10.1029/2008JD010077.

HEINOLD, B., TEGEN, I., ESSELBORN, M., FREUDENTHALER, V., GROSS, S., KANDLER, K., KNIPPERTZ, P., MÜLLER, D., SCHEPANSKI, K., SCHLADITZ, A., TESCHE, M., TOLEDANO, C., WEINZIERL, B., ANSMANN, A., ALTHAUSEN, D., MÜLLER, T., PETZOLD, A. AND

WIEDENSOHLER, A. (2011): Regional modelling of Saharan dust and land fire smoke: Model description and validation, Tellus B 63, submitted Oct. 2010.

HEINTZENBERG, J. (2009): The SAMUM-1 experiment over Southern Morocco: overview and introduction, Tellus B 61, 2–11.

HOFFER, A., GELENCSER, A., GUYON, P., KISS, G., SCHMID, O., FRANK, G. P., ARTAXO, P. AND ANDREAE, M. O. (2006): Optical properties of humic-like substances (HULIS) in biomass-burning aerosols, Atmospheric Chemistry and Physics 6, 3563–3570.

HUANG, J., ZHANG, C. AND PROSPERO, J. M. (2010): African dust outbreaks: A satellite perspective of temporal and spatial variability over the tropical Atlantic Ocean, Journal of Geophysical Research - Atmosphere 115, doi:10.1029/2009JD012516.

JAENICKE, R. AND SCHÜTZ, L. (1978): Comprehensive study of physical and chemical properties of surface aerosols in Cape-Verde-Islands region, Journal of Geophysical research – Oceans and atmospheres 83, 3585–3599.

JAFFE, H. W. (Ed.): Crystal chemistry and refractivity, Cambridge Univ. Press, Cambridge, 1988., Dover, Mineola, NY, 335 pp. 1996.

JASMUND, K. (Ed.): Tonminerale und Tone. Struktur, Eigenschaften, Anwendungen und Einsatz in Industrie und Umwelt, Steinkopff, Darmstadt, 490 pp. 1993.

KANDLER, K., SCHÜTZ, L., JAECKEL, S., LIEKE, K., EMMEL, C., MÜLLER-EBERT, D., EBERT, M., SCHEUVENS, D., SCHLADITZ, A., WIEDENSOHLER, A. AND WEINBRUCH, S. (2011): Ground-based off-line aerosol measurements at Praia, Cape Verde, during the Saharan Mineral dust experiment campaign - Part 1: Microphysical and mineralogical properties, Tellus B 63, submitted Oct. 2010.

KANDLER, K., LIEKE, K., BENKER, N., KÜPPER, M., EMMEL. C., MÜLLER-EBERT, D., EBERT, M., SCHEUVENS, D., SCHLADITZ, A., SCHÜTZ, L. AND WEINBRUCH, S. (2011b): Ground-based off-line aerosol measurements at Praia, Cape Verde, during the Saharan Mineral dust experiment campaign - Part 2: Electron-microscopical individual particle analysis, Tellus B 63, submitted Oct. 2010.

KANDLER, K., LIEKE, K., GLAHN, C. VON, WILHELM, K. D., EBERT, M., NILLIUS, B., PETZOLD, A., SCHÜTZ, L., WEINZIERL, B. AND WEINBRUCH, S. (2010): A giant particle collector (GPaC) for collection of super micron particles on an aircraft platform, International Aerosol Conference Helsinki, Aug. 29th - Sept. 3rd, Abstract P1E28.

KANDLER, K., SCHÜTZ, L., DEUTSCHER, C., EBERT, M., HOFMANN, H., JAECKEL, S., JAENICKE, R., KNIPPERTZ, P., LIEKE, K., MASSLING, A., PETZOLD, A., SCHLADITZ, A., WEINZIERL, B., WIEDENSOHLER, A., ZORN, S. AND WEINBRUCH, S. (2009): Size distribution, mass concentration, chemical and mineralogical composition and derived optical parameters of the boundary layer aerosol at Tinfou, Morocco, during SAMUM 2006, Tellus B 61, 32–50.

KANDLER, K., BENKER, N., BUNDKE, U., CUEVAS, E., EBERT, M., KNIPPERTZ, P., RODRÍGUEZ, S., SCHÜTZ, L. AND WEINBRUCH, S. (2007): Chemical composition and complex refractive index of Saharan Mineral Dust at Izaña, Tenerife (Spain) derived by electron microscopy, Atmospheric Environment 41, 8058–8074.

KARICKHOFF, S. W. AND BAILEY, G. W. (1973): Optical-absorption spectra of clay-minerals, Clays and Clay Minerals 21, 59–70.

KARYAMPUDI, V. M., PALM, S. P., REAGEN, J. A., FANG, H., GRANT, W. B., HOFF, R. M., MOULIN, C., PIERCE, H. F., TORRES, O., BROWELL, E. V. AND MELFI, S. H. (1999): Validation of the Saharan dust plume conceptual model using LIDAR, Meteosat, and ECMWF data, Bulletin of the American Meteorological Society 80, 1045–1075.

KAUFMAN, Y. J., TANRÉ, D. AND BOUCHER, O. (2002): A satellite view of aerosols in the climate system, Nature 419, 215–223.

KNIPPERTZ, P., DEUTSCHER, C., KANDLER, K., MÜLLER, T., SCHULZ, O. AND SCHÜTZ, L. (2007): Dust mobilization due to density currents in the Atlas region: Observations from the Saharan Mineral Dust Experiment 2006 field campaign, Journal of Geophysical Research 112, doi:10.1029/2007JD008774.

KNIPPERTZ, P., TESCHE, M., HEINOLD, B., KANDLER, K., TOLEDANO, C. AND ESSELBORN, M. (2011): Dust Mobilization and Aerosol Transport from West Africa to Cape Verde - A Meteorological Overview of SAMUM-2, Tellus B 63, submitted Sept. 2010.

KÖHLER, C., TRAUTMANN, T., LINDERMEIR, E., VREELING, W., LIEKE, K., KANDLER, K., WEINZIERL, B., GROß, S. AND TESCHE, M. (2011): Comparison of Ground Based Radiation Measurements in the Thermal IR during SAMUM-2 with Radiative Transfer Simulations, Tellus B 63, submitted Dec. 2010.

KOREN, I., KAUFMAN, Y. J., WASHINGTON, R., TODD, M. C., RUDICH, Y., MARTINS, V. J. AND ROSENFELD, D. (2006): The Bodélé depression: a single spot in the Sahara that provides most of the mineral dust to the Amazon forest, Environmental Research Letters 1, doi:10.1088/1748-9326/1/1/014005.

KRUEGER, B. J., GRASSIAN, V. H., COWIN, J. P. AND LASKIN, A. (2004): Heterogeneous chemistry of individual mineral dust particles from different dust source regions: the importance of particle mineralogy, Atmospheric Environment 38, 6253–6261.

LAFON, S., RAJOT, J.-L., ALFARO, S. C. AND GAUDICHET, A. (2004): Quantification of iron oxides in desert aerosol, Atmospheric Environment 38, 1211–1218.

LASKIN, A., COWIN, J. P. AND IEDEMA, M. J. (2006): Analysis of individual environmental particles using modern methods of electron microscopy and X-ray microanalysis, Journal of Electron Spectroscopy and Related Phenomena 150, 260–274.

LASKIN, A., IEDEMA, M. J. AND COWIN, J. P. (2003): Time-resolved aerosol collector for CCSEM/EDX single-particle analysis, Aerosol Science and Technology 37, 246–260.

LASKIN, A. AND COWIN, J. P. (2001): Automated Single-Particle SEM/EDX Analysis of Submicrometer Particles down to 0.1 Î¼m, Analytical Chemistry 73, 1023–1029.

LÁZARO, F. J., GUTIÉRREZ, L., BARRÓN, V. AND GELADO, M. D. (2008): The speciation of iron in desert dust collected in Gran Canaria (Canary Islands): Combined chemical, magnetic and optical analysis, Atmospheric Environment 42, 8987–8996.

LESINS, G., CHYLEK, P. AND LOHMANN, U. (2002): A study of internal and external mixing scenarios and its effect on aerosol optical properties and direct radiative forcing, Journal of Geophysical Research - Atmosphere 107, doi:10.1029/2001JD000973.

LEVIN, Z., TELLER, A., GANOR, E. AND YIN, Y. (2005): On the interactions of mineral dust, sea-salt particles, and clouds: A measurement and modeling study from the Mediterranean Israeli Dust Experiment campaign, Journal of Geophysical Research 110, doi:10.1029/2005JD005810.

LI, J., PÓSFAI, M., HOBBS, P. V. AND BUSECK, P. R. (2003): Individual aerosol particles from biomass burning in southern Africa: 2, Compositions and aging of inorganic particles, Journal of Geophysical Research 108, doi:10.1029/2002JD002310.

LI, W. J. AND SHAO, L. Y. (2009): Observation of nitrate coatings on atmospheric mineral dust particles, Atmospheric Chemistry and Physics 9, 1863–1871.

LIEKE, K. (2008): Chemische Zusammensetzung von Wüstenstaub, Biomasse-Verbrennungs- und urbanem Aerosol in der Region Kapverdische Inseln und West-Afrika während SAMUM II, Diplomarbeit, Technische Universität Darmstadt 44 pp.

LIEKE, K., KANDLER, K., SCHEUVENS, D., EMMEL, C., GLAHN, C. VON, PETZOLD, A., WEINZIERL, B., VEIRA, A., EBERT, M., WEINBRUCH, S. AND SCHÜTZ, L. (2011): Particle chemical

properties in the vertical column based on aircraft observations in the vicinity of Cape Verde, Tellus B 63, submitted Nov. 2010.

LIU, X., VAN ESPEN, P., ADAMS, F., CAFMEYER, J. AND MAENHAUT, W. (2000): Biomass Burning in Southern Africa: Individual Particle Characterization of Atmospheric Aerosols and Savanna Fire Samples, Journal of Atmospheric Chemistry 36, 135–155.

MARTICORENA, B. AND BERGAMETTI, G. (1995): Modelling the atmospheric dust cycle. 1. Design of a soil-derived dust emission scheme., Journal of Geophysical Research - Atmosphere 100, 16415–16430.

MASSLING, A., WIEDENSOHLER, A., BUSCH, B., NEUSUSS, C., QUINN, P., BATES, T. AND COVERT, D. (2003): Hygroscopic properties of different aerosol types over the Atlantic and Indian Oceans, Atmospheric Chemistry and Physics 3, 1377–1397.

MATSUKI, A., QUENNEHEN, B., SCHWARZENBOECK, A., CRUMEYROLLE, S., VENZAC, H., LAJ, P. AND GOMES, L. (2010): Temporal and vertical variations of aerosol physical and chemical properties over West Africa: AMMA aircraft campaign in summer 2006, Atmospheric Chemistry and Physics 10, 8437–8451.

MILLS, M. M., RIDAME, C., DAVEY, M., LA ROCHE, J. AND GEIDER, R. J. (2004): Iron and phosphorus co-limit nitrogen fixation in the eastern tropical North Atlantic, Nature 429, 292–294.

MORENO, T., QUEROL, X., CASTILLO, S., ALASTUEY, A., CUEVAS, E., HERRMANN, L., MOUNKAILA, M., ELVIRA, J. AND GIBBONS, W. (2006): Geochemical variations in aeolian mineral particles from the Sahara-Sahel Dust Corridor, Chemosphere 65, 261–270.

MOULIN, C., LAMBERT, C. E., DULAC, F. AND DAYAN, U. (1997): Control of atmospheric export of dust from North Africa by the North Atlantic oscillation, Nature 387, 691–694.

MUHS, D. R., BUDAHN, J. R., PROSPERO, J. M. AND CAREY, S. N. (2007): Geochemical evidence for African dust inputs to soils of western Atlantic islands: Barbados, the Bahamas, and Florida, Journal of Geophysical Research 112, F02009.

NOLI, W. (2010): personal communication, Plano, Wetzlar, Germany

NORMAND, C. W. B. (1920): The effect of high temperature, humidity, and wind on the human body, Quarterly Journal of the Royal Meteorological Society 46, 1–14.

OTTO, S., BIERWIRTH, E., WEINZIERL, B., KANDLER, K., ESSELBORN, M., TESCHE, M., SCHLADITZ, A., WENDISCH, M. AND TRAUTMANN, T. (2009): Solar radiative effects of a Saharan dust plume observed during SAMUM assuming spheroidal model particles, Tellus B 61, 270–296.

PELON, J., MALLET, M., MARISCAL, A., GOLOUB, P., TANRE, D., KARAM, D. B., FLAMANT, C., HAYWOOD, J., POSPICHAL, B. AND VICTORI, S. (2008): MicroLIDAR observations of biomass burning aerosol over Djougou (Benin) during African Monsoon Multidisciplinary Analysis Special Observation Period 0: Dust and Biomass-Burning Experiment, Journal of Geophysical Research - Atmosphere 113, doi:10.1029/2008JD009976.

PENNER, J. E., ANDREAE, M. O., ANNEGARN, H., BARRIE, L., FEICHTER, J., HEGG, D., JAYARAMAN, A., LEAITCH, R., MURPHY, D., NGANGA, J. AND PITARI, G.: Aerosols, their Direct and Indirect Effects. Intergovernmental Panel on Climate Change. Cambridge University Press, 89 pp., 2001.

PETZOLD, A., VEIRA, A., MUND, S., ESSELBORN, M., KIEMLE, C., WEINZIERL, B., HAMBURGER, G., EHRET, G., LIEKE, K. AND KANDLER, K. (2011): Mixing of mineral dust with urban

pollution aerosol over Dakar (Senegal) – Impact on dust physico-chemical and radiative properties, Tellus B 63, submitted Dec. 2010.

PETZOLD, A., RASP, K., WEINZIERL, B., ESSELBORN, M., HAMBURGER, T., DOERNBRACK, A., KANDLER, K., SCHUETZ, L., KNIPPERTZ, P., FIEBIG, M. AND VIRKKULA, A. (2009): Saharan dust absorption and refractive index from aircraft-based observations during SAMUM 2006, Tellus B 61, 118–130.

POSFAI, M., XU, H. F., ANDERSON, J. R. AND BUSECK, P. R. (1998): Wet and dry sizes of atmospheric aerosol particles: An AFM-TEM study, Geophysical Research Letters 25, 1907–1910.

PROSPERO, J. M., GLACCUM, R. A. AND NEES, R. T. (1981): Atmospheric transport of soil dust from Africa to South-America, Nature 289, 570–572.

PROSPERO, J., BARRETT, K., CHURCH, T., DENTENER, F., DUCE, R., GALLOWAY, J., LEVY, H., MOODY, J. AND QUINN, P. (1996): Atmospheric deposition of nutrients to the North Atlantic Basin, Biogeochemistry 35, 27–73.

PROSPERO, J. M. (1999a): Long-range transport of mineral dust in the global atmosphere: Impact of African dust on the environment of the southeastern United States, Proceedings of the national academy of sciences of the United States of America 96, 3396–3403.

PROSPERO, J. M. (1999b): Long-term measurements of the transport of African mineral dust to the southeastern United States: Implications for regional air quality, Journal of Geophysical Research - Atmosphere 104, 15917–15927.

PROSPERO, J. M., GINOUX, P., TORRES, O., NICHOLSON, S. E. AND GILL, T. E. (2002): Environmental characterization of global sources of atmospheric soil dust identified with the NIMBUS 7 Total Ozone Mapping Spectrometer (TOMS) absorbing aerosol product, Reviews of Geophysics 40, doi:10.1029/2000RG000095.

QUIJANO, A. L., IN SOKOLIK AND TOON, O. B. (2000): Influence of the aerosol vertical distribution on the retrievals of aerosol optical depth from satellite radiance measurements, Geophysical Research Letters 27, 3457–3460.

REDELSPERGER, J.-L., THORNCROFT, C. D., DIEDHIOU, A., LEBEL, T., PARKER, D. J. AND POLCHER, J. (2006): African monsoon multidisciplinary analysis - An international research project and field campaign, Bulletin of the American Meteorological Society 87, 1–20.

REED, S. J. B.: Electron microprobe analysis and scanning electron microscopy in geology, 2. ed., Cambridge Univ. Press, Cambridge, 189 pp. 2005.

REID, J. S., PIKETH, S. J., WALKER, A. L., BURGER, R. P., ROSS, K. E., WESTPHAL, D. L., BRUINTJES, R. T., HOLBEN, B. N., HSU, C., JENSEN, T. L., KAHN, R. A., KUCIAUSKAS, A. P., ALUMINIUM MANDOOS, A., ALUMINIUM MANGOOSH, A., MILLER, S. D., PORTER, J. N., REID, E. A. AND TSAY, S.-C. (2008): An overview of UAE(2) flight operations: Observations of summertime atmospheric thermodynamic and aerosol profiles of the southern Arabian Gulf, Journal of Geophysical Research - Atmosphere 113, doi:10.1029/2007JD009435.

REID, J. S., KINNEY, J. E., WESTPHAL, D. L., HOLBEN, B. N., WELTON, E. J., TSAY, S. C., ELEUTERIO, D. P., CAMPBELL, JR, CHRISTOPHER, S. A., COLARCO, P. R., JONSSON, H. H., LIVINGSTON, J. M., MARING, H. B., MEIER, M. L., PILEWSKIE, P., PROSPERO, J. M., REID, E. A., LA REMER, RUSSELL, P. B., SAVOIE, D. L., SMIRNOV, A. AND TANRE, D. (2003): Analysis of measurements of Saharan dust by airborne and ground-based remote sensing methods during the Puerto Rico Dust Experiment (PRIDE), Journal of Geophysical Research - Atmosphere 108, doi:10.1029/2002JD002493.

REIMER, L.: Transmission electron microscopy. Physics of image formation and microanalysis, 4. ed., Springer series in optical sciences 36, Springer, Berlin, 584 pp. 1997.

RO, C. U., KIM, H., OH, K. Y., YEA, S. K., LEE, C. B., JANG, M. AND GRIEKEN, R. V. (2002): Single-particle characterization of urban aerosol particles collected in three Korean cities using low-Z electron probe X-ray microanalysis, Environmental Science and Technology 36, 4770–4776.

ROSEN, H., HANSEN, A. D. A., GUNDEL, L. AND NOVAKOV, T. (1978): Identification of the optically absorbing component in urban aerosols, Applied Optics 17, 3858–3859.

SCHEPANSKI, K. (2008): Characterising Saharan Dust Sources and Export using Remote Sensing and Regional Modelling, Dissertation, Christian-Albrechts-Universiät Kiel, 96 pp.

SCHEPANSKI, K., TEGEN, I., LAURENT, B., HEINOLD, B. AND MACKE, A. (2007): A new Saharan dust source activation frequency map derived from MSG-SEVIRI IR-channels, Geophysical Research Letters 34, doi:10.1029/2007GL030168.

SCHEUVENS, D., KANDLER, K., KÜPPER, M., K., LIEKE, K., ZORN, S., EBERT, M., SCHÜTZ, L. AND WEINBRUCH, S. (2011): Indiviual-particle analysis of airborne dust samples from Morocco: source characterization and height dependence of composition, Tellus B 63, submitted Nov. 2010.

SCHEUVENS, D., KANDLER, K., SCHUETZ, L., EBERT, M. AND WEINBRUCH, S. (2009): XRD data of Saharan and Sahelian dusts and soils - A compilation, Geochimica et Cosmochimica Acta 73, Abstract 1172.

SCHKOLNIK, G., CHAND, D., HOFFER, A., ANDREAE, M. O., ERLICK, C., SWIETLICKI, E. AND RUDICH, Y. (2007): Constraining the density and complex refractive index of elemental and organic carbon in biomass burning aerosol using optical and chemical measurements, Atmospheric Environment 41, 1107–1118.

SCHLADITZ, A., MÜLLER, T., NOWAK, A., KANDLER, K., LIEKE, K., MAßLING, A. AND WIEDENSOHLER, A. (2011): In situ aerosol characterization at Cape Verde. Part 1: Particle number size distributions, growth factors and hygroscopic mixing state of mixed marine and Saharan dust aerosol, Tellus B 63, submitted Oct. 2010.

SCHNAITER, M., LINKE, C., MÖHLER, O., NAUMANN, K. H., SAATHOFF, H., WAGNER, R., SCHURATH, U. AND WEHNER, B. (2005): Absorption amplification of black carbon internally mixed with secondary organic aerosol, J. Geophys. Res. 110, doi:10.1029/2005JD006046.

SCHÜTZ, L., KANDLER, K., DEUTSCHER, C., LIEKE, K., MASSLING, A., NOWAK, A., SCHLADITZ, A., WIEDENSOHLER, A., EBERT, M., WEINBRUCH, S., KNIPPERTZ, P., ZORN, S., JAENICKE, R., WEINZIERL, B. AND PETZOLD, A. (2008): Boundary layer aerosol size distributions during SAMUM I-II, Morocco 2006 and Cape Verde 2008, 3rd International Workshop on Mineral Dust, Leipzig Sept. 15th - 17th, Abstract 2-10.

SCHÜTZ, L. AND SEBERT, M. (1987): Mineral Aerosols and Source Identification, Journal of Aerosol Science 18, doi:10.1016/0021-8502(87)90002-4.

SCHÜTZ, L. (1980): Long range transport of desert dust with special emphasis on the Sahara, Annals of the New York Academy of Sciences 338, 515–532.

SHAO, Y., MYSAK, L. A. AND HAMILTON, K. (Eds.): Physics and Modelling of Wind Erosion, Atmospheric and Oceanographic Sciences Library 37, Springer Netherlands, Dordrecht 2009.

SOKOLIK, I. N. AND TOON, O. B. (1999): Incorporation of mineralogical composition into models of the radiative properties of mineral aerosol from UV to IR wavelengths, Journal of Geophysical Research - Atmosphere 104, 9423–9444.

SOKOLIK, I. N. AND TOON, O. B. (1996): Direct radiative forcing by anthropogenic airborne mineral aerosols, Nature 381, 681–683.

SOLOMON, S. (Ed.): Climate change 2007. The physical science basis; contribution of Working Group I to the Fourth Assessment Report of Intergovernmental Panel on Climate Change. Cambridge University Press, 996 pp., 2007.

SUN, D., LAU, K. M. AND KAFATOS, M. (2008): Contrasting the 2007 and 2005 hurricane seasons: Evidence of possible impacts of Saharan dry air and dust on tropical cyclone activity in the Atlantic basin, Geophysical Research Letters 35, doi:10.1029/2008GL034529.

SWAP, R., GARSTANG, M., GRECO, S., TALBOT, R. AND KALLBERG, P. (1992): Saharan dust in the Amazon Basin, Tellus B 44, 133–149.

SWIETLICKI, E., ZHOU, J. C., COVERT, D. S., HAMERI, K., BUSCH, B., VAKEVA, M., DUSEK, U., BERG, O. H., WIEDENSOHLER, A., AALTO, P., MAKELA, J., MARTINSSON, B. G., PAPASPIROPOULOS, G., MENTES, B., FRANK, G. AND STRATMANN, F. (2000): Hygroscopic properties of aerosol particles in the northeastern Atlantic during ACE-2, Tellus B 52, 201–227.

TAKAHAMA, S., LIU, S. AND RUSSELL, L. M. (2010): Coatings and clusters of carboxylic acids in carbon-containing atmospheric particles from spectromicroscopy and their implications for cloud-nucleating and optical properties, Journal of Geophysical Research - Atmosphere 115, doi:10.1029/2009JD012622.

TANAKA, T. Y. AND CHIBA, M. (2006): A numerical study of the contributions of dust source regions to the global dust budget, Global and Planetary Change 52, 88–104.

TANG, I. N. AND MUNKELWITZ, H. R. (1993): Composition and temperature dependence of the deliquescence properties of hygroscopic aerosols, Atmospheric Environment 27, 467–473.

TANRÉ, D., HAYWOOD, J., PELON, J., LEON, J. F., CHATENET, B., FORMENTI, P., FRANCIS, P., GOLOUB, P., HIGHWOOD, E. J. AND MYHRE, G. (2003): Measurement and modeling of the Saharan dust radiative impact: overview of the Saharan dust Experiment (SHADE), Journal of Geophysical Research 108, doi:10.1029/2002JD003273.

TEGEN, I. AND LACIS, A. A. (1996): Modeling of particle size distribution and its influence on the radiative properties of mineral dust aerosol, Journal of Geophysical Research 101, 19237–19244.

TEGEN, I., LACIS, A. A. AND FUNG, I. (1996): The influence on climate forcing of mineral aerosols from disturbed soils, Nature 380, 419–422.

TESCHE, M., ANSMANN, A., MUELLER, D., ALTHAUSEN, D., MATTIS, I., HEESE, B., FREUDENTHALER, V., WIEGNER, M., ESSELBORN, M., PISANI, G. AND KNIPPERTZ, P. (2009): Vertical profiling of Saharan dust with Raman LIDARs and airborne HSRL in southern Morocco during SAMUM, Tellus B 61, 144–164.

TOLEDANO, C., WIEGNER, M., GARHAMMER, M., SEEFELDNER, M., GASTEIGER, J., MUELLER, D. AND KOEPKE, P. (2009): Spectral aerosol optical depth characterization of desert dust during SAMUM 2006, Tellus B 61, 216–228.

TWOMEY, S. (1991): Aerosols, clouds and radiation, Atmospheric Environment 25, 2435–2442.

TWOMEY, S. (1977): The Influence of Pollution on the Shortwave Albedo of Clouds, Journal of the Atmospheric Sciences 34, 1149–1152.

VESTER, B. P., EBERT, M., BARNERT, E. B., SCHNEIDER, J., KANDLER, K., SCHÜTZ, L. AND WEINBRUCH, S. (2007): Composition and mixing state of the urban background aerosol in the Rhein-Main area (Germany), Atmospheric Environment 41, 6102–6115.

WANG, K.-S., CHIANG, K.-Y., TSAI, C.-C., SUN, C.-J., TSAI, C.-C. AND LIN, K.-L. (2001): The effects of FeCl3 on the distribution of the heavy metals Cd, Cu, Cr, and Zn in a simulated multimetal incineration system, Environment International 26, 257–263.

WEINBRUCH, S., WENTZEL, M., KLUCKNER, M., HOFFMANN, P. AND ORTNER, H. M. (1997): Characterization of individual atmospheric particles by element mapping in electron probe microanalysis, Mikrochimica Acta 125, 137–141.

WEINZIERL, B., SAUER, D., ESSELBORN, M., MUND, S., PETZOLD, A., VEIRA, A., TESCHE, M., ANSMANN, A. AND WIRTH, M. (2011): Airborne observations of microphysical and optical properties of dust and biomass burning aerosol layers in the Cape Verde region during SAMUM 2008, Tellus B 63, submitted Dec. 2010.

WEINZIERL, B., PETZOLD, A., ESSELBORN, M., WIRTH, M., RASP, K., KANDLER, K., SCHÜTZ, L., KOEPKE, P. AND FIEBIG, M. (2009): Airborne measurements of dust layer properties, particle size distribution and mixing state of Saharan dust during SAMUM 2006, Tellus B 61, 96–117.

WENTZEL, M., GORZAWSKI, H., NAUMANN, K. H., SAATHOFF, H. AND WEINBRUCH, S. (2003): Transmission electron microscopical and aerosol dynamical characterization of soot aerosols, Journal of Aerosol Science 34, 1347–1370.

WILLEKE, K. (Ed.): Aerosol measurement. Principles, techniques and applications, Wiley, New York, XVIII, 876 pp., 1993.

WILLIAMS, D. B. AND CARTER, C. B.: Transmission electron microscopy. A textbook for materials science, Plenum Press, New York, NY, 729 pp. 1996.

WORRINGEN, A., EBERT, M., TRAUTMANN, T., WEINBRUCH, S. AND HELAS, G. (2008): Optical properties of internally mixed ammonium sulfate and soot particles--a study of individual aerosol particles and ambient aerosol populations, Applied Optics 47, 3835–3845.

ZHANG, D. Z., IWASAKA, Y., MATSUKI, A., UENO, K. AND MATSUZAKI, T. (2006b): Coarse and accumulation mode particles associated with Asian dust in southwestern Japan, Atmospheric Environment 40, 1205–1215.

ZHANG, D. AND IWASAKA, Y. (2006a): Comparison of size changes of Asian dust particles caused by sea salt and sulfate, Journal of the Meteorological Society of Japan 84, 939–947.

ZHANG, D., ZANG, J., SHI, G., IWASAKA, Y., MATSUKI, A. AND TROCHKINE, D. (2003b): Mixture state of individual Asian dust particles at a coastal site of Qingdao, China, Atmospheric Environment 37, 3895–3901.

ZHANG, D. Z., IWASAKA, Y., SHI, G. Y., ZANG, J. Y., MATSUKI, A. AND TROCHKINE, D. (2003a): Mixture state and size of Asian dust particles collected at southwestern Japan in spring 2000, Journal of Geophysical Research - Atmosphere 108, doi:10.1029/2003JD003869.

ZIEGER, P., FIERZ-SCHMIDHAUSER, R., GYSEL, M., STROM, J., HENNE, S., YTTRI, K. E., BALTENSPERGER, U. AND WEINGARTNER, E. (2010): Effects of relative humidity on aerosol light scattering in the Arctic, Atmospheric Chemistry and Physics 10, 3875–3890.

Curriculum Vitae

von Kirsten Inga Lieke

Ausbildung

12/2008 – 1/2011	Dissertation
bis 9/2008	Abschluss als Dipl.-Ing. Geowissenschaften
	Diplomarbeit
4/2001 – 9/2007	Technische Universität Darmstadt
	Studium Angewandte Geowissenschaften
1998	Abitur

Praktika und Auslandsaufenthalte

6/2009 – 3/2010	Prefectural University of Kumamoto, Kumamoto, Japan
5/2008 – 6/2008	Messkampagne SAMUM II, Kapverdische Inseln, Fogo
1/2008 – 2/2008	Messkampagne SAMUM II, Kapverdische Inseln, Praia
10/2007 – 12/2007	Praktikum Leibniz-Institut für Troposphärenforschung, Leipzig

Forschungsinteressen und Projekte

2006 – heute	SAMUM: Saharan Mineral Dust Experiment, DFG-Forschergruppe. chemische Charakterisierung und Mischungszustand von afrikanischem Mineralstaub und Biomasse-Verbrennungsaerosol
2009 – heute	Asian Dust, Vergleich von afrikanischem und asiatischem transportierten Aerosol, Mischungszustand und innerer Aufbau von Partikeln
2010 – heute	Volcanic Ash, chemische Charakterisierung und mineralogische Zusammensetzung von Vulkanascheproben des isländischen Vulkans „Eyjafjallajöküll“. Analyse der DLR-Falcon-Flugproben

Publikationsliste Kirsten Inga Lieke

2011

LIEKE, K., KANDLER, K., SCHEUVENS, D., EMMEL, C., GLAHN, C. VON, PETZOLD, A., WEINZIERL, B., VEIRA, A., EBERT, M., WEINBRUCH, S. AND SCHÜTZ, L. (2011): Particle chemical properties in the vertical column based on aircraft observations in the vicinity of Cape Verde, Tellus B 63, submitted Nov. 2010.

PETZOLD, A., VEIRA, A., MUND, S., ESSELBORN, M., KIEMLE, C., WEINZIERL, B., HAMBURGER, G., EHRET, G., LIEKE, K. AND KANDLER, K. (2011): Mixing of mineral dust with urban pollution aerosol over Dakar (Senegal) – Impact on dust physico-chemical and radiative properties, Tellus B 63, submitted Dec. 2010.

KÖHLER, C., TRAUTMANN, T., LINDERMEIR, E., VREELING, W., LIEKE, K., KANDLER, K., WEINZIERL, B., GROß, S. AND TESCHE, M. (2011): Comparison of Ground Based Radiation Measurements in the Thermal IR during SAMUM-2 with Radiative Transfer Simulations, Tellus B 63, submitted Dec. 2010.

ENGELMANN, R., ANSMANN, A., HORN, S., ESSELBORN, M., FRUNTKE, J., SEIFERT, P., ALTHAUSEN, D., TESCHE, M. AND LIEKE, K. (2011): Doppler LIDAR studies of heat island effects on vertical mixing of aerosols during SAMUM-2, Tellus B 63, submitted Nov. 2010.

SCHEUVENS, D., KANDLER, K., KÜPPER, M., K., LIEKE, K., ZORN, S., EBERT, M., SCHÜTZ, L. AND WEINBRUCH, S. (2011): Indiviual-particle analysis of airborne dust samples from Morocco: source characterization and height dependence of composition, Tellus B 63, submitted Nov. 2010.

KANDLER, K., LIEKE, K., BENKER, N., KÜPPER, M., EMMEL. C., M.-E. D., EBERT, M., SCHEUVENS, D., SCHLADITZ, A., SCHÜTZ, L. AND WEINBRUCH, S. (2011): Ground-based off-line aerosol measurements at Praia, Cape Verde, during the Saharan Mineral dust experiment campaign - Part 2: Electron-microscopical individual particle analysis, Tellus B 63, submitted Oct. 2010.

KANDLER, K., SCHÜTZ, L., JAECKEL, S., LIEKE, K., EMMEL, C., MÜLLER-EBERT, D., EBERT, M., SCHEUVENS, D., SCHLADITZ, A., WIEDENSOHLER, A. AND WEINBRUCH, S. (2011): Ground-based off-line aerosol measurements at Praia, Cape Verde, during the Saharan Mineral dust experiment campaign - Part 1: Microphysical and mineralogical properties, Tellus B 63, submitted Oct. 2010.

SCHLADITZ, A., MÜLLER, T., NOWAK, A., KANDLER, K., LIEKE, K., MAßLING, A. AND WIEDENSOHLER, A. (2011): In situ aerosol characterization at Cape Verde. Part 1: Particle number size distributions, growth factors and hygroscopic mixing state of mixed marine and Saharan dust aerosol, Tellus B 63, submitted Oct. 2010.

2010

SCHUMANN, U., WEINZIERL, B., REITEBUCH, O., SCHLAGER, H., MINIKIN, A., FORSTER, C., BAUMANN, R., SAILER, T., GRAF, K., MANNSTEIN, H., VOIGT, C., RAHM, S., SIMMET, R., SCHEIBE, M., LICHTENSTERN, M., STOCK, P., RÜBA, H., SCHÄUBLE, D., TAFFERNER, A., RAUTENHAUS, M., GERZ, T., ZIEREIS, H., KRAUTSTRUNK, M., MALLAUN, C., GAYET, J. F., LIEKE, K., KANDLER, K., EBERT, M., WEINBRUCH, S., STOHL, A., GASTEIGER, J., OLAFSSON, H. AND STURM, K. (2010): Airborne observations of the Eyjafjalla volcano ash cloud over Europe during air space closure in April and May 2010, Atmos. Chem. Phys. Discuss. 10, 22131–22218.

2009

KANDLER, K., SCHÜTZ, L., DEUTSCHER, C., EBERT, M., HOFMANN, H., JAECKEL, S., JAENICKE, R., KNIPPERTZ, P., LIEKE, K., MASSLING, A., PETZOLD, A., SCHLADITZ, A., WEINZIERL, B., WIEDENSOHLER, A., ZORN, S. AND WEINBRUCH, S. (2009): Size distribution, mass concentration, chemical and mineralogical composition and derived optical parameters of the boundary layer aerosol at Tinfou, Morocco, during SAMUM 2006, Tellus B 61, 32–50.

Ausgewählte Konferenzbeiträge

2010

KANDLER, K., LIEKE, K., GLAHN, C. VON, WILHELM, K. D., EBERT, M., NILLIUS, B., PETZOLD, A., SCHÜTZ, L., WEINZIERL, B. AND WEINBRUCH, S. (2010): A giant particle collector (GPaC) for collection of super micron particles on an aircraft platform, International Aerosol Conference Helsinki, Aug. 29th - Sept.3rd, Abstract P1E28. ***Poster***.

LIEKE, K., KANDLER, K., EMMEL, C., EBERT, M., WEINZIERL, B., SCHÜTZ, L., PETZOLD, A. AND WEINBRUCH, S. (2010): Vertical distribution and state of mixing of aged Saharan dust and biomass burning aerosol at Cape Verde region during SAMUM II, International Aerosol Conference Helsinki, Aug. 29th - Sept.3rd, Abstract 2F2. ***Vortrag***.

LIEKE, K., KANDLER, K., EMMEL, C., EBERT, M., WEINZIERL, B., SCHÜTZ, L., PETZOLD, A. AND WEINBRUCH, S. (2010): Mixing state and size-resolved chemical composition of Saharan aerosol in the Cape Verde region - results of airplane taken samples, Geophysical Research Abstracts 12, EGU2010-2931. ***Vortrag***.

LIEKE, K., ZHANG, D., KANDLER, K. AND EMMEL, C. (2009): First approach to a comparison study of Asian desert dust particles from Amakusa and African dust particles of Cape Verde Islands, Geophysical Research Abstracts 12, EGU2010-2925. ***Poster***

2009

LIEKE, K., KANDLER, K., DEUTSCHER, C., EBERT, M., WEINZIERL, B., SCHÜTZ, L., PETZOLD, A. AND WEINBRUCH, S. (2009): Size-resolved chemical composition showing the vertical heterogeneity of Saharan aerosol in the Cape Verde region, Japanese Association of Aaerosol Science and Technology General Assembly Okayama, Abstract P16. ***Vortrag***.

LIEKE, K., KANDLER, K., DEUTSCHER, C., EBERT, M., JAECKEL, S., MÜLLER-EBERT, D., SCHÜTZ, L. AND WEINBRUCH, S. (2008):): The distribution and mixing state of aeolian African dust, urban and biomass burning aerosol as observed in the Cape Verde region (compared with results from southern Morocco), Japanese Association of Aaerosol Science and Technology General Assembly Okayama, Abstract B08. ***Poster***.

KANDLER, K., LIEKE, K., SCHÜTZ, L., DEUTSCHER, C., EBERT, M., JAENICKE, R., MÜLLER-EBERT, D. AND WEINBRUCH, S. (2009): Single particle chemical composition and shape of fresh and aged Saharan dust in Morocco and at Cape Verde Islands during SAMUM I and II, Geophysical Research Abstracts 11, EGU2009-4524. ***Poster***.

KANDLER, K., LIEKE, K., SCHÜTZ, L. ET AL. (2009): Boundary layer aerosol size distribution, mass concentration and mineralogical composition in Morocco and at Cape Verde Islands during SAMUM I-II, Geophysical Research Abstracts 11, EGU2009-3445. ***Poster***.

LIEKE, K., KANDLER, K., DEUTSCHER, C., EBERT, M., WEINZIERL, B., SCHÜTZ, L., PETZOLD, A. AND WEINBRUCH, S. (2009): Size-resolved chemical composition showing the vertical heterogeneity of Saharan aerosol in the Cape Verde region, Geophysical Research Abstracts 11, EGU2009-4522. ***Vortrag***.

2008

LIEKE, K., KANDLER, K., DEUTSCHER, C., EBERT, M., SCHÜTZ, L. AND WEINBRUCH, S. (2008): Chemical and mineralogical composition and morphology of aged Saharan dust, marine, urban and biomass burning aerosol at Cape Verde, European Aerosol Conference Thessaloniki, Aug. 24th - 29th, Abstract T06A088P. ***Poster***.

LIEKE, K., KANDLER, K., SCHÜTZ, L., DEUTSCHER, C., EBERT, M., MÜLLER-EBERT, D., PETZOLD, A., RASP, K., WEINZIERL, B. AND WEINBRUCH, S. (2008): Chemical and mineralogical composition and morphology of aged Saharan dust, marine, urban and biomass burning aerosol at Cape Verde, 3rd International Workshop on Mineral Dust, Leipzig Sept. 15th - 17th, Abstract 2-13. ***Poster***.

Erklärung der Urheberschaft

Ich erkläre hiermit an Eides statt, dass ich die vorliegende Arbeit ohne Hilfe Dritter und ohne Benutzung anderer als der angegebenen Hilfsmittel angefertigt habe. Die aus fremden Quellen direkt oder indirekt übernommenen Gedanken sind als solche kenntlich gemacht. Die Arbeit wurde bisher in gleicher oder ähnlicher Form keiner anderen Prüfungsbehörde vorgelegt und auch noch nicht veröffentlicht.

Darmstadt, den _____

(Datum, Unterschrift)

Appendix A

class	*group*	*criteria*	*size range*	*refractive index*
other	biological*	(K+ Na+ S+ P+ Ca)/AE=[0.4;1.1], P/AE=[0.05;0.8], Na/AE=[0.05;0.8], Ca/AE=[0.05;1.1], K/AE=[0.025;0.8], S/AE=[0.025;0.8], Mg/(Na+ S+ P+ Ca)<0.1, Al/(Na+ S+ P+ Ca)<0.05, Si/(Na+ S+ P+ Ca)<0.1, Cl/(Na+ S+ P+ Ca)<0.05, Ti/(Na+ S+ P+ Ca)<0.05, Cr/(Na+ S+ P+ Ca)<0.05, Mn/(Na+ S+ P+ Ca)<0.05, Fe/(Na+ S+ P+ Ca)<0.1	d>0.3	-
secondary	Na-rich*	Na/AE=[0.2;1.1], Cl/AE<0.02499, Mg/Na<1.1, Al/Na<0.75, Si/Na<0.25, P/Na<0.1, S/Na<0.1, C/Na<0.05, K/Na<0.5, Ca/Na<0.5, Ti/Na<0.05, Cr/Na<0.05, Mn/Na<0.1, Fe/Na<0.1		sulf
secondary	ammonium sulphate*	S/AE=[0.3;1.1], Na/S<0.1, Mg/S<0.1, Al/S<0.2, Si/S<0.25, P/S<0.1, Cl/S<0.1, K/S<0.1, Ca/S<0.1, Ti/S<0.05, Cr/S<0.05, Mn/S<0.05, Fe/S<0.1		sulf
soot mixtures	soot*	Mg/AE<0.05, K/AE<0.3, S/AE<0.05, Al/AE<0.05, Fe/AE<0.03, Cl/AE<0.05, Cl/Si<0.05	0.03<d<0.20	soot
soot mixtures	soot+ ammonium sulphate*	Mg/AE<0.05, Si/AE<1.1, K/AE<0.3, S/AE=[0.05;1.1], Al/AE<0.05, Fe/AE<0.03, Cl/AE<0.05, Cl/Si<0.05	0.03<d<0.20	sulf+ soot**
sulphates	Na sulphate	Na/S=[0.101;10], (Na+ S)/AE=[0.1;1.1], Na/AE=[0.025;1.1], S/AE=[0.025;1.1], Mg/(S+ Na)<0.5, Al/(S+ Na)<0.1, Si/(S+ Na)<0.15, P/(S+ Na)<0.5, Cl/(S+ Na)<0.1, K/(S+ Na)<0.1, Ca/(S+ Na)<0.05, Ti/(S+ Na)<0.05, Cr/(S+ Na)<0.05, Mn/(S+ Na)<0.5, Fe/(S+ Na)<0.1		sulf
sulphates	Ca Na sulphate	(Na+ S+ Ca)/AE=[0.15;1.1], Na/AE=[0.025;1.1], S/AE=[0.025;1.1], Ca/AE=[0.025;1.1], Na/Ca=[0.1;10], Mg/(S+ Na+ Ca)<0.5, Al/(S+ Na+ Ca)<0.05, Si/(S+ Na+ Ca)<0.05, P/(S+ Na+ Ca)<0.2, Cl/(S+ Na+ Ca)<0.1, K/(S+ Na+ Ca)<0.1, Ti/(S+ Na+ Ca)<0.05, Cr/(S+ Na+ Ca)<0.1, Mn/(S+ Na+ Ca)<0.5, Fe/(S+ Na+ Ca)<0.1, Ca/(S+ Na)=[0.1001;10]		sulf
sulphates	Ca sulphate	Ca/S=[0.20;10], (Ca+ S)/AE=[0.2;1.1], Na/(Ca+ S)<0.1, Mg/(S+ Ca)<0.35, Al/(S+ Ca)<0.1, Si/(S+ Ca)<0.1, P/(S+ Ca)<0.1, Cl/(S+ Ca)<0.1, K/(S+ Ca)<0.1, Ti/(S+ Ca)<0.05, Cr/(S+ Ca)<0.05, Mn/(S+ Ca)<0.5, Fe/(S+ Ca)<0.1		calc
sulphates	other sulphates	sulfate S/AE=[0.2;1.1], Na/S<2, Mg/S<2, Al/S<2.5, Si/S<0.25, P/S<0.2, Cl/S<0.2, K/S<10, Ca/S<2, Ti/S<0.5, Cr/S<0.5, Mn/S<2, Fe/S<2		sulf
carbonates	Ca carbonate	Ca/AE=[0.2;1.1], Na/Ca<0.11, Mg/Ca<0.5, Al/Ca<0.151, Si/Ca<0.11, P/Ca<0.1, S/Ca<0.1, Cl/Ca<0.1, K/Ca<0.1, Ti/Ca<0.1, Cr/Ca<0.05, Mn/Ca<0.5, Fe/Ca<0.1		hem+ sil+ calc
carbonates	Ca Mg carbonate	(Ca+ Mg)/AE=[0.4;1.1], Mg/Ca=[0.501;2], Na/(Ca+ Mg)<0.5, Al/(Ca+ Mg)<0.1, Si/(Ca+ Mg)<0.2, P/(Ca+ Mg)<0.1, S/(Ca+ Mg)<0.1, Cl/(Ca+ Mg)<0.1, Ti/(Ca+ Mg)<0.1, Cr/(Ca+ Mg)<0.05, Fe/(Ca+ Mg)<0.1		hem+ sil+ calc
phosphates	phosphate	P/AE=[0.05;1.1], Al/(Ca+ P)<0.2, Si/(Ca+ P)<0.1		-
chlorides	Na chloride	(Na+ Cl)/AE=[0.25;1.1], Na/AE=[0.01;1.1], Cl/AE=[0.01;1.1], Si/AE<0.0499, Al/AE<0.0299, Mg/(Na+ Cl)<2, P/(Na+ Cl)<0.2, S/(Na+ Cl)<0.25, K/(Na+ Cl)<0.15, Ti/(Na+ Cl)<0.25, Cr/(Na+ Cl)<0.25, Mn/(Na+ Cl)<2, Fe/(Na+ Cl)<0.25		nchl+ sulf
chlorides	K chloride	(K+ Cl)/AE=[0.3;1.1], Na/AE=[0.01;1.1], Cl/AE=[0.01;1.1], Na/(K+ Cl)<0.15, Mg/(K+ Cl)<0.1, Al/(K+ Cl)<0.2, Si/(K+ Cl)<0.25,		kchl

		P/(K+ Cl)<0.2, S/(K+ Cl)<0.25, Ca/(K+ Cl)<0.5, Ti/(K+ Cl)<0.25, Cr/(K+ Cl)<0.25, Mn/(K+ Cl)<2, Fe/(K+ Cl)<0.25		
chlorides	other chloride	Cl/AE=[0.25;1.1], Si/AE<0.0699, Al/AE<0.0099, Na/Cl<2, Mg/Cl<2, P/Cl<0.1, S/Cl<0.2, K/Cl<2, Ca/Cl<2, Ti/Cl<0.1, Cr/Cl<0.1, Mn/Cl<2, Fe/Cl<10		-
oxides	Fe oxide	Fe/AE=[0.25;1.1], Na/Fe<0.1, Mg/Fe<0.25, Al/Fe<0.2, Si/Fe<0.25, P/Fe<0.2, S/Fe<0.2, Cl/Fe<0.1, K/(Fe<0.1, Ca/Fe<0.1, Ti/Fe<0.25, Cr/Fe<0.05, Mn/Fe<1		hem+ sil
oxides	Ti oxide	Ti/AE=[0.25;1.1], Na/Ti<0.18, Mg/Ti<0.1, Al/Ti<0.2, Si/Ti<0.25, P/Ti<0.2, S/Ti<0.2, Cl/Ti<0.1, K/Ti<0.1, Ca/Ti<0.1, Cr/Ti<0.05, Mn/Ti<0.25, Fe/Ti<0.25		rut+ sil
oxides	Fe Ti oxide	Ti/Fe=[0.2501;4], (Fe+ Ti)/AE=[0.25;1.1], Na/(Ti+ Fe)<0.2, Mg/(Ti+ Fe)<0.1, Al/(Ti+ Fe)<0.2, Si/(Ti+ Fe)<0.25, P/(Ti+ Fe)<0.2, S/(Ti+ Fe)<0.2, Cl/(Ti+ Fe)<0.1, K/(Ti+ Fe)<0.1, Ca/(Ti+ Fe)<0.1, Cr/(Ti+ Fe)<0.05, Mn/(Ti+ Fe)<0.05		rut+ sil
oxides	Al oxide	Al/AE=[0.2;1.1], Na/Al<0.2, Mg/Al<0.1, Si/Al<0.2499, P/Al<0.2, S/Al<0.2, Cl/Al<0.1, K/Al<0.1, Ca/Al<0.1, Ti/Al<0.1, Fe/Al<1		-
quartz	quartz	Si/AE=[0.4;1.1], Al/Si<0.2, Na/Si<0.1, Mg/Si<0.1, P/Si<0.2, S/Si<0.2, Cl/Si<0.05, K/Si<0.1, Ca/Si<0.05, Ti/Si<0.1, Cr/Si<0.05, Mn/Si<0.25, Fe/Si<0.1	d>0.2	hem+ qtz
silicates	SiAl	Al/Si=[0.201;4], (Al+ Si)/AE=[0.4;1.1], Al/AE=[0.05;1.1], Na/(Si+ Al)<0.05, Mg/(Si+ Al)<0.05, P/(Si+ Al)<0.2, S/(Si+ Al)<0.2, Cl/(Si+ Al)<0.1, K/(Si+ Al)<0.05, Ca/(Si+ Al)<0.05, Ti/(Si+ Al)<0.1, Cr/(Si+ Al)<0.1, Mn/(Si+ Al)<0.5, Fe/(Si+ Al)<0.1		hem+ sil
silicates	SiAlK	K/(Si+ Al)=[0.101;3], Al/Si=[0.2;2], (K+ Al+ Si)/AE=[0.4;1.1], K/AE=[0.0025;1.1], Na/(Si+ Al+ K)<0.05, Mg/(Si+ Al+ K)<0.08, P/(Si+ Al+ K)<0.2, S/(Si+ Al+ K)<0.1, Cl/(Si+ Al+ K)<0.1, Ca/(Si+ Al+ K)<0.1, Ti/(Si+ Al+ K)<0.05, Cr/(Si+ Al+ K)<0.05, Mn/(Si+ Al+ K)<0.05, Fe/(Si+ Al+ K)<0.05		hem+ sil
silicates	SiAlNa	Na/(Si+ Al)=[0.101;3], Al/Si=[0.2;2], Ca/Na<0.25, (Na+ Al+ Si)/AE=[0.4;1.1], Mg/(Si+ Al+ Na)<0.15, P/(Si+ Al+ Na)<0.2, S/(Si+ Al+ Na)<0.1, Cl/(Si+ Al+ Na)<0.05, K/(Si+ Al+ Na)<0.05, Ca/(Si+ Al+ Na)<0.05, Ti/(Si+ Al+ Na)<0.05, Cr/(Si+ Al+ Na)<0.05, Mn/(Si+ Al+ Na)<0.05, Fe/(Si+ Al+ Na)<0.15		hem+ sil
silicates	SiAlNaCa	(Ca+ Na)/(Si+ Al)=[0.101;3], Ca/(Si+ Al)=[0.101;3], Al/Si=[0.2;2], Ca/Na=[0.2501;5.5], (Na+ Ca+ Al+ Si)/AE=[0.4;1.1], Mg/(Si+ Al+ Na+ Ca)<0.1, P/(Si+ Al+ Na+ Ca)<0.2, S/(Si+ Al+ Na+ Ca)<0.2, Cl/(Si+ Al+ Na+ Ca)<0.05, K/(Si+ Al+ Na+ Ca)<0.1, Ti/(Si+ Al+ Na+ Ca)<0.05, Cr/(Si+ Al+ Na+ Ca)<0.05, Mn/(Si+ Al+ Na+ Ca)<0.05, Fe/(Si+ Al+ Na+ Ca)<0.1		hem+ sil+ calc
silicates	SiAlNaK	(K+ Na)/(Si+ Al)=[0.101;3], Al/Si=[0.2;2], K/Na=[0.25;4], (K+ Na+ Al+ Si)/AE=[0.4;1.1], Na/AE=[0.05;1.1], K/AE=[0.05;1.1],		hem+ sil

		Mg/(Si+ Al+ Na+ K)<0.05, P/(Si+ Al+ Na+ K)<0.2, S/(Si+ Al+ Na+ K)<0.2, Cl/(Si+ Al+ Na+ K)<0.05, Ca/(Si+ Al+ Na+ K)<0.1, Ti/(Si+ Al+ Na+ K)<0.05, Cr/(Si+ Al+ Na+ K)<0.05, Mn/(Si+ Al+ Na+ K)<0.05, Fe/(Si+ Al+ Na+ K)<0.05		
silicates	SiAlCaFeMg	(Ca+ Fe+ Mg)/(Si+ Al)=[0.101;3], Al/Si=[0.2;2], Ca/(Fe+ Mg)=[0.25;10], (Ca+ Fe+ Mg+ Al+ Si)/AE=[0.4;1.1], Ca/AE=[0.05;1.1], Fe/AE=[0.025;1.1], Mg/AE=[0.025;1.1], Ca/(Si+ Al)<0.5, Na/(Si+ Al+ Ca+ Fe+ Mg)<0.05, P/(Si+ Al+ Ca+ Fe+ Mg)<0.2, S/(Si+ Al+ Ca+ Fe+ Mg)<0.2, Cl/(Si+ Al+ Ca+ Fe+ Mg)<0.1, K/(Si+ Al+ Ca+ Fe+ Mg)<0.05, Ti/(Si+ Al+ Ca+ Fe+ Mg)<0.05, Cr/(Si+ Al+ Ca+ Fe+ Mg)<0.05, Mn/(Si+ Al+ Ca+ Fe+ Mg)<0.05		hem+ sil+ calc
silicates	SiAlKFeMg	K+ Fe+ Mg)/(Si+ Al)=[0.101;3], K/(Si+ Al)=[0.101;3], (Fe+ Mg)/(Si+ Al)=[0.101;3], K/(Fe+ Mg)=[0.25;4], (K+ Mg+ Fe+ Al+ Si)/AE=[0.4;1.1], Ca/AE<0.05, Na/(Si+ Al+ K+ Fe+ Mg)<0.1, P/(Si+ Al+ K+ Fe+ Mg)<0.2, S/(Si+ Al+ K+ Fe+ Mg)<0.2, Cl/(Si+ Al+ K+ Fe+ Mg)<0.1, Ca/(Si+ Al+ K+ Fe+ Mg)<0.05, Ti/(Si+ Al+ K+ Fe+ Mg)<0.05, Cr/(Si+ Al+ K+ Fe+ Mg)<0.05, Mn/(Si+ Al+ K+ Fe+ Mg)<0.05		hem+ sil
silicates	SiAlFeMg	Al/AE=[0.1;0.8], Fe/AE=[0.05;0.8], Mg/AE=[0.05;0.8], Ca/AE<0.05, (Fe+ Mg)/(Si+ Al)=[0.101;3], Al/Si=[0.201;2], K/(Si+ Al)<0.1, (Al+ Si+ Fe+ Mg)/AE=[0.5;1.1], Na/(Si+ Al+ Fe+ Mg)<0.05, P/(Si+ Al+ Fe+ Mg)<0.2, S/(Si+ Al+ Fe+ Mg)<0.2, Cl/(Si+ Al+ Fe+ Mg)<0.05, K/(Si+ Al+ Fe+ Mg)<0.1, Ca/(Si+ Al+ Fe+ Mg)<0.1, Ti/(Si+ Al+ Fe+ Mg)<0.05, Cr/(Si+ Al+ Fe+ Mg)<0.05, Mn/(Si+ Al+ Fe+ Mg)<0.05		hem+ sil
silicates	SiMgFe	Fe/(Si+ Mg)=[0.201;10], (Mg+ Fe)/Si=[0.25;4], Al/Si<0.2, (Fe+ Mg+ Si)/AE=[0.4;1.1], Na/(Si+ Fe+ Mg)<0.1, Al/(Si+ Fe+ Mg)<0.05, P/(Si+ Fe+ Mg)<0.2, S/(Si+ Fe+ Mg)<0.2, Cl/(Si+ Fe+ Mg)<0.1, K/(Si+ Fe+ Mg)<0.1, Ca/(Si+ Fe+ Mg)<0.1, Ti/(Si+ Fe+ Mg)<0.05, Cr/(Si+ Fe+ Mg)<0.05, Mn/(Si+ Fe+ Mg)<0.05		hem+ sil
silicates	SiMg	Mg/Si=[0.25;4], Al/Si<0.2, (Mg+ Si)/AE=[0.4;1.1], Na/(Si+ Mg)<0.1, Al/(Si+ Mg)<0.1, P/(Si+ Mg)<0.2, S/(Si+ Mg)<0.2, Cl/(Si+ Mg)<0.1, K/(Si+ Mg)<0.1, Ca/(Si+ Mg)<0.1, Ti/(Si+ Mg)<0.05, Cr/(Si+ Mg)<0.05, Mn/(Si+ Mg)<0.05, Fe/(Si+ Mg)<0.2		hem+ sil
silicates	SiCaTi	Ca/Ti=[0.25;4], Al/Si<0.2, (Si+ Ca+ Ti)/AE=[0.4;1.1], Ca/Si=[0.101;10], Ti/Si=[0.101;10], Na/(Si+ Ca+ Ti)<0.1, Mg/(Si+ Ca+ Ti)<0.1, P/(Si+ Ca+ Ti)<0.2, S/(Si+ Ca+ Ti)<0.2, Cl/(Si+ Ca+ Ti)<0.1, K/(Si+ Ca+ Ti)<0.1, Cr/(Si+ Ca+ Ti)<0.05, Mn/(Si+ Ca+ Ti)<0.05, Fe/(Si+ Ca+ Ti)<0.2		rut+ sil
mixtures	mixtures Si+ S	Al/AE<0.05, S/AE=[0.05;0.9], S/Si=[0.5;4], Al/Si<0.2, (Si+ S)/AE=[0.3;1.1], Na/(Si+ S)<2, Mg/(Si+ S)<2, Al/(Si+ S)<0.2, P/(Si+ S)<0.2, Cl/(Si+ S)<0.05, K/(Si+ S)<2, Ca/(Si+ S)<2, Ti/(Si+ S)<0.2, Cr/(Si+ S)<0.1, Mn/(Si+ S)<0.1, Fe/(Si+ S)<5	d>0.2	hem+ sil+ sulf
mixtures	mixtures AlSi+ S	Al/AE=[0.05;0.9], Si/AE=[0.1;0.9], S/AE=[0.1;0.9], S/Si=[0.5;10], Al/Si=[0.201;5], (Al+ Si+ S)/AE=[0.3;1.1], Na/(Al+ Si+ S)<5,		hem+ sil+ sulf

		Mg/(Al+ Si+ S)<5, P/(Al+ Si+ S)<0.2, Cl/(Al+ Si+ S)<0.05, K/(Al+ Si+ S)<5, Ca/(Al+ Si+ S)<5, Ti/(Al+ Si+ S)<0.2, Cr/(Al+ Si+ S)<0.2, Mn/(Al+ Si+ S)<0.2, Fe/(Al+ Si+ S)<5		
mixtures	mixtures Cl+ S	Cl/S=[0.201;10], (S+ Cl)/AE=[0.2;1.1], Cl/AE=[0.025;1.1], S/AE=[0.025;1.1], S/(Na+ Cl)=[0.1;20], Na/(S+ Cl)<3, Mg/(S+ Cl)<3, Al/(S+ Cl)<0.2, Si/(S+ Cl)<0.25, P/(S+ Cl)<0.25, K/(S+ Cl)<3, Fe/(S+ Cl)<2		nchl+ sulf
mixtures	mixtures NaCl+ Si	/(Na+ Cl)=[0.05;100], Al/Si<0.2, (Si+ Na+ Cl)/AE=[0.2;1.1], Cl/AE=[0.05;1.1], Na/AE=[0.05;1.1], Si/AE=[0.01;1.1]		hem+ sil+ nchl+ sulf
mixtures	mixtures NaCl+ AlSi	(Si+ Al)/(Na+ Cl)=[0.075;100], Al/Si=[0.201;100], (Si+ Na+ Cl)/AE=[0.2;1.1], Cl/AE=[0.05;1.1], Na/AE=[0.05;1.1], Si/AE=[0.025;1.1], Al/AE=[0.01;1.1]		hem+ sil+ nchl+ sulf
mixtures	mixtures Ca+ Si	Si/Ca=[0.2501;4], Al/Si<0.2, (Ca+ Si)/AE=[0.2;1.1], Si/AE=[0.01;1.1], Ca/AE=[0.05;1.1], Si/Ca=[0.1001;100], Mg/(Si+ Ca)<0.1, Al/(Si+ Ca)<0.2, P/(Si+ Ca)<0.2, S/(Si+ Ca)<0.2		hem+ sil+ calc
mixtures	mixtures Ca+ AlSi	Al/Si=[0.201;20], (Ca+ Si+ Al)/AE=[0.2;1.1], Al/AE=[0.01;1.1], Si/AE=[0.01;1.1], Ca/AE=[0.05;1.1], Si/Ca=[0.1001;100], Na/(Si+ Ca)<0.2, Mg/(Si+ Ca)<2, P/(Si+ Ca)<0.2, S/(Si+ Ca)<0.2, Cl/(Si+ Ca)<0.05, K/(Si+ Ca)<1		hem+ sil+ calc
silicates	other Si-dominated	Si/AE=[0.1;1.1]		hem+ sil+ sulf
other	steel	(Fe+ Ti+ Mn+ Cr)/AE=[0.2;1.1], Fe/AE=[0.2;1.1]		-
other	other Mg-dominated	Mg/AE=[0.35;1.1]		-
other	other K-dominated	K/AE=[0.25;1.1]		-
other	other Ca-dominated	Ca/AE=[0.15;1.1]		-
other	other			-

Appendix B

Date	Start Time	Sample	Start Lat	Start Lon	Start Alt	Biological	Secondary	Soot	Sulphates	Carbonates	Phosphates	Chlorides	Oxides	Quartz	Silicates	Mixtures	Other
2008_0122	15:13:00	FA_108	10.449	-19.048	100	0	51	222	1	1	1	0	7	1	25	2	2
2008_0123	16:59:10	FA_112	10.394	-19.081	100	0	331	335	43	0	3	0	0	1	16	4	1
2008_0123	16:52:00	FA_109	10.034	-19.384	900	3	87	1137	20	0	1	4	0	0	39	1	28
2008_0123	16:44:25	FA_111	9.6209	-19.722	2000	0	85	0	27	0	2	0	0	1	7	6	0
2008_0123	16:36:50	FA_110	9.2111	-20.057	3000	1	96	70	43	0	1	3	0	2	44	7	2
2008_0125	17:04:57	FA_114	14.932	-23.487	200	0	4	3	0	0	0	3	2	1	113	30	0
2008_0125	16:56:30	FA_116	14.886	-23.514	500	0	2	14	0	0	0	1	0	0	453	152	6
2008_0125	16:50:00	FA_119	14.955	-23.472	700	0	1	359	5	0	0	0	0	0	10	3	0
2008_0125	16:42:28	FA_118	14.931	-23.487	2000	0	7	278	0	0	0	0	0	1	4	4	12
2008_0125	16:35:00	FA_117	14.986	-23.553	3300	1	0	548	9	0	0	0	0	2	29	11	103
2008_0129	17:22:50	FA_127	14.963	-18.747	900	0	3	69	0	0	0	8	0	4	181	19	1
2008_0129	17:10:25	FA_128	14.858	-18.042	900	0	1	30	1	0	0	4	1	16	360	56	0
2008_0129	15:17:00	FA_129	15.003	-16.121	940	0	0	18	0	0	0	0	2	12	151	16	0
2008_0129	15:01:40	FA_130	15	-15.092	940	0	0	10	0	0	0	1	0	1	311	41	0
2008_0204	17:49:00	FA_139	10.291	-19.163	500	6	13	255	39	0	0	7	0	4	377	104	25
2008_0204	17:42:40	FA_140	9.9433	-19.437	900	0	0	217	15	0	0	44	0	2	21	4	39
2008_0204	17:36:50	FA_141	9.7596	-19.58	1300	1	9	1257	15	0	0	12	1	2	57	1	127
2008_0204	17:30:35	FA_142	9.4089	-19.854	1800	2	0	981	14	0	0	7	0	2	47	3	18
2008_0204	17:22:23	FA_143	8.9091	-20.243	3300	0	0	22	0	0	0	1	0	15	175	19	5
2008_0205	16:40:10	FA_148	-19.081	14.279	500	0	1436	12	3	0	0	0	0	0	28	87	0
2008_0205	17:03:30	FA_144	-18.064	14.633	700	0	2	23	2	0	0	1	3	9	331	36	12
2008_0205	17:11:20	FA_145	-17.68	14.717	700	0	8	21	1	0	0	6	0	11	457	97	38
2008_0205	16:28:50	FA_147	-18.133	14.152	2200	0	19	809	28	0	0	14	1	4	52	8	76
2008_0206	15:44:20	FA_154	14.823	-23.46	3600	3	32	336	70	0	4	10	1	0	100	24	9
2008_0206	16:48:50	FA_150	14.932	-23.476	3700	0	16	198	88	0	0	0	0	1	20	5	52
2008_0206	15:55:30	FA_153	15.675	-23.645	4000	0	1	150	23	0	0	0	0	0	18	2	51

Tab. 1: Sampling time (start time UTC), coordinates (start) and chemical composition in number of all collected samples; particle diameters < 0.5µm

Date	Start Time	Sample	Start Lat	Start Lon	Start Alt	Biological	Secondary	Soot	Sulphates	Carbonates	Phosphates	Chlorides	Oxides	Quartz	Silicates	Mixtures	Other
2008_0122	15:13:00	FA_108	10.449	-19.048	100	0	2	1	7	5	1	1	31	48	231	19	0
2008_0123	16:59:10	FA_112	10.394	-19.081	100	0	8	4	88	2	2	0	22	35	167	20	6
2008_0123	16:52:00	FA_109	10.034	-19.384	900	0	22	3	65	9	1	1	7	41	124	25	2
2008_0123	16:44:25	FA_111	9.6209	-19.722	2000	0	12	0	72	4	1	0	17	48	221	29	3
2008_0123	16:36:50	FA_110	9.2111	-20.057	3000	0	5	0	42	9	3	1	7	90	257	37	1
2008_0125	17:04:57	FA_114	14.932	-23.487	200	0	15	0	158	0	1	0	5	9	205	81	1
2008_0125	16:56:30	FA_116	14.886	-23.514	500	0	10	0	58	2	1	2	13	40	228	54	1
2008_0125	16:50:00	FA_119	14.955	-23.472	700	0	14	0	157	0	0	0	1	35	234	93	1
2008_0125	16:42:28	FA_118	14.931	-23.487	2000	0	9	0	57	1	2	0	12	19	146	37	0
2008_0125	16:35:00	FA_117	14.986	-23.553	3300	0	0	0	5	0	1	0	6	20	86	13	2
2008_0129	17:22:50	FA_127	14.963	-18.747	900	0	20	0	95	1	2	1	3	23	187	49	0
2008_0129	17:10:25	FA_128	14.858	-18.042	900	0	33	0	81	2	0	0	0	24	243	82	0
2008_0129	15:17:00	FA_129	15.003	-16.121	940	0	6	0	29	0	0	0	0	18	152	38	0
2008_0129	15:01:40	FA_130	15	-15.092	940	0	17	0	78	2	0	0	5	29	224	59	1
2008_0130	19:08:00	FA_132	16.717	-25.321	500	0	3	0	3	2	2	2	22	31	159	12	30
2008_0130	18:50:30	FA_133	17.669	-25.965	500	0	2	0	17	0	1	6	3	20	90	10	12
2008_0130	18:46:00	FA_134	17.891	-26.103	100	0	0	0	7	1	4	6	17	36	142	19	1
2008_0130	18:41:40	FA_135	18.118	-26.327	500	0	0	0	12	1	0	0	2	14	65	9	2
2008_0130	18:33:20	FA_136	18.453	-26.657	500	0	6	0	55	3	3	4	22	110	717	61	3
2008_0130	18:29:55	FA_137	18.651	-26.854	100	0	6	0	81	0	1	0	7	30	213	60	21
2008_0204	17:49:00	FA_139	10.291	-19.163	500	0	15	0	69	1	1	8	7	37	255	100	21
2008_0204	17:42:40	FA_140	9.9433	-19.437	900	0	14	0	58	1	6	0	10	40	282	77	3
2008_0204	17:36:50	FA_141	9.7596	-19.58	1300	0	5	16	27	2	0	0	0	21	199	48	4
2008_0204	17:30:35	FA_142	9.4089	-19.854	1800	0	25	0	107	4	5	0	5	63	259	71	5
2008_0204	17:22:23	FA_143	8.9091	-20.243	3300	0	0	0	1	0	0	0	0	5	20	5	0
2008_0205	16:40:10	FA_148	-19.081	14.279	500	0	3	0	11	1	0	90	3	18	99	24	0
2008_0205	17:03:30	FA_144	-18.064	14.633	700	0	15	0	114	8	4	1	24	64	344	67	2
2008_0205	17:11:20	FA_145	-17.68	14.717	700	0	16	0	106	12	2	1	32	75	392	89	0
2008_0205	16:28:50	FA_147	-18.133	14.152	2200	0	19	1	57	5	1	0	4	65	261	65	8
2008_0206	16:57:58	FA_151	14.879	-23.451	2000	0	12	0	66	1	0	0	8	22	116	16	1
2008_0206	15:44:20	FA_154	14.823	-23.46	3600	0	1	0	2	0	0	0	0	0	24	17	0
2008_0206	16:48:50	FA_150	14.932	-23.476	3700	0	33	0	107	1	1	1	0	45	169	59	5
2008_0206	15:55:30	FA_153	15.675	-23.645	4000	0	5	0	38	33	2	0	9	50	250	80	3

Tab. 2: Sampling time (start time UTC), coordinates (start) and chemical composition in number of all collected samples; particle diameters 0.5 µm - 2.5 µm

Date	Start Time	Sample	Start Lat	Start Lon	Start Alt	Bio	Secondary	Soot	Sulphates	Carbonates	Phosphates	Chlorides	Oxides	Quartz	Silicates	Mixtures	Other
2008_0122	15:13:00	FA_108	10.449	-19.048	100	0	0	0	5	0	0	0	14	45	286	17	0
2008_0123	16:59:10	FA_112	10.394	-19.081	100	0	4	0	24	3	2	1	2	23	161	10	3
2008_0123	16:52:00	FA_109	10.034	-19.384	900	0	2	0	16	12	4	21	2	48	262	77	3
2008_0123	16:44:25	FA_111	9.6209	-19.722	2000	0	1	0	22	5	0	1	2	34	211	33	3
2008_0123	16:36:50	FA_110	9.2111	-20.057	3000	0	6	0	14	18	0	1	2	59	266	59	4
2008_0125	17:04:57	FA_114	14.932	-23.487	200	0	4	0	16	0	0	1	2	6	146	46	1
2008_0125	16:56:30	FA_116	14.886	-23.514	500	0	2	0	13	10	2	11	9	85	791	85	0
2008_0125	16:50:00	FA_119	14.955	-23.472	700	0	4	0	25	7	0	0	9	82	617	69	0
2008_0125	16:42:28	FA_118	14.931	-23.487	2000	0	2	0	14	17	1	0	5	45	446	89	4
2008_0125	16:35:00	FA_117	14.986	-23.553	3300	0	1	0	6	11	0	0	0	11	72	27	0
2008_0129	17:22:50	FA_127	14.963	-18.747	900	0	4	0	28	0	0	0	1	14	163	36	0
2008_0129	17:10:25	FA_128	14.858	-18.042	900	0	2	0	17	0	0	0	0	5	156	27	0
2008_0129	15:17:00	FA_129	15.003	-16.121	940	0	1	0	3	1	0	0	5	40	432	34	0
2008_0129	15:01:40	FA_130	15	-15.092	940	0	2	0	24	0	1	0	1	15	249	43	0
2008_0130	19:08:00	FA_132	16.717	-25.321	500	0	2	0	1	4	0	28	6	30	237	26	6
2008_0130	18:50:30	FA_133	17.669	-25.965	500	0	1	0	5	4	0	17	3	28	289	28	6
2008_0130	18:46:00	FA_134	17.891	-26.103	100	0	1	0	5	6	3	1	7	81	648	113	0
2008_0130	18:41:40	FA_135	18.118	-26.327	500	0	1	0	9	2	0	0	0	16	244	26	0
2008_0130	18:33:20	FA_136	18.453	-26.657	500	0	1	0	0	1	0	9	1	16	174	70	0
2008_0130	18:29:55	FA_137	18.651	-26.854	100	0	1	0	16	0	0	0	2	28	229	23	5
2008_0204	17:49:00	FA_139	10.291	-19.163	500	0	1	0	7	3	2	88	0	13	234	102	7
2008_0204	17:42:40	FA_140	9.9433	-19.437	900	0	5	0	7	3	1	2	3	39	381	43	3
2008_0204	17:36:50	FA_141	9.7596	-19.58	1300	0	0	0	1	0	1	0	0	5	96	11	0
2008_0204	17:30:35	FA_142	9.4089	-19.854	1800	0	6	0	11	5	1	0	3	41	230	54	0
2008_0205	16:40:10	FA_148	-19.081	14.279	500	0	1	0	1	4	0	491	0	14	108	55	0
2008_0205	17:03:30	FA_144	-18.064	14.633	700	0	4	0	18	6	1	6	9	44	341	32	1
2008_0205	17:11:20	FA_145	-17.68	14.717	700	0	3	0	15	0	1	7	8	29	259	33	1
2008_0205	16:28:50	FA_147	-18.133	14.152	2200	0	3	0	23	15	4	0	6	101	495	208	5
2008_0206	16:57:58	FA_151	14.879	-23.451	2000	0	0	0	0	0	0	0	2	10	63	11	0
2008_0206	16:48:50	FA_150	14.932	-23.476	3700	0	16	0	5	5	10	6	1	29	256	55	5
2008_0206	15:55:30	FA_153	15.675	-23.645	4000	0	20	0	24	5	10	4	2	105	602	115	5

Tab. 3: Sampling time (start time UTC), coordinates (start) and chemical composition in number of all collected samples; particle diameters > 2.5µm

Appendix C

Jan. 25th, Praia

FA_117, 3300 m a.s.l.														
from, µm	to, µm	number	N_355	N_380	N_441	N_467	N_532	N_630	N_660	N_670	N_869	N_1021	N_1638	N_2000
0.05	0.1	316	1.48	1.56	1.67	1.70	1.71	1.74	1.75	1.75	1.78	1.80	1.88	1.93
0.1	0.25	255	1.50	1.56	1.64	1.67	1.68	1.70	1.71	1.71	1.74	1.75	1.81	1.85
0.25	0.5	28	1.52	1.55	1.60	1.62	1.63	1.64	1.64	1.64	1.65	1.66	1.69	1.72
0.5	1	22	1.77	1.76	1.75	1.75	1.75	1.73	1.73	1.73	1.71	1.70	1.69	1.69
1	2	88	1.59	1.59	1.59	1.59	1.59	1.59	1.59	1.59	1.58	1.57	1.57	1.57
2	4	99	1.58	1.58	1.58	1.59	1.59	1.59	1.58	1.58	1.58	1.58	1.57	1.57
4	8	48	1.61	1.61	1.61	1.61	1.61	1.60	1.60	1.60	1.60	1.60	1.59	1.59
8	16	1	1.62	1.62	1.61	1.61	1.61	1.61	1.61	1.61	1.61	1.60	1.60	1.59
from, µm	to, µm	number	K_355	K_380	K_441	K_467	K_532	K_630	K_660	K_670	K_869	K_1021	K_1638	K_2000
0.05	0.1	316	6.98E-01	6.69E-01	6.21E-01	6.11E-01	5.82E-01	5.62E-01	5.62E-01	5.62E-01	5.72E-01	5.82E-01	6.79E-01	7.56E-01
0.1	0.25	255	5.61E-01	5.38E-01	4.99E-01	4.91E-01	4.67E-01	4.51E-01	4.51E-01	4.51E-01	4.59E-01	4.66E-01	5.44E-01	6.06E-01
0.25	0.5	28	3.35E-01	3.21E-01	2.98E-01	2.93E-01	2.79E-01	2.69E-01	2.69E-01	2.69E-01	2.74E-01	2.79E-01	3.25E-01	3.62E-01
0.5	1	22	8.06E-02	7.64E-02	6.50E-02	5.37E-02	3.48E-02	5.33E-03	3.58E-03	3.00E-03	1.59E-03	1.26E-03	1.88E-03	2.10E-03
1	2	88	2.67E-02	2.80E-02	2.46E-02	2.19E-02	1.42E-02	2.18E-03	1.49E-03	1.26E-03	6.88E-04	5.69E-04	9.37E-04	1.10E-03
2	4	99	2.16E-02	2.31E-02	2.04E-02	1.84E-02	1.19E-02	1.85E-03	1.27E-03	1.08E-03	5.98E-04	5.04E-04	8.57E-04	1.03E-03
4	8	48	1.02E-02	1.08E-02	9.56E-03	8.62E-03	5.58E-03	8.71E-04	6.12E-04	5.29E-04	3.04E-04	2.70E-04	4.95E-04	6.31E-04
8	16	1	5.46E-03	5.78E-03	5.07E-03	4.58E-03	2.95E-03	4.70E-04	3.43E-04	3.04E-04	1.85E-04	1.77E-04	3.60E-04	4.81E-04

Feb. 4th, south

FA_139, 500 m a.s.l.														
from, µm	to, µm	number	N_355	N_380	N_441	N_467	N_532	N_630	N_660	N_670	N_869	N_1021	N_1638	N_2000
0.05	0.1	442	1.53	1.56	1.60	1.61	1.61	1.62	1.62	1.62	1.63	1.64	1.66	1.68
0.1	0.25	308	1.54	1.56	1.58	1.59	1.59	1.60	1.60	1.60	1.60	1.60	1.61	1.63
0.25	0.5	50	1.55	1.55	1.55	1.55	1.55	1.54	1.54	1.54	1.54	1.53	1.52	1.54
0.5	1	41	1.60	1.60	1.59	1.59	1.59	1.58	1.58	1.58	1.58	1.57	1.56	1.57
1	2	383	1.57	1.57	1.57	1.57	1.57	1.57	1.57	1.57	1.56	1.56	1.55	1.56
2	4	338	1.57	1.56	1.57	1.57	1.56	1.56	1.56	1.56	1.56	1.55	1.55	1.56
4	8	142	1.57	1.57	1.57	1.57	1.56	1.56	1.56	1.56	1.56	1.55	1.55	1.55
8	16	32	1.57	1.56	1.56	1.56	1.55	1.55	1.55	1.55	1.55	1.54	1.54	1.54
FA_139, 500 m a.s.l.														
from, µm	to, µm	number	K_355	K_380	K_441	K_467	K_532	K_630	K_660	K_670	K_869	K_1021	K_1638	K_2000
0.05	0.1	442	2.41E-01	2.31E-01	2.14E-01	2.10E-01	1.99E-01	1.91E-01	1.91E-01	1.91E-01	1.94E-01	1.97E-01	2.30E-01	2.57E-01
0.1	0.25	308	1.57E-01	1.51E-01	1.40E-01	1.37E-01	1.29E-01	1.21E-01	1.21E-01	1.21E-01	1.23E-01	1.25E-01	1.46E-01	1.63E-01

0.25	0.5	50	4.91E-03	4.88E-03	4.41E-03	4.19E-03	3.47E-03	2.50E-03	2.46E-03	2.44E-03	2.44E-03	2.49E-03	3.05E-03	3.38E-03
0.5	1	41	1.91E-02	1.82E-02	1.55E-02	1.30E-02	8.39E-03	1.30E-03	8.92E-04	7.60E-04	4.20E-04	3.54E-04	6.32E-04	7.28E-04
1	2	383	1.88E-02	1.99E-02	1.76E-02	1.57E-02	1.02E-02	1.57E-03	1.08E-03	9.16E-04	5.02E-04	4.19E-04	7.28E-04	8.33E-04
2	4	338	8.34E-03	8.85E-03	7.79E-03	7.03E-03	4.54E-03	7.16E-04	5.12E-04	4.49E-04	2.65E-04	2.45E-04	5.01E-04	6.23E-04
4	8	142	8.14E-03	8.66E-03	7.63E-03	6.88E-03	4.45E-03	6.99E-04	4.96E-04	4.32E-04	2.52E-04	2.29E-04	4.63E-04	5.63E-04
8	16	32	5.32E-03	5.65E-03	4.98E-03	4.49E-03	2.90E-03	4.57E-04	3.28E-04	2.87E-04	1.70E-04	1.58E-04	3.38E-04	4.02E-04

Feb. 5th, Dakar

from, µm	to, µm	number	N_355	N_380	N_441	N_467	N_532	N_630	N_660	N_670	N_869	N_1021	N_1638	N_2000
FA_144, 700 m a.s.l.														
0.05	0.1	159	1.58	1.59	1.60	1.60	1.61	1.61	1.61	1.61	1.60	1.60	1.60	1.60
0.1	0.25	215	1.59	1.60	1.61	1.62	1.62	1.63	1.62	1.62	1.62	1.61	1.61	1.62
0.25	0.5	36	1.59	1.59	1.60	1.60	1.60	1.60	1.60	1.60	1.59	1.58	1.58	1.58
0.5	1	99	1.63	1.63	1.63	1.64	1.64	1.64	1.63	1.63	1.63	1.62	1.61	1.61
1	2	469	1.59	1.59	1.59	1.60	1.60	1.60	1.59	1.59	1.59	1.58	1.57	1.58
2	4	343	1.60	1.60	1.61	1.61	1.61	1.61	1.61	1.61	1.60	1.59	1.59	1.59
4	8	164	1.58	1.58	1.58	1.58	1.58	1.58	1.58	1.58	1.57	1.57	1.57	1.57
8	16	18	1.58	1.58	1.58	1.58	1.59	1.59	1.59	1.59	1.58	1.58	1.58	1.58
16	32	1	1.58	1.58	1.58	1.58	1.58	1.59	1.58	1.58	1.58	1.58	1.58	1.58
FA_148, 500 m a.s.l.														
0.05	0.1	329	1.54	1.54	1.55	1.55	1.54	1.53	1.53	1.53	1.53	1.52	1.51	1.53
0.1	0.25	1078	1.54	1.54	1.54	1.54	1.53	1.52	1.52	1.52	1.52	1.51	1.50	1.52
0.25	0.5	159	1.54	1.54	1.54	1.54	1.53	1.52	1.52	1.52	1.52	1.51	1.49	1.52
0.5	1	41	1.56	1.56	1.56	1.56	1.55	1.55	1.55	1.55	1.55	1.54	1.53	1.54
1	2	156	1.58	1.58	1.58	1.58	1.58	1.57	1.57	1.57	1.57	1.56	1.55	1.56
2	4	399	1.56	1.55	1.55	1.55	1.55	1.54	1.54	1.54	1.54	1.53	1.52	1.54
4	8	263	1.56	1.55	1.55	1.55	1.54	1.53	1.53	1.53	1.53	1.53	1.51	1.53
8	16	53	1.55	1.55	1.55	1.55	1.54	1.53	1.53	1.53	1.53	1.52	1.51	1.53
16	32	4	1.57	1.56	1.56	1.56	1.56	1.55	1.55	1.55	1.55	1.55	1.54	1.55
FA_147, 2200 m a.s.l.														
from, µm	to, µm	number	K_355	K_380	K_441	K_467	K_532	K_630	K_660	K_670	K_869	K_1021	K_1638	K_2000
FA_144, 700 m a.s.l.														
0.05	0.1	159	6.50E-02	6.69E-02	6.02E-02	5.61E-02	4.31E-02	2.38E-02	2.27E-02	2.24E-02	2.18E-02	2.20E-02	2.60E-02	2.91E-02
0.1	0.25	215	9.14E-02	9.41E-02	8.48E-02	7.91E-02	6.11E-02	3.43E-02	3.28E-02	3.23E-02	3.16E-02	3.18E-02	3.76E-02	4.19E-02
0.25	0.5	36	4.92E-02	5.30E-02	4.69E-02	4.23E-02	2.74E-02	4.20E-03	2.83E-03	2.38E-03	1.27E-03	1.01E-03	1.56E-03	1.74E-03
0.5	1	99	5.66E-02	5.86E-02	5.13E-02	4.51E-02	2.92E-02	4.49E-03	3.03E-03	2.55E-03	1.36E-03	1.08E-03	1.65E-03	1.88E-03
1	2	469	4.03E-02	4.32E-02	3.82E-02	3.43E-02	2.22E-02	3.41E-03	2.30E-03	1.94E-03	1.04E-03	8.29E-04	1.30E-03	1.45E-03

2	4	343	4.39E-02	4.64E-02	4.08E-02	3.64E-02	2.36E-02	3.63E-03	2.45E-03	2.07E-03	1.11E-03	8.93E-04	1.40E-03	1.60E-03
4	8	164	1.45E-02	1.54E-02	1.35E-02	1.21E-02	7.84E-03	1.22E-03	8.58E-04	7.42E-04	4.25E-04	3.76E-04	6.90E-04	8.75E-04
8	16	18	2.04E-02	2.18E-02	1.93E-02	1.74E-02	1.12E-02	1.75E-03	1.22E-03	1.04E-03	5.89E-04	5.12E-04	9.06E-04	1.13E-03
16	32	1	2.20E-02	2.35E-02	2.07E-02	1.87E-02	1.21E-02	1.88E-03	1.31E-03	1.12E-03	6.32E-04	5.48E-04	9.66E-04	1.21E-03
FA_148, 500 m a.s.l.														
0.05	0.1	329	1.37E-02	1.32E-02	1.22E-02	1.19E-02	1.12E-02	1.06E-02	1.06E-02	1.06E-02	1.08E-02	1.10E-02	1.29E-02	1.43E-02
0.1	0.25	1078	4.21E-03	4.05E-03	3.74E-03	3.66E-03	3.44E-03	3.25E-03	3.24E-03	3.24E-03	3.29E-03	3.35E-03	4.02E-03	4.38E-03
0.25	0.5	159	1.11E-04	1.12E-04	9.67E-05	8.74E-05	5.58E-05	9.66E-06	8.23E-06	7.99E-06	5.76E-06	6.55E-06	1.13E-04	2.29E-05
0.5	1	41	6.33E-03	6.75E-03	5.95E-03	5.37E-03	3.47E-03	5.43E-04	3.82E-04	3.31E-04	1.91E-04	1.71E-04	3.64E-04	4.05E-04
1	2	156	2.03E-02	2.13E-02	1.87E-02	1.66E-02	1.08E-02	1.66E-03	1.13E-03	9.56E-04	5.19E-04	4.26E-04	7.28E-04	8.12E-04
2	4	399	4.44E-03	4.74E-03	4.18E-03	3.77E-03	2.44E-03	3.80E-04	2.66E-04	2.30E-04	1.31E-04	1.16E-04	2.76E-04	2.66E-04
4	8	263	2.79E-03	2.97E-03	2.62E-03	2.36E-03	1.53E-03	2.39E-04	1.69E-04	1.46E-04	8.43E-05	7.55E-05	2.11E-04	1.80E-04
8	16	53	4.13E-03	4.45E-03	3.94E-03	3.55E-03	2.30E-03	3.53E-04	2.40E-04	2.02E-04	1.09E-04	8.86E-05	2.24E-04	1.63E-04
16	32	4	7.11E-03	7.55E-03	6.65E-03	6.00E-03	3.87E-03	6.10E-04	4.37E-04	3.83E-04	2.26E-04	2.09E-04	4.31E-04	5.30E-04

Tab. 1: refractive Indices (real part n, "N" and imaginary part ik, "K") at different wavelength for Jan. 25th, Feb. 4th, and Feb. 5th. The values are arithmetic averages for all particles in the size class. For source and method of RI calculation of the single particles refer to Kandler et al. (2011)

Values for all other days can be derived from the electronic supplement: RI_Falcon.xls file.